UNIVERSITY OF WISCONSIN
DEPARTMENT OF METEOROLOGY
MADISON, DECEMBER 1964

Annual Report 1964

STUDIES OF THE EFFECTS OF VARIATIONS IN BOUNDARY CONDITIONS ON THE ATMOSPHERIC BOUNDARY LAYER

Heinz H. Lettau
Project Supervisor

Contributions by
Charles R. Stearns
Arlin B. Super
John C. Turner

Contract DA-36-039-AMC-00878
DA Task 1-A-O-11001-B-021-08

Sponsored by the Department of Meteorology
U. S. Army Electronics Research and Development Activity
Fort Huachuca, Arizona

University of Wisconsin
Department of Meteorology
Madison, December 1964

ANNUAL REPORT 1964

STUDIES OF THE EFFECTS OF VARIATIONS IN BOUNDARY CONDITIONS ON THE ATMOSPHERIC BOUNDARY LAYER

Heinz H. Lettau
Project Supervisor

Contributions by

Charles R. Stearns
Arlin B. Super
John C. Turner

Contract DA-36-039-AMC-00878
DA Task 1-A-0-11001-B-021-08

Sponsored by the Department of Metoeorology

U. S. Army Electronics Research and Development Activity

Fort Huachuca, Arizona

Scanner's note:

This page is blank.

General Introduction

In this second Annual Report, results are summarized which concern four phases specified in the objectives of the contract. These include (1) Micrometeorological studies of the interaction at an air/water interface and the resulting airmass modification over a scale of several kilometers of windfetch, (2) A series of thermal-response experiments utilizing the shading-technique of the sun's radiation on natural surfaces, (3) Controlled experiments on wind profile modification in airflow over the ice of Lake Mendota using fields of Christmas trees, and (4) A theoretical investigation of the processes which may explain the occasional formation of extreme wind-speed maxima known as the "low-level jet stream" of the atmospheric boundary layer.

Each of the four individual papers of this report is accompanied by an abstract which summarizes the specific problems discussed and details of the results.

Heinz H. Lettau
Madison, Wisconsin

December 1964

Table of Contents

LIST OF ILLUSTRATIONS

Section 1

Preliminary Results of an Air Mass Modification Study over Lake Mendota

Arlin B. Super

Department of Meteorology
University of Wisconsin

Abstract: Case studies of air mass modification in the lowest 3m above Lake Mendota (41 km^2 surface area) made with the aid of a specially instrumented pontoon boat, are discussed. The instrumentation on this boat is described in detail. Measurements include wind speed, air temperature and wet-bulb temperature at five levels above the air-water interface, and water temperature. Vertical profile structure is studied as a function of several kilometers of horizontal fetch by making runs across the lake into the mean wind. Budgets based on horizontal and vertical mean-motion transports of momentum, sensible heat, and latent heat and eddy transfer are calculated and graphed. Especially interesting conditions prevail on summer days; when the air flow is from rough and heated land to the smooth water surface with changes to inversion, wind speed increases first, and decreases after about 2 km of fetch.

1. Introduction

The primary purpose of this study has been to investigate the air mass modification in the lowest 3 m above Lake Mendota, a lake of 41 km^2 surface area. Air flowing from the surrounding terrain unto the lake encounters an abrupt change in boundary conditions. The aerodynamic surface roughness of the lake will be less than that of the land resulting in a decrease in the downward momentum flux and an increase in the mean wind over the lake. The air will not normally be in thermal adjustment with the water and a transfer of sensible heat will take place. An air-water vapor pressure gradient will generally exist resulting in a moisture flux.

Although boundary conditions vary significantly from the land to the lake, little variation is to be expected over the lake itself. Moreover, any variation with fetch that does occur might be expected to be systematic. For these reasons the lake affords an excellent site for the study of small-scale air mass modification over distances of 2 to 8 km.

The classical air mass modification study is usually attributed to G. I. Taylor (1915) who investigated the influence of the horizontal gradient of sea surface temperature on the lowest 1 km of the atmosphere off Newfoundland. Many modification studies have been recorded since Taylor's, and on size-scales ranging from the synoptic to the micro-scale. However, most studies have been conducted on the large or synoptic-scale. Notable examples include Wexler (1936), Craddock (1951), Riehl (1951), and others. Several meso-scale modification studies have been made over water surfaces. Bunker (1949) studied the moisture flux in continental air flowing over coastal waters. The influence of Hudson Bay on cP air was investigated by Burbidge (1951). "Steam Fog over Lake Michigan in Winter," by Church (1945) is another noteworthy example. Most of the few micro-scale studies that have been published consider the modification over a solid boundary. Kutzbach (1961), and Stearns and Lettau (1963) have studied the modification caused by introducing roughness elements on a smooth ice surface. Rider, Philip, and Bradley (1963) have investigated the effect of a 50 m^2 grass plot on air flowing off a large expanse of blacktop.

In those cases where substantial data has been collected over or around a lake, the primary purpose has been to estimate evaporation. The Lake Hefner (1954) and Lake Mead (1958) studies are outstanding examples as is the Lake Eucumbene study reported by Webb (1961). These studies utilized measurements of vertical profiles obtained at fixed masts either slightly offshore or slightly onshore or from moored rafts, with the exception of the Lake Eucumbene study which had some data available from a mobile barge.

1 Equipment and Instrumentation

Lettau (1959) has suggested an approach to the study of horizontal differences in micrometeorological profile structure, as provided by sensors mounted on moving vehicles, such as light airplanes, sailplanes, etc. In this study, a pontoon boat was used to investigate the horizontal variability of wind, tempera-

ture, and humidity profiles over Lake Mendota. Simultaneous observations were generally made at a base tower on the lake. The 27 × 8 foot pontoon boat (see Fig. 1) was powered by an 18 hp outboard engine during the 1963 season and a 28 hp engine during the 1964 season. It was driven at full throttle on all runs maintaining a speed ranging from 2.0 to 4.5 m/sec. depending upon surface roughness and wind. The boat carried the following equipment, which will later on be described in more detail:

a) A 3 kw 115/230 vac Onan gasoline generator which provided instrument power was located near the rear of the pontoon boat deck.

b) A wind vane was mounted between the pontoon tips about 2m above water level. The boat was driven into the mean wind by maintaining this vane in as close to a "dead-ahead" position as possible.

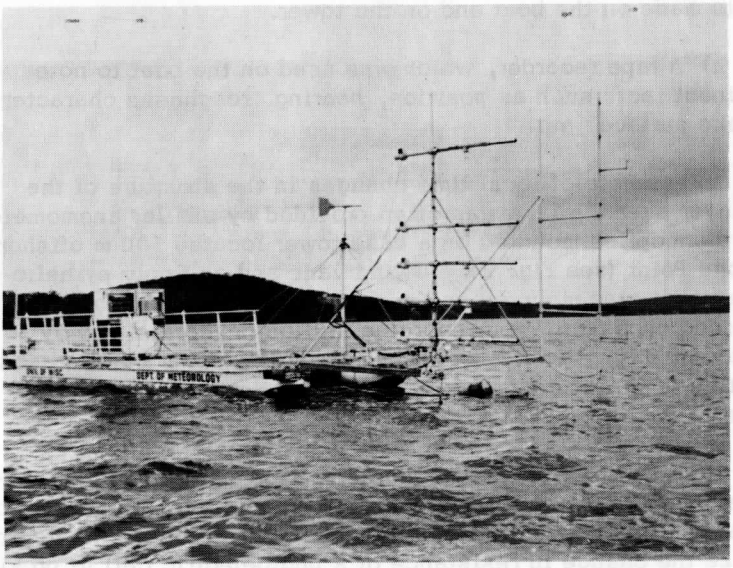

Fig. 1 Instrumented Pontoon Boat used in the air mass modification study over Lake Mendota.

c) Twin masts which held temperature, wet-bulb, and wind probes were fastened to the deck and extended 12 feet ahead of the pontoon tips. Anemometers were mounted at five levels (0.8, 1.2, 1.6, 2.0, and 2.8 m above mean water level) on the port mast, and ventilated thermopiles were mounted at the same five levels on the starboard mast.

d) Two thermopiles which extended into the lake which served as a reference bath. A thermistor or diode monitored lake temperature.

e) A "distance meter" which measured the movement of the boat relative to the lake.

f) A recording system for all thermopiles, which consisted of a 24 position stepping switch to dc amplifier to digital voltmeter to digital recorder. Anemometers and the distance meter were recorded by electro-mechanical counters which were photographed once per minute.

g) A two-way radio link between the boat and the instrument shack which provided an accurate synchronization of measurements made on the boat and on the tower.

h) A tape recorder, which was used on the boat to note pertinent facts such as position, bearing, roughness character of lake surface, etc.

An estimate of local time changes in the structure of the air layer over the lake was often provided by similar anemometers and thermopiles mounted on a base tower located 500 m offshore Second Point (see Fig. 2). A wind vane and an Epply pyrheliometer were also mounted on the tower. All tower sensors were recorded once/min. at a recording station onshore either by photographing counters, or on punch cards. For a detailed description of this micrometeorological installation reference is made to Stearns (1962).

The wind profile was measured by five matched cup anemometers manufactured by Thornthwaite Associates. These anemometers and their counting circuits, as modified by C. R. Stearns, utilize the change in resistance of a photoelectric cell to provide a signal. This signal is detected by an amplifier which triggers a relay which activates an electro-mechanical counter (see Fig. 3). The counters were photographed once/min. simultaneously with

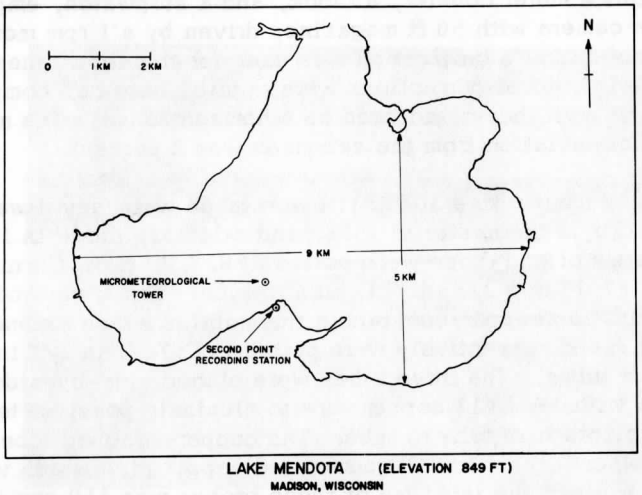

Fig. 2 Lake Mendota, Madison, Wisconsin — showing the location of the Department of Meteorology, University of Wisconsin, Micrometeorological tower.

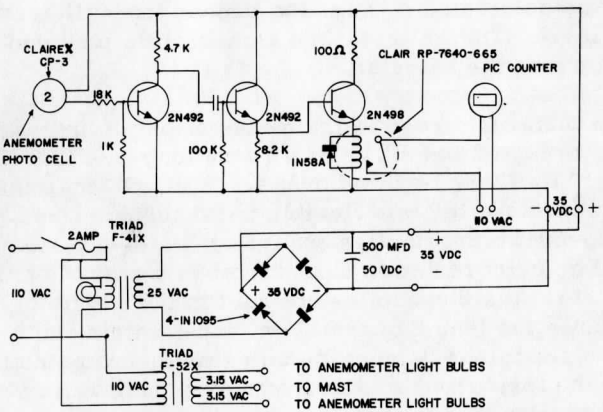

Fig. 3 Anemometer counting circuit and power supply.

the distance meter counter, a clock, and a stopwatch, employing a 35 mm camera with 50 ft magazine, driven by a 1 rpm motor. The manufacturer's calibration was used for the set of anemometers although individual corrections were applied based on comparison-runs made with the set mounted on a horizontal bar. The maximum individual deviation from the set-mean was 2 percent.

Water temperature at 0.3 m below mean water level was measured by a thermistor in 1963, and a 1N2326 diode in 1964. The thermistor and diode were potted in R.T.V. (Dow Corning Silastic #731) in a 3/8 in. OD plastic tube. The lower ends of two 2-junction copper-constantan thermopiles which extended to 0.8 and 2.8 m respectively were potted in R.T.V. in 1/4 in. OD aluminum tubes. The three tubes were placed side-by-side and wrapped with AWG #17 copper wire to eliminate possible temperature gradients from tube to tube. The copper-wrapped tubes were finally placed in a 1 in. OD perforated copper pipe which was painted white. The lag-time of these probes was 110 sec in still water.

Air temperature differences at 0.8 to 1.2, 1.2 to 1.6, 1.6 to 2.0, and 2.0 to 2.8 m were measured by 10-junction copper-constantan thermopiles having a lag-time of about 48 sec. The thermopile extending from 0.3 m below water surface to 0.8 m in the air gave the temperature difference relative to the absolute temperature of the water. The absolute temperatures at the other levels were calculated by summing temperature differences from level to level. The water-to-2.8 m thermopile provided an additional check on the calculation.

Each thermopile used in the measurement of air temperature gradients is potted in R.T.V. in a 10 cm long-1/4 in. OD aluminum tube. This tube is fitted over a 3/8 in. OD stainless steel tube which is inserted into flexible tygon tubing. (See Fig. 4). At each level two thermopiles are inserted side-by-side into an inner and an outer radiation shield through a plexiglass nozzle (see Fig. 5). The thermopiles are held in the middle of and midway down the length of the 12 in. inner shield, with the aid of a small plexiglass "spider." Both shields are painted flat black on the inside and are covered with aluminized mylar on the outside. Ventilation between the shields is provided through eight 1/4 diameter holes located around the rear of the inner shield. The plexiglass nozzle is attached to a 1 m long 1-1/4 in. aluminum pipe which has a 110 vac blower on the other end. Nozzle, pipe, and blower are painted white. Tests made using

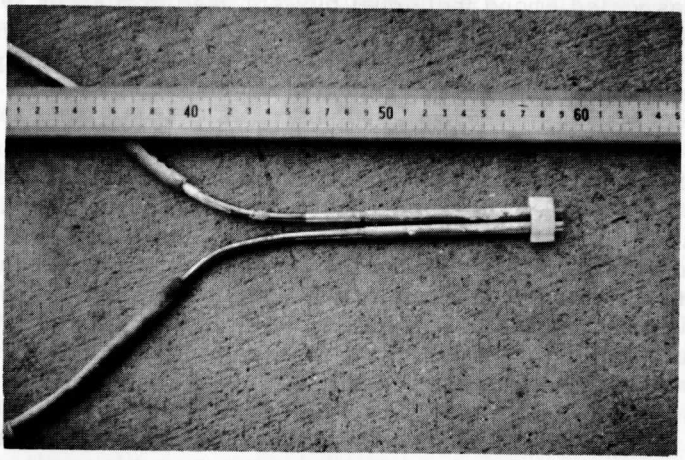

Fig. 4 Two thermopiles used in temperature difference measurement held together by a plexiglass "spider." Units shown on measuring stick are centimeters.

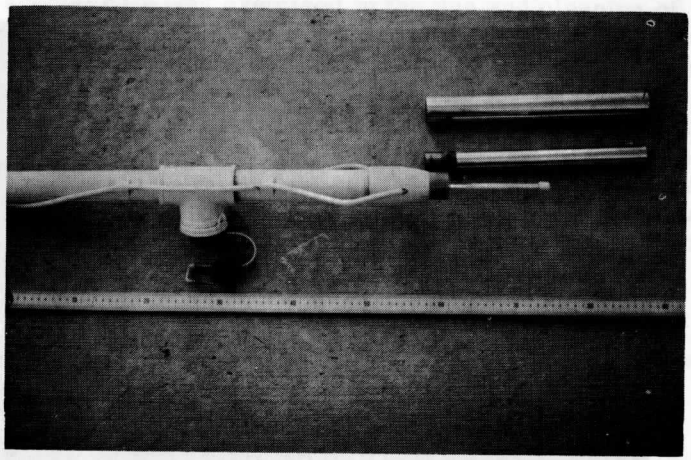

Fig. 5 Air temperature and wet-bulb depression probes with housings and radiation shields. A meter stick is also shown.

a pitot tube and pressure transducer indicated that ventilation rates varied among individual blowers used from about 390 to 420 cm/sec in still air with the probes in place. The ventilation rate was found to increase by about 10 percent when the probes were pointed into a 5 m/sec wind.

All thermopiles and the absolute temperature probes were individually calibrated in agitated water baths with the aid of mercury-in-glass precision thermometers. Several checks were made on the absolute temperature probes during both the 1963 and 1964 seasons by measuring water temperature near the probes with a precision thermometer. It is estimated that the accuracy of absolute temperature obtained with the thermistor was $\pm$ 0.1°C, while that obtained with the diode was $\pm$ 0.05°C, assuming no error for the thermometer reading.

The wet-bulb to dry-bulb temperature depressions were also measured at 0.8, 1.2, 1.6, 2.0, and 2.8 m above mean water level. Specially designed probes (see Fig. 6) were inserted into "tees" in the 1 - 1/4 in. pipe located 45 cm behind the 10-junction thermopiles. It was assumed that this dry-bulb probe was at the same temperature as the thermopiles in the radiation shields.

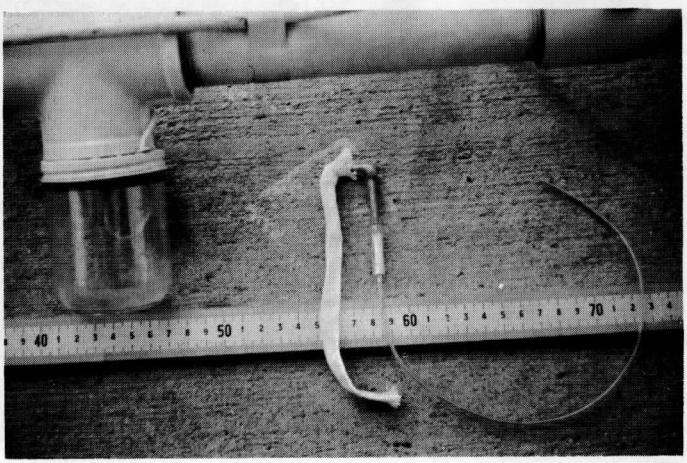

Fig. 6 Wet-bulb depression probe with wick, housing, and meter stick.

All wet-to-dry bulb thermopiles were compared in agitated baths and checked with precision thermometers. This proved to be difficult because of the small size of the probes (only a 1.4 cm thick styrofoam wall separated the baths and the two ends of the probes). However, individual differences from the group mean were less than ± 0.03°C at a mean bath temperature difference of 3.5°C. Calculation of the temperature differences between the two baths using standard tables for copper-constantan thermocouple outputs yielded values which agreed within ± 0.05°C with measured differences.

Cotton wicks were used to feed distilled water to the wet-bulb probes, by capillary attraction. The wicks fitted somewhat loosely over the 3/8 in. OD aluminum tube but snugly over the 1/4 in. OD plastic tube into which the aluminum tube was inserted. Better results were obtained with these wicks than with smaller diameter wicks which fitted over the aluminum tube only. In practice, the wicks were extended about 1.5 cm onto the plastic "U" (see Fig. 6).

Horizontal comparisons of the entire thermopile assemblys were made by mounting them side-by-side on a horizontal bar about 4 ft above water level and 12 ft ahead of the moving pontoon boat. The results indicated that it was possible to obtain agreement of individual wet-bulb depressions within ± 0.1°C only if special care was exercised in the use and cleaning of the wicks. In practice, wicks were cleaned by boiling first in a weak Alconox solution, second in clean tap water, and third in distilled water. They were then stored in a closed container of distilled water until used. Clean wicks were put on for each day of cruises. The same horizontal comparisons indicated that temperature differences between the shielded thermopiles were less than 0.02°C even when some were shaded from direct solar radiation while others were not. This indicates that no significant radiation errors were present.

The "distance meter" which measured boat speed relative to the lake was mounted between the pontoon tips 25 cm below mean water level (see Fig. 7). It consists of twin screws mounted on a horizontal shaft which drives a vertical shaft through a 20:1 worm-gear. Both shafts turn on ball bearings which are sealed in an oil-filled housing. A cam on the vertical shaft activates a micro-switch which, in turn, activates a relay-driven counter through an electrical circuit. The counter is photographed once/min.

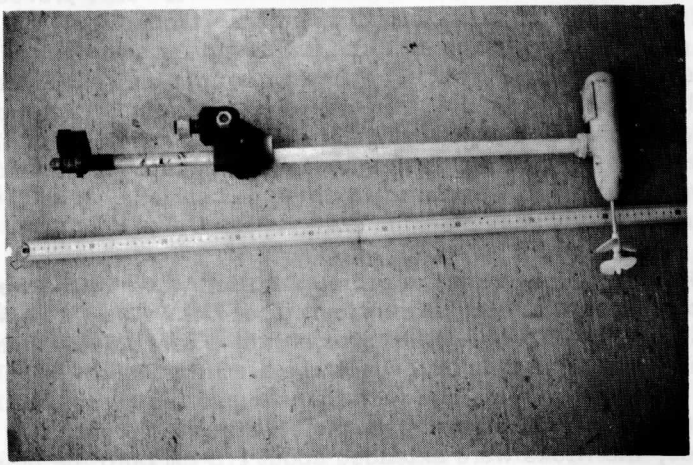

Fig. 7 Propellor-driven "distance meter" and meter stick.

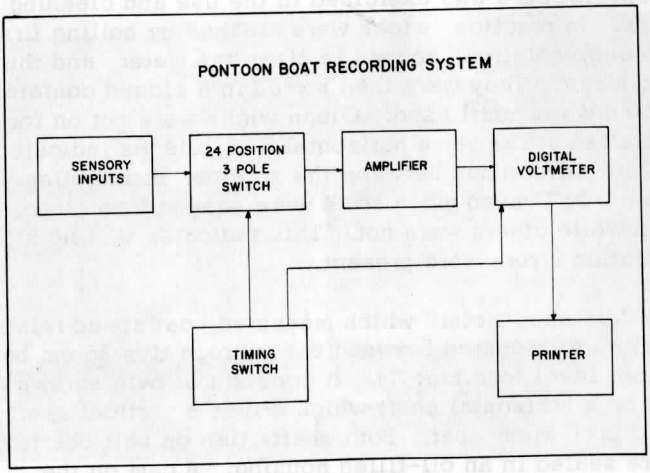

Fig. 8 Layout of temperature and wet-bulb depression recording system.

The calibration of the distance meter was accomplished by two methods. One method was to make comparisons with the anemometers during periods of very light winds. The simultaneous minute by minute record of "measured wind speed" and distance-meter counts/min for these runs contained several cases of negligible wind shear for which a scatter diagram was plotted. Obviously, "measured wind speed" at any level consists of the actual wind speed at that level plus the speed of the boat which is driven into the mean wind. It was assumed that the lowest values of wind speed recorded for given rates of distance meter counting represented cases of zero actual wind speed. In such cases "measured wind speed" and boat speed would be equivalent. The scatter diagram of readings obtained throughout the range of the boat's cruising speed suggested that the distance meter was essentially linear in this range. This was confirmed by making straight-line runs between fixed points on the lake at several different speeds.

A second independent means of calibrating the distance meter was obtained by estimating the distances covered for several timed runs over 3 km with the aid of a U. S. Geodetic Survey map of Lake Mendota. This method consistently yielded speeds about 6 percent higher than the anemometer comparison method. The production of a certain amount of "dead air" by the boat might cause such a discrepancy. However, several simultaneous 5 to 10 min wind profile measurements made on the base tower off Second Point and on the boat which was moored within 50 m of the tower revealed no significant differences in wind speed at any level. Errors in the map and its scale and/or in the manufacturer's anemometer calibration might also cause this discrepancy. A careful measurement over the frozen lake of the distance between two fixed landmarks about 1.75 km apart was in good agreement with the map. A means of checking the anemometer calibration was not readily available. However, the anemometer comparison method of distance meter calibration was used because it was necessary to calculate the portion of "measured wind speed" due not to actual wind but to the boat's movement into the mean wind. This portion has the same magnitude at all levels and is equivalent to true boat speed if the anemometer calibration is correct. It is estimated that this portion was calculated with $\pm$ 10 cm/sec of its actual value.

All temperature and wet-bulb depression sensors were recorded by the system depicted as Figure 8. A 24 position stepping switch driven by a 1 rpm motor sampled each thermopile once/30 sec with the exception of the water to 2.8 m probe which was sampled once/min. Water temperature was also sampled once/min. The stepping

switch alternately connected each probe to a Honeywell Accudata II dc amplifier which was operated on single-ended input capable of 2 vdc output for 1 mv full scale input. According to the manufacturer's specification, this amplifier possesses gain stability and linearity better than 99.99 percent, with noise and drift less than $\pm$ 2 microvolts for the range used. Frequent checking of the system with a reference voltage seemed to confirm these claims. Amplifier output was measured by a Hewlett-Packard 405/CR digital voltmeter which was read by a Hewlett-Packard 561B digital recorder. Recorder output was printed on paper tape. Inherent noise in the entire recording system was about $\pm$ 0.02°C or less for all thermopile probes. The recording equipment is shown in Fig. 9 mounted on the rear of the pontoon boat deck.

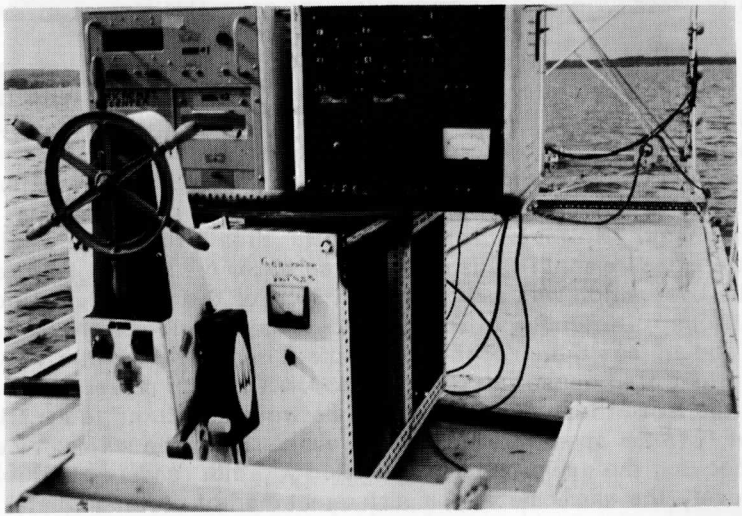

Fig. 9 3 kw generator, recording equipment, and pontoon boat controls located at rear of pontoon deck.

1.3 Observational Program and Preliminary Results

A typical measurement cruise with the pontoon boat would begin either near the micrometeorological tower or just offshore the downwind shoreline. The boat would be driven at full throttle across the lake into the mean wind. The cruise would terminate within 100 m of the upwind shoreline. In all, some 90 cruises

ranging from 2 to 8.5 km in length were made during the fall of 1963 and the spring and summer of 1964. The temperature gradient in the 0 to 3 m air layer ranged from strong inversion to strong lapse while wind speeds varied from calm to over 10 m/sec.

It was hoped that the data recorded at the tower would serve as a reference to estimate local or time changes of the various parameters involved. However, examination of simultaneously recorded wind speeds on the moving boat and on the tower revealed large fluctuations of a few minutes period that appeared to be essentially random. Also, comparisons were made between the wind speed as recorded on the tower and on the boat moored from 2 to 3.5 km upwind. These one hour comparisons revealed little correlation. In view of this, no attempt has been made to estimate local wind speed variations. It appears that the tower data may yield estimates of local variations of temperature and moisture which vary in a more gradual and apparently organized manner. However, in the following preliminary results, no such estimates have been made. Rather, it has been assumed that local changes are essentially random and can be eliminated by the grouping of the results of several cruises obtained under similar conditions.

Because of the large quantity of data involved, it was convenient to utilize an automatic computer for most of the data analysis. Parameters at each level of measurement were averaged for each 0.5 km section off the upwind shoreline for each individual cruise. The percent departures of these 0.5 km means from the mean for the entire fetch under consideration (3.5 km in the following results) were calculated. The percent departures for each particular 0.5 km section (e.g., 0 to 0.5 km, 0.5 to 1 km, etc.), were then averaged for all cruises in a particular class of conditions. Finally, these average percent departures were multiplied by the average of the mean values of the parameter for individual cruises. Thus, the percent departures from the means of individual cruises were averaged yielding a more meaningful result than simple averaging of the 0.5 km parameter means.

The preliminary results which follow all represent inversion conditions. That is, they depict the typical daytime case of the summer season, i.e., warm air flowing over cool water. The results are separated into two classes depending upon the mean wind speed at 2.8 m for the 3.5 km section. The strong wind class is composed of 20 cruises for which the mean 2.8 m wind speed was greater than 6 m/sec. The light wind class represents 14 cruises each with a mean 2.8 m wind speed below 5 m/sec. In both

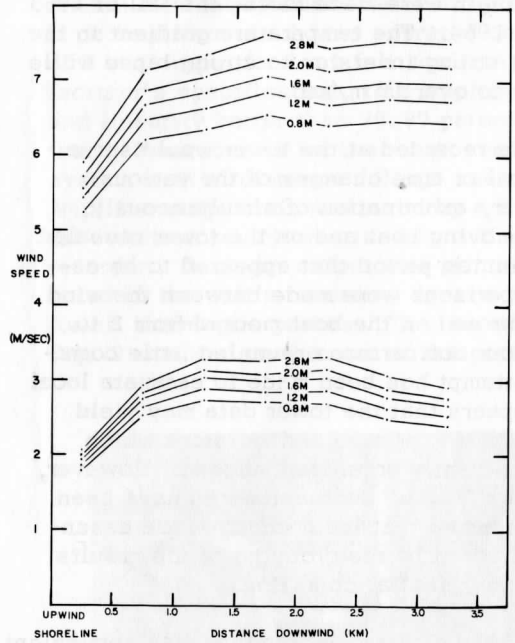

Fig. 10. 0.5 km means of wind speed at each level of measurement plotted as a function of distance downwind for both the strong and light wind classes.

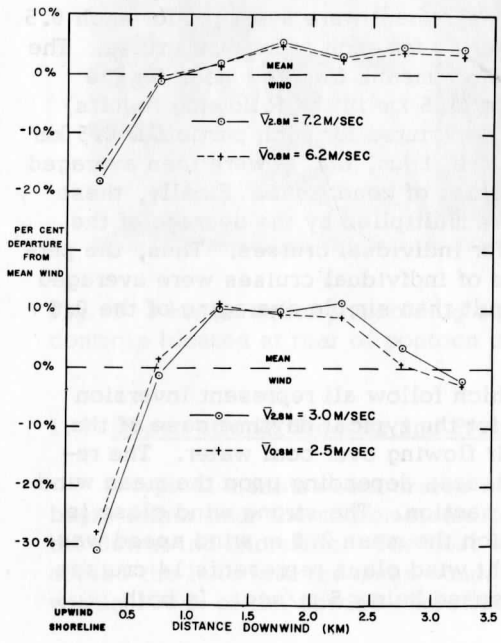

Fig. 11. Percent departures from the mean wind at 0.8 m and 2.8 m plotted as functions of distance downwind.

classes conditions for the first 3.5 km downwind of the upwind shoreline were studied in detail.

Figure 10 represents the 0.5 km means of wind speed for each measurement level as a function of distance downwind for both the strong and the light wind class. In each case the air accelerates rapidly after encountering the lake. As is especially evident in the light wind class, the wind speed appears to reach a maximum about 2 km offshore after which it gradually diminishes. Similar plots have been made representing fewer cruises but extending out to 6 km offshore. This wind speed maximum is again evident at about 2 km offshore followed by a gradual decrease across the remainder of the lake. Similar plots for lapse conditions reveal no such maximum but rather an increase of wind speed with fetch across the entire lake.

This wind speed maximum might be explained by considering the variations in boundary conditions along the trajectories. The air, driven primarily by the synoptic-scale pressure gradient, encounters a relatively smooth surface upon reaching the lake and accelerates. However, as the air flows across the relatively cool lake thermal stratification increases tending to supress turbulence. The air exhibited marked stability in the cases under consideration. The average Richardson Number at 1 m was 0.05 for the strong wind class and 0.19 for the light wind class.

The percent departures from the mean wind at 0.8 m and 2.8 m are plotted as functions of distance downwind in Figure 11 for both the strong and the light wind class. It can be seen that in each class the curves representing the highest and lowest levels of measurement (2.8 m and 0.8 m) are quite similar. However, the 2.8 m curve lags slightly behind the 0.8 m curve across the entire 3.5 km section. It appears that the wind at the lower level responds to the variations in boundary conditions before the wind at the higher level. Thus, the wind speed maximum at the lower level occurs nearer the upwind shoreline. As would be expected, this effect is more pronounced in the light wind class. Similar plots made for lapse conditions have revealed no such lag but rather a close overlapping of the 0.8 m and 2.8 m curves. This might also be expected because of the increased mixing associated with lapse conditions.

Figure 12 reveals a continuous and rather large decrease in air temperature with fetch for both classes. As would be expected, the rate of decrease lessens downwind as the air-water temperature

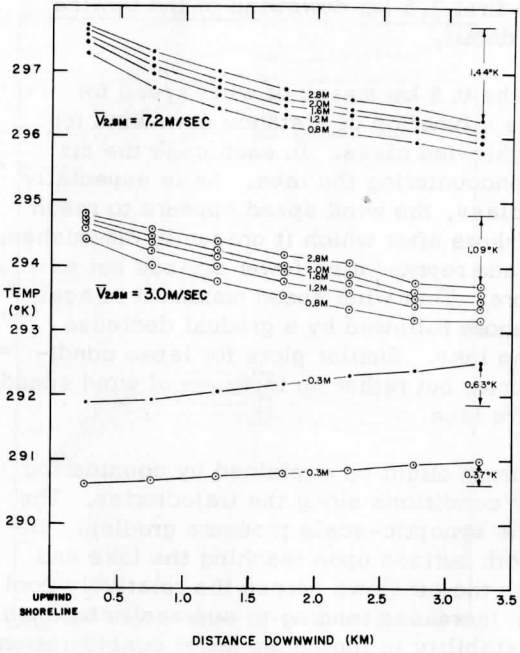

Fig. 12. 0.5 km means of temperature at each level of measurement plotted as a function of distance downwind for both the strong and light wind classes.

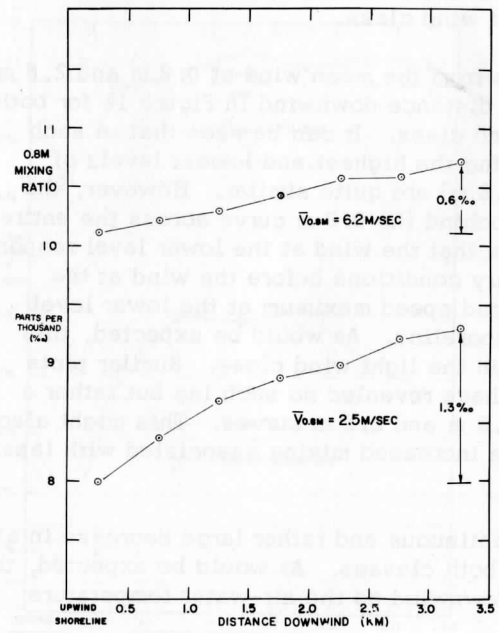

Fig. 13. 0.5 km means of mixing ratio at 0.8 m plotted as a function of distance downwind.

gradient decreases. In both classes the water temperature at -0.3 m increases almost linearly with distance downwind. This large increase must be primarily due to the wind-driven circulation in the lake. The warm surface layers are replaced by the upwelling of deeper cooler water. It is significant that the horizontal gradient of water temperature is larger for the strong wind class.

The downwind increase in the mixing ratio at 0.8 m is shown as Figure 13 for both classes. The higher levels of measurement were not depicted because of obvious measurement errors at some of these levels for some of the light-wind cruises. It appears that the mixing ratio increase for the light wind class is over twice that for the strong wind class. The air-water vapor pressure gradient was approximately the same for both classes. Thus, if the bulk aerodynamic method had been applied, the rate of evaporation would be directly proportional to wind speed, or about 2.5 times greater for the strong wind class. However, since the air in the light wind class takes about 2.5 times as long to cross the 3.5 km section one might expect a similar increase in water vapor content in both classes. Since this does not occur, it can be concluded that the water vapor is being mixed through a deeper layer in the strong wind class.

The momentum budget from the interface to 2.8 m for the 3.5 km section is considered in Figure 14 for both classes. A scheme similar to that used by Stearns and Lettau (1963) is utilized to construct these budgets. Thus, in calculating that portion of the budget due to mean motion it is assumed that steady states and two-dimensional flow exists. Also, the effects of the pressure gradient force, of the Coriolis force, of viscous forces, and of air compressibility are neglected. The surface shearing stress, τ_0, is calculated from Lettau's (1964) model of the diabatic wind profile. The eddy transport through the top of the layer then becomes the residue. It is seen that τ_0 is relatively invarient with fetch for the strong wind class. In the light wind class τ_0 is, of course, much less and apparently has a maximum roughly corresponding to the wind speed maximum.

Similarity theory suggests that it is reasonable to assume the equality of the coefficients of eddy conductivity, eddy diffusivity, and eddy viscosity. This assumption was made in order to calculate budgets of sensible and latent heat transfer similar to the momentum budget. Fig. 15 represents such a budget for sensible heat transfer. It is apparent that the air to water heat flux decreases rapidly with fetch in both cases and that this flux is about twice as large for the strong wind class.

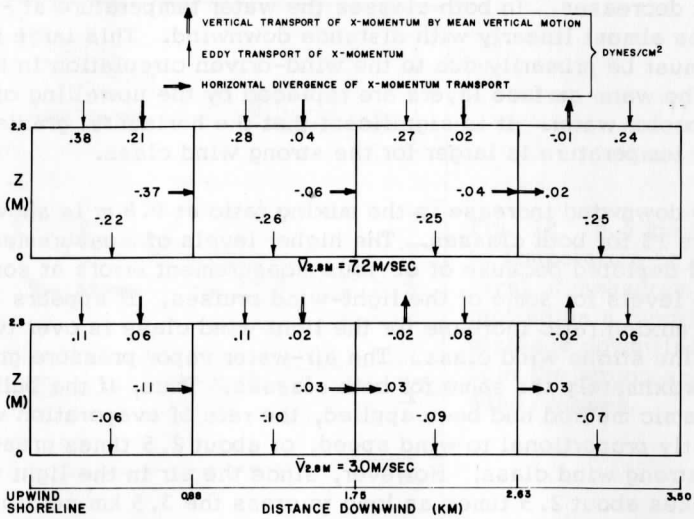

Fig. 14 Local momentum budget constituents for four air volumes along the 3.5 km trajectory for both strong and light winds.

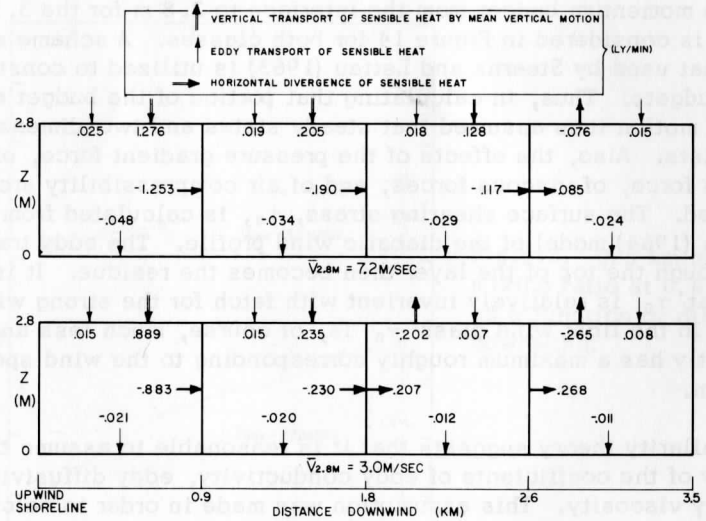

Fig. 15 Local sensible heat budget constituents for four air volumes along the 3.5 km trajectory for both strong and light winds.

For practical applications it is interesting to know how well profile measurements made at only one point along the 3.5 km section would represent the mean air to water heat flux for the section. It can be seen on Fig. 15 that such measurements made in the center of the last "box" (about 3 km downwind) would yield an underestimation of the mean sensible heat flux to the water of about 30 percent. Similarly, measurements made about 0.5 km downwind would yield a 36 percent overestimate. Measurements made at the center of the 3.5 km section would also result in an overestimation but of only about 4 percent.

The budget of latent heat transfer for the strong wind class is depicted as Fig. 16. No budget was calculated for light winds because of the previously mentioned measurement errors. The rate of evaporation is seen to decrease downwind. The air-water latent heat flux is almost twice as large at the sensible heat flux but, of course, in the opposite direction. The mean rate of evaporation for the section represents the loss of a 0.17 cm layer of water per day. Let us again consider the representativeness of measurements made about 3 km downwind. They would result in a 13 percent underestimation of evaporation. Measurements made 0.5 km downwind and at the center of the section would yield overestimates of evaporation amounting to 16 percent and 2 percent respectively.

This study clearly points out the need for exercising care in choosing representative recording points over a given site. If it is necessary to limit profile measurements to a single point it appears that the best position is lightly downwind of the center of the site.

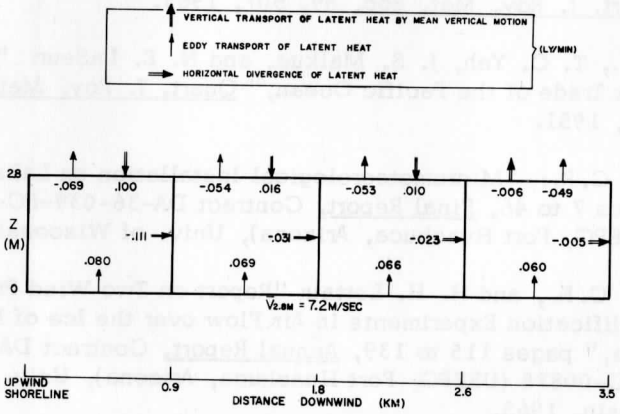

Fig. 16 Local latent heat budget constituents for four air volumes along the 3.5 km trajectory for the strong wind class.

1.4 References

Bunker, A. F.: "Transport of Water Vapor by Eddy Diffusion in Continental Air Masses flowing over Coastal Waters, Sept. 23, 1947 - Nov. 16, 1948," Woods Hole Ocean. Institution Contract N6onr-277, Task Order 2, Tech. Report #2, March 1949.

Burbidge, F. E.: "The Modification of Continental Polar Air over Hudson Bay," Quart. J. Roy. Met. Soc. 77, 365, 1951.

Church, D. E.: "Steam Fog over Lake Michigan in Winter," Trans. Amer. Geophys. Union, 26, 353, 1945.

Craddock, Y. M.: "Warming of Arctic Air Masses over the Eastern North Atlantic," Quart. J. Roy. Met. Soc. 77, 355, 1951.

Kutzbach, J. E.: "Investigations of the Modification of Wind Profiles by Artificially Controlled Surface Roughness," pages 71 to 114 of Annual Report, Contract DA-36-039-SC-80282 (USEPG, Fort Huachuca, Arizona) Univ. of Wisconsin, 1961.

Lettau, H. H.: "Research Problems in Micrometeorology," Final Report, Contract DA-36-039-SC-80063 (USEPG, Fort Huachuca, Arizona) Univ. of Wisconsin, 1959.

Lettau, H. H.: Personal Correspondence, 1964.

Rider, N. E., J. R. Philip, and E. F. Bradley: "The Horizontal Transport of Heat and Moisture — a Micrometeorological Study," Quart. J. Roy. Met. Soc. 89, 507, 1963.

Riehl, H., T. C. Yeh, J. S. Malkus, and N. E. LaSeur: "The North-East Trade of the Pacific Ocean," Quart. J. Roy. Met. Soc. 77, 598, 1951.

Stearns, C. R.: "Micrometeorological Installation on Lake Mendota," pages 7 to 46, Final Report, Contract DA-36-039-SC-80282 (USEPG, Fort Huachuca, Arizona), Univ. of Wisconsin, 1962.

Stearns, C. F., and H. H. Lettau: "Report on Two Wind Profile Modification Experiments in Air Flow over the Ice of Lake Mendota," pages 115 to 139, Annual Report, Contract DA-36-039-AMC-00878 (USEPG, Fort Huachuca, Arizona), Univ. of Wisconsin, 1963.

Taylor, G. I.: "Eddy Motion in the Atmosphere," Phil. Trans. Roy. Soc. 215, 1, 1915 (reprinted in The Scientific Papers of Sir Geoffrey Ingram Taylor, Vol. II, Cambridge Univ. Press, 1960.)

U. S. Geological Survey, Water-Loss Investigations — Lake Hefner Studies, technical report: U. S. Geol. Survey Prof. Paper 269, 1954.

U. S. Geological Survey, Water-Loss Investigations — Lake Mead Studies, U. S. Geol. Survey Prof. Paper 298, 1958.

Webb, E. K.: "An Investigation of the Evaporation from Lake Eucumbene," Division of Met. Physics Tech. Paper #10, (CSIRO, Melbourne, Australia), 1960.

Wexler, H.: "Cooling in the Lower Atmosphere and the Structure of Polar Continental Air," Mon. Weather Rev. 64, 122, 1936.

Scanner's note:

This page is blank.

2

A Thermal Response Experiment on Lake Ice*

John Colin Turner

Department of Meteorology
University of Wisconsin

Abstract: A preliminary experiment was carried out to examine the thermal response of lake ice to a square-wave radiation forcing function, induced by alternate shading and unshading of the surface by a mobile screen, with a range of periods from 4 to 40 minutes. The results indicated a general agreement with theoretical predictions but were inconclusive because of measurement deficiencies. Suggestions for future studies are made, including possible modifications of surface roughness and albedo, and the harmonic analysis of results to separate out the first harmonics.

2.1. Introduction

2.1.1 Definition of thermal response

Thermal response experiments in micrometeorology have been defined by Lettau (1959) as empirical determinations of the ratio of the amplitude of surface temperature (ΔT_0) to the amplitude of a radiation forcing function which is assumed to be a harmonic time function. Earlier, Lettau (1951, 1952) put forward a two-layer theory the aim of which was to predict the proportioning of incoming radiant energy at the interface into sensible heating of the air (A_0) and heat flow into the underlying medium (B_0), and the phase relationships of the partitioned energy. Thermal response,

*Part of this work was submitted to the University of Wisconsin in partial fulfillment of the requirements for the degree of Master of Science.

as defined above, was also predicted. Apart from the influence of the intrinsic thermal properties of the media, conveniently expressed for each by the quantity termed "thermal admittance" $((\lambda c)^{\frac{1}{2}}$, cal/cm^2 deg C min$^{\frac{1}{2}}$, where λ is the thermal conductivity and c the volumetric heat capacity) by Lettau and "conductive capacity" by Priestley (1959, a), allowance was made for the action of three independent variables: surface roughness parameter (z_0), friction velocity (w*) and period of the forcing function. Some of the assumptions of the theory were:

(1) evaporation independent of time —
(2) eddy diffusivity a linear function of z near the surface; and wind speed and temperature measurements to be made within this layer —
(3) underlying medium homogeneous with respect to thermal admittance —
(4) at the interface, the net radiation (R_n) is a given harmonic function of time.

Priestley (1959, b) has pointed out that the theory predicts only the amplitudes of A_0, B_0, and T_0 during a cycle of the forcing function, and not the absolute amounts involved throughout the course of the cycle.

2.1.2 Experimental approaches to testing the theory

Lettau (1959) described a method by which the working of his theory and its predictions about thermal response could be examined experimentally. The principle was to induce ranges of the three independent variables, z_0, w* and period, by deliberate modification, selection and control. The possibility of the experimental control of period of the forcing function in the field by a sun-screen technique was as then untried. Since 1959, two workers at the University of Wisconsin, Lienesch (1961) and Federer (1962) have carried out semi-controlled experiments along the lines suggested by Lettau.

Lienesch, working on a soil surface closely covered with short grass, found that such a surface presented uncontrollable variables (evaporation rate, soil moisture content and surface roughness) which tended to confound results. Federer then used a smooth concrete surface (which was artificially roughened at will by the distribution of pebbles on the surface) to eliminate these variables. He obtained results which in most respects

substantiated the theory. After his work there was a continuing need to improve measurement techniques in and above the concrete, and to extend the ranges of variables and the types of surfaces over which the theory was tested.

2.1.3 Aim

The aim therefore, of the present work, was to extend the empirical testing of Lettau's model to another surface type: winter ice on Lake Mendota. Lake ice as an underlying medium in thermal response experiments, has some of the advantages of the concrete used by Federer; the surface is satisfactorily smooth and flat, the medium approaches three-dimensional homogeneity in physical properties, large up-wind fetches can be chosen, and evaporation, at least when surface temperatures are well below freezing point, can reasonably be neglected (Scott and Ragotzkie, 1961).

Ice differs from concrete however, in two major ways for thermal response applications: (1) it has a wave-length-dependent transmissivity to the short wave forcing function, i.e., incoming radiation is absorbed in depth rather than at the interface; and (2) the water underlying the ice represents a near-isothermal fluid heat source of high thermal admittance.

These two properties conflict with one of the assumptions of Lettau's theory: that all radiation transformations occur at the interface and that there are no energy sources or sinks in the atmosphere or underlying medium for $z \neq 0$. It was with the background of these potential complications that the measuring equipment was assembled and shading trials carried out.

2.2. Experimental Details

2.2.1 Site

The measurements were made at the winter instrument installation of the Department of Meteorology on Lake Mendota, about 450 m north of the instrument shelter near Second Point. A description of the site and general instrumentation is given by Stearns (1962). The equipment for the shading experiment was placed about 15 m west of the general electrical junction and control center (see Fig. 1), giving undisturbed fetches in excess of 2000 m to both the west and north.

2.2.2 Equipment for measurements in ice

A modified version of the ice "conduction" instrument described by Scott and Ragotzkie (1961) was constructed. Horizontal pairs of arms of plexiglass tubing (1/4" outside and 1/8" inside diameter) carried leads (which were kept as fine as possible to minimize heat conduction) from sensors mounted on their ends. The sensor-carrying arms were attached at 5 cm depth intervals between 5 and 35 cm to two vertical plexiglass tubes (3/4" outside and 1/2" inside diameter), which carried leads vertically and acted as the primary structural basis of the instrument (see Fig. 2). One of the vertical 3/4" tubes was made 2 m long in order to maintain thermopile reference junctions in the lake water, which had a very stable temperature. The other was made only 45 cm long. The two tubes were joined by cross pieces, and a horizontal 3/4" O.D. tube of plexiglass attached to the bottom crosspiece extended out for 47 cm, supporting from below by slender plexiglass braces, the sensor array. An essential minimum of plexiglass supports and spacers was also included between the sensor arms themselves. The instrument was designed to be installed so that the sensor-carrying arms faced south. The arms were made increasingly longer the lower they were (29 to 66 cm) to minimize possible shading and other interference effects.

An upper mobile sensor-carrier was included on the instrument, attached above the 5 cm arms by a flexible polyethylene tube. It was designed to be placed at or just below the ice surface. Nominal zero depth was taken to be at the top of the two 3/4" vertical tubes. When the two tube ends were finally sealed by a single strip of 1/4" plexiglass sheet, a levelling bubble placed on the sheet was used to level the whole instrument before it was frozen in; the sensors having been aligned relative to this surface when they were attached to the arms.

The following sensors were included on the instrument:

(1) 2-junction copper-constantan thermopiles at 0, 5, 15, 25 and 35 cm, reference junctions being at 2 m depth in lake water. These thermopiles were meant to measure absolute temperature in conjunction with an independent temperature measurement at 2 m.
(2) 4-junction thermopiles to measure temperature differences over the intervals 0-5, 5-15, 15-25, 25-35 cm.
(3) 100-junction heat flux plates at 10, 20 and 30 cm.
(4) Solar cells at 10, 20 and 30 cm; one at each depth facing upwards and one facing downwards.

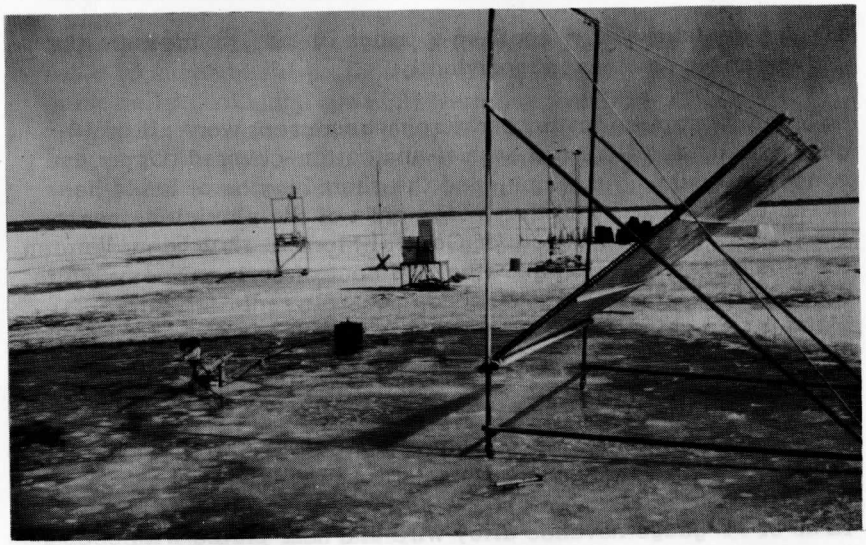

Fig. 1. Experimental site, Feb. 24, 1963, facing east. Net radiometer, Eppley pyrheliometer (on black box) and sun-screen in foreground, control box in center background.

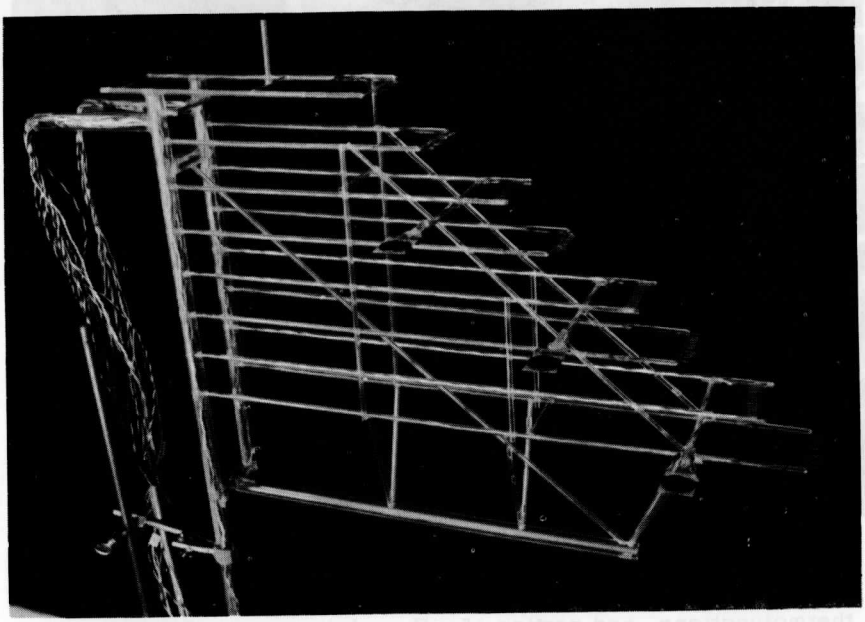

Fig. 2. General view of instrument for ice-gradient measurements

(5) A thermistor at 2 m depth in a bridge circuit, to measure the water temperature independently.

The termopiles for temperature measurement were all of 30-gauge Leeds and Northrup enamel and cotton-covered copper and constantan wire. Junctions, and the short lengths of leads between the junctions and the sealed ends of the plexiglass sensor arms, were given two coats of General Electric 1202 Clear Varnish for electrical insulation and finally a coat of Krylon Glossy White Spray Enamel, No. 1501, to reduce possible radiation errors. About 1 cm behind the thermojunctions, the leads were cemented with an epoxy resin to cross pieces of solid transparent polystyrene (8 cm long, 1/8" × 1/16" across) at each of the temperature-sensing levels (see Fig. 3). The leads were evenly spaced along the cross pieces so that some degree of horizontal integration of measurement was attained. The flux plates were 3" × 1" × 1 mm glass microscope slides, lathewound with 100 turns of 34-gauge Advance alloy wire and half-plated with copper

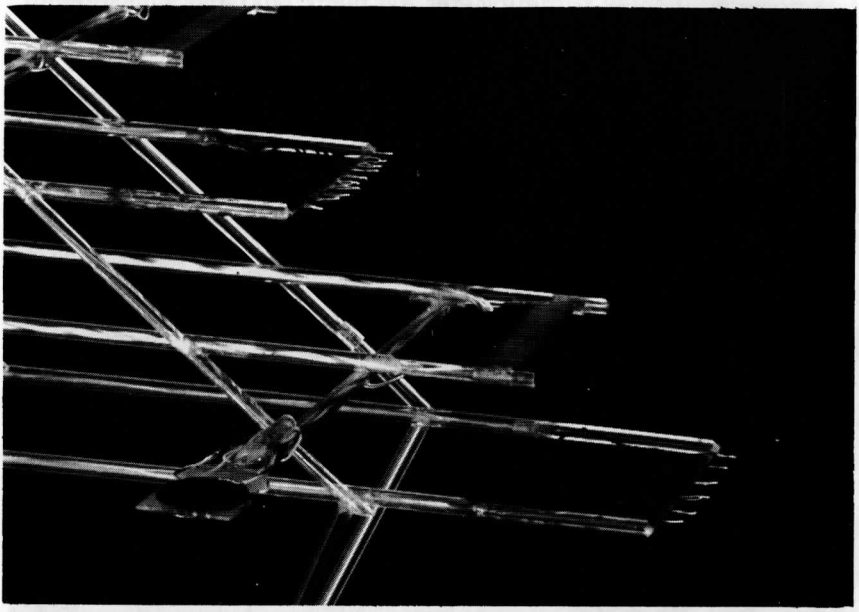

Fig. 3 Details of sensor arrangement. From bottom to top: thermojunctions, solar cell and flux plate at the same level, thermojunctions, and portion of a flux plate at top. 5 cm vertical distance between successive sensors.

by an alkaline process. The plates were then coated with epoxy resin for mechanical protection and electrical insulation. The solar cells (Hoffman, type S2) were supported by side-arms (12 cm long) of plexiglass tube, away from the bulk of the instrument assembly. The up- and down-facing solar cells at each level were cemented to a single piece of 1/16" sheet polystyrene (Fig. 3). No attempt was made to insulate electrically the solar cell surfaces from the surrounding liquid water or ice.

All plexiglass-to-plexiglass and polystyrene-to-plexiglass junctions were joined and sealed with a cement made by dissolving plexiglass scraps in ethylene dichloride. Epoxy was used to seal tube ends wherever leads emerged. Experience showed however, that epoxy was liable to effect only weak adhesion with smooth plastics surfaces, so a precautionary coat of Pliobond 20 adhesive (which also has good electrical insulation properties) was finally applied over all epoxy surfaces, including the heat flux plates.

None of the plexiglass tubes was filled with epoxy after the leads had been installed, in contrast to the procedure followed by Scott and Ragotzkie (1961). For the present work it was reasoned that the numbers or arrangement of leads might need to be changed in future uses — an impossible task after sealing with epoxy. The horizontal sensor-carrying arms were so long that it is considered that possible heat transfer from the water below, up the vertical tubes and then horizontally to the sensors was negligible.

The thermojunctions and the thermistor at the 2 m depth were placed in a 5/8" diameter aluminum alloy bulb, sealed to the bottom end of the long plexiglass tube. The thermistor was soon found to give unreliable signals and readings from it were discontinued. Instead, on each day of shading trials, and on several other occasions, a Whitney Underwater Electric Thermometer was lowered to 2 m depth through a nearby hole in the ice and a spot reading taken. It was assumed (Scott, personal communication) that diurnal amplitudes of temperature at 2 m in late February, would be negligible or certainly less than 0.1°C.

2.2.3 Installation of the ice-profile instrument, and ice-surface management

Installation was done on 26 January 1963, during a calm and cloudless day of temperature about -15°C. This was an ideal weather situation for rapid and effective freeze-in. Wind is undesirable because it may blow surrounding snow onto the semi-frozen water surface about the instrument and produce a roughened and non-uniform surface. A 4' × 3' hole was cut in the snow-cleared ice, which was about 25 cm thick. The cut-out block of ice was pushed about 2 m away under the main ice-sheet. All chips of ice resulting from the cutting were ladled from the water and carried away, to eliminate the chance of possible damage to the instrument when it was lowered in, and to achieve greater uniformity of composition of the final ice about the instrument.

Initial support of the instrument was by several strings radiating from it and tied to bricks on the surrounding ice. A brick had also to be tied to the bottom of the 2 m tube to get the instrument to sink in the water. Levelling of course, had to be completed at this time. In addition, an open-sided 2.5' × 3' × 3' rectangular prism made from a medium gauge fencing wire was lowered into the hole about the sensing instrument so that its uppermost side was about 1 cm below water level, and supported with strings in the same way. This served as an electrical shield for the solar cells which — experience the previous winter had shown — produced large noise signals unless shielded. After it was frozen in, the shield was connected to ground at the control center.

Because of the favourable weather, freezing-in was very rapid. It was estimated by visual inspection that there was 5 cm of ice in the hole after two days. The photograph in Fig. 4 was taken on January 28. A day or two later, the strings were cut where they emerged from the ice and an additional 1/2" of water was added to the hole to bring the new ice surface up to the level of the surrounding original ice. Numerous ice-pick chippings and water spreadings were carried out in the immediate area during the following month, with the aim of producing a smooth surface. The nominally zero level temperature sensor, clearly visible in Fig. 4, was gently removed from the existing ice and raised in level as more water was added to the surface, so that finally it was close below the surface. On the occasions of the three experimental runs reported here, it was 0.3 cm below the ice surface (Fig. 5). It should be noted also that the

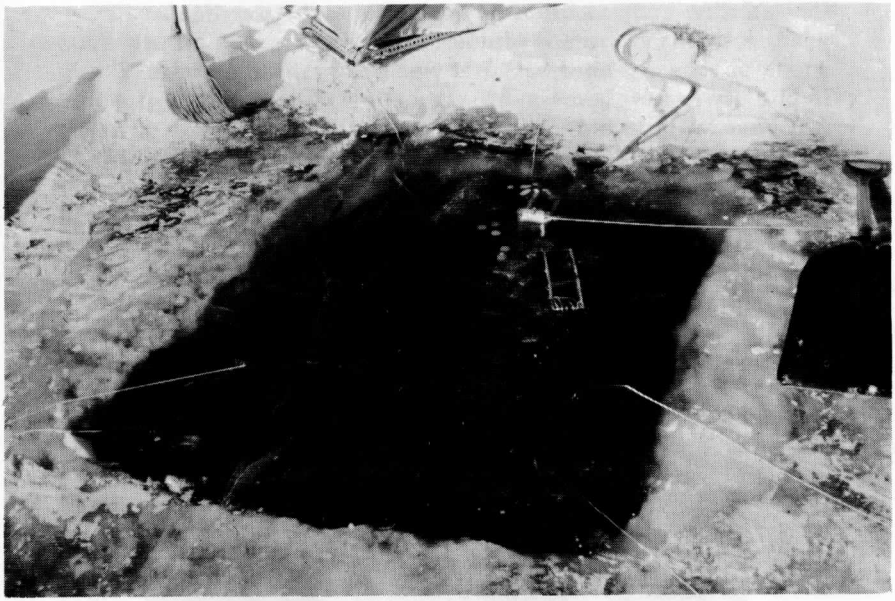

Fig. 4. 28 January 1963. Ice-gradient instrument two days after installation in the ice.

actual depths of the other sensors were not the same as the nominal depths. Actual depths were all less than the corresponding nominal depths by 1 cm; i.e., 4, 14, 24 and 34 cm. Henceforth, all depths quoted which refer to sensor placement and which are multiples of five, should be considered to be nominal, and really refer to the corresponding actual depths.

Snow was removed by shovelling and sweeping from the immediate area of the experiment (an approximately circular area of 5 m radius) whenever it fell, and dragged 50 m or more to the east. A hand-made and jeep-drawn snow-plough was then used to smooth out the height inequality at the periphery of the cleared area. The considerable labour involved in the snow removal was considered worthwhile in order to maintain an exposed ice surface for experimentation. Ice had the advantage of being unaffected by the inevitable maintenance traffic and in addition, instrumentation had not been provided for measurements within a snow cover, with its complexities

of a continually shifting surface and vague gradation into the ice beneath.

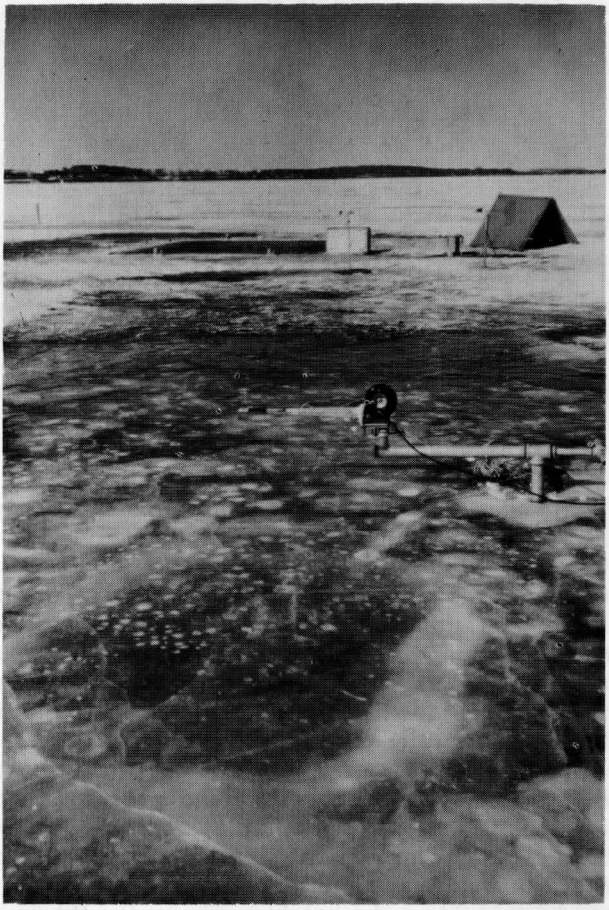

Fig. 5. Experimental site, 24 February 1963, facing north. 0.3 cm temperature sensor visible in ice in immediate foreground. Net radiometer on its stand in center of picture.

2.2.4 Ice depth measurement

Ice depth was determined by periodic borings with an ice-auger in the south-western and south-eastern corners of the 4' × 3' area containing the new ice. Borings were made about 30 cm from the nearest sensors. The method was crude and at times misleading results were obtained. Mention is made later (Section 2.3.5) of an occasion when a boring suggested that all the sensors were in ice, whereas the temperature records strongly suggested that the 35 cm sensors were in liquid water.

It seems likely that ice growth was most rapid at the sides of the hole. To obviate this uncertainty in the future, an electrical resistance method (Houle, 1961) will be tried which promises to enable depth readings to be made close to the sensors without undue distortion of the natural conditions. Apart from knowing whether particular sensors are in ice or not, accurate knowledge of the rate of ice accretion is useful information because it enables an independent and in situ calibration to be made of heat flux plates.

2.2.5 Radiation measurements above the ice

A 10-junction Eppley pyrheliometer and a Suomi-type ventilated net radiometer were used to measure total incident short-wave radiation and total net radiation respectively. The radiometer was mounted 18" above the surface, on the same stand as used by Federer (Figs. 1 and 5). The pyrheliometer was placed on the ice surface nearby, during shading trials. For the first trial the Eppley was not available, and a solar cell, mounted directly on the end of the net radiometer sensor, was used instead. Both the Eppley and the radiometer were disposed within the shaded area during runs in such a way as seemed to cause a minimum of mutual interference. They were, of course, always to the north of the ice-sensors.

2.2.6 Wind and temperature profiles in the atmosphere

Unfortunately, because of personnel shortages and equipment failures at the time, it was possible to run wind profiles during only one of the shading trials. Thornthwaite equipment, as described by Stearns (1962) was used on that occasion; anamometers being mounted 20, 40, 80 and 160 cm above the surface, and successive 15-minute runs being made. Nor was

it possible to obtain atmospheric temperature data for the same reasons. A special instrument had been made to sweep fine-wire (0.001" diameter) thermocouples horizontally backwards and forwards through an arc of about 1 m — temperatures and temperature differences being obtained at nominal heights of 1, 2, 3, and 4 cm above the surface. This instrument was designed to overcome some of the difficulties and errors in aerial temperature measurements encountered by both Lienesch and Federer: radiation errors due to bulk of the sensors, thermometers insufficiently close to the surface to escape advection errors during shading cycles, possible calibration changes in thermistors, forced ventilation disturbing the profiles to be measured, and the potentially disturbing presence of a person manually operating a horizontal sweep.

Trial use of the instrument was made during the second part of the second shading run, but there were uncertainties in the amplifiers to which the thermocouple outputs were attached, and the data have not been examined. Mechanically and structurally however, the sweep seems satisfactory (it was also used successfully on the concrete slab at Arlington — where Federer carried out his experiments — in the autumn of 1962), and it is planned to use it in the future over both concrete and ice.

2.2.7 Mobile sun-shield

The same radiation screen as used by Federer was used in the present study. It is shown in the "unshaded" position in Fig. 1. The screen itself is eight feet square. Some trouble was encountered in keeping the frame stationary on the smooth ice during windy conditions, and small holes were chipped in the ice as necessary, to anchor the castors. In general, the shield worked satisfactorily on ice, although even in late February, when the noon altitude of the sun at Madison's latitude is only about 38°, one wished for a larger shaded area to enclose more effectively the sensing devices.

2.2.8 Data recording

Signals from the sensors in the ice, and the two radiation-measuring instruments above the surface, were led to the switch-amplifier-digital volt meter-card punch system described by Stearns (1962). Outputs from the pyreheliometer and radiometer

had first to be reduced by suitable resistors to be comparable to the other signals. The amplifier-digital voltmeter system was adjusted so that 1000 volt-meter units were equivalent to 1.900 mv, or 50°C for 1 junction of copper-constantan with a near-0°C temperature coefficient of 0.038 mv/°C. In essence then, all the data which it was found possible to obtain during the shading trials were available minute by minute on single cards. For subsequent analysis of the data, the initial digitalisation was found to be invaluable. A 1620 IBM computer, jointly operated by the Departments of Astronomy and Meteorology and the U. S. Weather Bureau, was used for the analysis.

2.2.9 Calibrations

The Eppley pyrheliometer and the aerial solar cell were calibrated against another Eppley known to have a reliable calibration constant, on July 2, 1963. At the same time, the net radiometer was calibrated against the Eppleys by the standard shading and unshading technique. Its symmetry of ventilation was also checked and found to be satisfactory. It was not possible to compare or calibrate the below-surface solar cells before they were installed in the ice. After removal from the ice in the spring, both solar cells at 10 cm were found to be too seriously cracked to be worth calibrating. Another of the sensors at 30 cm was also slightly cracked. All four of the lowest solar cells were compared in air against Eppleys on July 2 1963. The calibrations obtained however, could not in any way be sensibly related to the readings obtained within the ice. Thus the solar cells were unsatisfactory in ice, as far as they were tested. However, they need more thorough and rigorous testing and the subject of possible future testing is taken up later. The heat flux plates were calibrated in the sand-bath equipment described by Federer (1962, p. 25). The copper-constantan thermopiles were from spools which, in the light of general Department of Meteorology experience, were known to have the standard thermoelectric output° namely 0.038 mv/°C at 0°C.

2.3. Results

2.3.1 Description of times of data collection

Shading trials were carried out on three occasions, on each of which the weather was almost ideal for experimentation. Desirable weather criteria were:

(1) cloudless skies, particularly around noon, which is the best time for experimentation from the point of view of a near-constant forcing function; (2) below-freezing temperatures at the surface; (3) wind from the west (in order to be more or less parallel to the sun-screen), and no so strong as to cause blowing of loose snow.

Such conditions usually occur on at least one day during the passage of each winter high pressure system across the southern Wisconsin region.

In addition, data were collected automatically on cards, from the unshaded site, for most of the remainder of the period from the night of 22-23 February to noon of 2 March 1963. Most of this information was obtained at 15-minute intervals, as compared with the 1-minute sampling during the three shading trials. Data at 5-minute intervals were gathered during the night of 25-26 February prior to Run 2. The night was near-calm, cloudless and cold, and because of these favourable conditions, some aspects of the information obtained have been examined for this thesis. In Table 1 the meteorological and limnological conditions of the three shading trials and the nocturnal run are summarized.

Table 1. General Conditions During the Analysed Runs

	Run 1	Run 2	Run 3	Nocturnal Run
Date (1963)	24 Feb.	26 Feb.	1 Mar.	25-26 Feb.
Time (CST)	11:28 - 13:30	11:19 - 14:28	11:44- 13:58	17:45 - 06:56
Wind direction	NW to WSW	W to WSW	W to SW	-----
Ice thickness 30 cm from sensors (cm)	44	46	47	(45 ?)
Water temp. at 2 m (°C)	0.5	0.6	0.8	(0.6 ?)
Range of temps. at 0.3 cm in ice during the run (°C)	-4.3 to -1.9	-10.7 to - 8.1	-4.0 to -2.9	-11.1 to -16.6

Notes and Comments:

Run 1 Wind about 10 mph. Ice surface mottled and translucent in appearance due to water-spreading 22 February (see Figs. 1 and 5 taken at the end of this run).

Run 2 Wind estimated at 6-8 mph. Ice surface similar in appearance to that in Run 1. The period 12:13 to 13:12 lost owing to switching failure.

Run 3 Wind light, estimated at about 5 mph. Ice surface covered with 2" of snow, settled from an original fall of 3" on 27 February.

Noctural Run—Near-calm conditions. Ice surface as for Runs 1 and 2. Sunset about 17:40, sunrise about 0.6:40 hrs.

The sequence and lengths of shaded and unshaded periods were in general the same as those employed by both Lienesch and Federer. Occasional mishaps occurred, unavoidably changing the lengths of some of the half-periods. The chronology of the runs is described in Table 2.

Table 2. Sequence of Half-periods (minutes) in Shading Trials

U: unshaded S: shaded	U	S	U	S	U	S	U	S	U	S	U	S	U	S	U
Run 1		5	5	10	10	20	20*	23	11		9	5	5		
Run 2	2	2	5	5	10	10	20	20	20	10	10	5	7	2	2
Run 3	2	2	5	5	10	10	20	20	20	10	10	5	5	2	2

(*For about 5 minutes of this 20-minute interval, the experimental area was unshaded because the screen temporarily could not be restrained from sailing away during an unusually strong gust of wind.)

There was occasionally greater electrical noise than usual in the signals (the minimum noise level attainable with the entire system is about $\pm$ 1 scale division of the divital voltmeter, which is approximately equivalent to an input of $\pm$ 1 v). Noise was

especially prominent during Run 3 and least apparent during the nocturnal run. The latter fact suggests that the noise level is at least partially temperature dependent. Expert help was not available during the period of experimentation to attempt to reduce the noise level.

2.3.2 Radiation measurements

Information about values of solar radiation (Rs) and net radiation (Rn) measured during the runs is given in Table 3.

Table 3. Net and Solar Radiation During Runs (ly/min)

U: unshaded S: shaded			Run 1	Run 2	Run 3	Nocturnal Run
Mean values first period	R_s	U	1.131	1.110	1.174	
		S	0.093	0.163	0.247	
	R_n	U	0.561	0.554	0.097	-0.146
		S	-0.062	-0.049	-0.101	
Highest mean value in any period	R_s	U	1.148	1.148	1.177	
		S	0.093	0.173	0.247	
	R_n	U	0.593	0.556	0.104	-0.146
		S	-0.066	-0.082	-0.131	
Mean values final period	R_s	U	1.032	0.871	0.941	
		S	0.091	0.164	0.206	
	R_n	U	0.486	0.368	0.045	-0.110
		S	-0.066	-0.081	-0.131	

Both Lienesch and Federer used a relationship from which the albedo of the experimental surface can be estimated, knowing the differences in R_s and R_n values within individual periods (i.e., between the unshaded and shaded half-periods). The expression is:

$$r = 1 - (\Delta R_n)/(\Delta R_s) \quad (1)$$

An assumption made in the derivation is that the long-wave radiation balance remains unchanged throughout individual periods, i.e., in effect, that the surface temperature remains constant. Calculation shows that for a surface temperature decrease of 2°C, from -3°C to -5°C, during shading (a reasonable value for the 20-minute interval on ice) the emission of the surface (assuming black-body) would be reduced by about 3 percent. Consideration of the terms of the surface energy budget during a shaded interval reveals that the net out-going long-wave radiation is given by the sum of the magnitudes of the sky radiation (short-wave diffuse) and the recorded net radiation at that time. Reference to the results from Run 1 in Table 3 for instance, shows that the Rn_{long} value was about 0.15 ly/min. Assuming this figure as an initial value, the Rn_{long} would drop therefore by about 0.0045 ly/min during a 20-minute shaded interval. For ΔRn values of approximately 0.6 ly/min, the change due to shading is thus less than 1 percent, well below the $\pm$ 5 percent error levels of the above-surface radiation sensors.

The results of albedo and sky radiation calculations for the three runs are summarized in Table 4. ΔR_s and ΔR_n values were calculated from the mean values of successive half-periods.

Table 4

Albedo, and Sky Radiation Fraction During Shading Trials

Run		1/2-period intervals in sequence (min)								Mean
		2	5	10	20	20	10	5	2	
1	albedo	----	0.40	0.40	0.38	0.37	0.40	0.41	----	0.39
	sky	----	0.08	0.08	0.08	0.08	0.08	0.09	----	0.08
2	albedo	0.36	0.34	0.38	----	0.35	0.38	0.39	0.36	0.37
	sky	0.15	0.15	0.15	----	0.16	0.17	0.18	0.19	0.16
3	albedo	0.78	0.76	0.76	0.76	0.77	0.76	0.76	0.76	0.76
	sky	0.21	0.20	0.21	0.20	0.21	0.21	0.24	0.22	0.21

The albedo values for the snow and ice surfaces are in general agreement with values quoted in the literature (e.g., Scott

and Ragotzkie, 1961; Smithsonian Meteorological Tables, 1951), but the range of possible values is so great that no detailed comparisons can be made. We would expect that values for Runs 1 and 2 would be similar, and they do, in fact, show fairly close agreement.

The sky radiation fraction is defined by the ratio of diffuse short wave radiation scattered from the sky to total short wave radiation (diffuse and beam), both incident on a horizontal surface. In Table 4 we see that the fraction showed marked changes from run to run, and also evidence of temporal change within each run. It is not immediately clear whether these figures reflect actual physical changes, or perhaps some measurement error. Supplementary data in the form of sky and visibility conditions at Truax Field, about 10 km northeast of the experimental site, together with air mass information are given in Table 5.

Table 5
Sky, Visibility and Air Mass Conditions During Shading Runs

	Run 1	Run 2	Run 3
Visibility throughout hours of run (miles)	15	15	10 to 15
Cloud ceiling	unlimited	unlimited	unlimited
Cloud cover (tenths)	0	0	0
Air mass origin (cA : continental arctic)	cA	cA	cA

From these data there is no evidence to provide a physical explanation for the large changes in the proportion of sky radiation from run to run. Accordingly, we must suspect a measurement error. Experience suggests that the lowest value of sky radiation fraction obtained in any of the runs (0.08 in Run 1, using a solar cell mounted on the net radiometer) was the most reasonable; especially having regard to the generally high visibility within winter high pressure systems. Hence we must suspect, in particular, a defect in the characteristics of the Eppley which was used or — as seems more likely — an error in its placement. The amounts of radiation involved in the error are small relative to the ΔRs and ΔRn values, so the resulting error in albedo is probably quite small.

2.3.3 Estimates of the penetration and absorption of solar radiation in ice

As was noted in Section 1.4, attention must be paid to the absorption of radiation in depth, by the ice. Because no quantitative data were obtained from the solar cells, we must assume a value for the absorption coefficient of ice and a knowledge of the spectral composition of the penetrating radiation. Scott and Ragotzkie (1961) adopted an absorption coefficient of 0.0115 cm^{-1} for ice intermediate in transmissivity between "bubbly" and clear. This figure referred only to wavelengths less than 0.7μ, it being assumed that all radiation of longer wavelength was absorbed at the surface. Reference to the Smithsonian Meteorological Tables (1951) reveals that about 48 percent of the total solar radiation reaching the surface on a cloudless day, at the end of February, at Madison's latitude is of wavelength less than 0.7μ. Then, if Rs_0 is the short-wave radiation penetrating downwards through the surface, its value is given by the expression:

$$Rs_0 = 0.48\ Rs\ (1 - r) \qquad (2)$$

With the additional assumptions that the ice is homogeneous in optical properties with depth and perfectly diffuse, we may apply the Bouguer-Lamberg law, giving the radiation Rs_z passing downwards at any depth z:

$$Rs_z = Rs_0 e^{-Kz} \qquad (3)$$

where K is the absorption coefficient. Calculations using this equation were carried out for Run 2, and the results are summarized in Table 6.

These calculations provide reasonable order-of-magnitude estimates, which clearly are also applicable to Run 1. No attempt has beenmade to derive similar estimates for the more complex situation during Run 3, but obviously the heating rate due to absorption in depth in the ice layer would be very much less because of the higher albedo of the snow surface. The figures in Table 6 suggest that during a 20-minute unshaded interval, the mean temperature of the top 10 cm layer woulr rise by about 0.15°C due to radiation absorption alone. Examination of actual temperature results from Run 2 show a mean rise of about 0.8°C in 20 minutes for the same layer.

Table 6
Estimates of the Absorption of Solar Radiation in Ice During Run 2

	Radiation (ly/min)	Percent of Rs_0	Mean temp. rise due to absorption (°C/min)*
Mean Rs_0 for unshaded intervals	0.311		
Absorbed in layer 0-10cm	0.034	10.9	0.0074
" " " 10-20cm	0.030	9.7	0.0065
" " " 20-30cm	0.027	8.6	0.0059
" " " 30-40cm	0.024	7.7	0.0052
Total, layer 0-40cm	0.115	36.9	0.0063

(*volumetric heat capacity of ice was taken as 0.460 cal/cm^3 degC)

It is of interest to mention an aspect of the qualitative information obtained from the solar cells in the ice. All the downward facing cells gave small signals during Runs 1 and 2, and at 10 and 20cm depth, the sequence of shading and unshading was clearly apparent, with a fall of about 80 percent in output during shading. Preliminary indications are, therefore, that there is an upward component of short wave radiation in lake ice, at least in the top 30cm.

2.3.3 Estimates of the thermal conductivity of ice

For attempts to determine heat flux at the ice surface during shading trials, an estimate of the thermal conductivity of ice was required. The following two methods were used:

(1) The temperature gradient across a flux plate was compared with the corresponding vertical temperature gradient in the surrounding ice for the nocturnal run. Then, assuming a value for the thermal conductivity of glass, the thermal conductivity of ice, λ_{ice}, is given by the expression:

$$\lambda_{ice} = \lambda_{glass} \cdot (\Delta T/\Delta z)_{flux\text{-}plate} / (\Delta T/\Delta z)_{ice} \qquad (4)$$

The temperature gradient data are plotted in Fig. 6. Data from the shaded intervals of the first two shading runs are also included. There is more scatter in these points, one reason probably being that profile equilibrium was not fully attained during the shading trials. It was found that there was a very marked radiation error in the flux plates during the unshaded intervals. In addition, results from the 10cm plate were not consistent at any time with those from the two lower plates, nor with the temperature gradient in the 4 to 14cm layer. Accordingly, data from it have not been used. It is considered that periodic melting of the ice about this plate may have been sufficient to permanently change its in situ calibration constant.

Scott and Ragotzkie (1961), using a value for λ_{glass} of 0.0020 cal/cmsecdegC, found a mean λ_{ice} value of 0.0052 cal/cm sec degC. The mean value determined from the present data, using the same λ_{glass} value together with the mean slope of the two nocturnal relationships in Fig. 6 (the mean slopes of the two relationships were found to be equal) was 0.0057 cal/cm sec degC. The slightly curved form of the relationship in Fig. 6

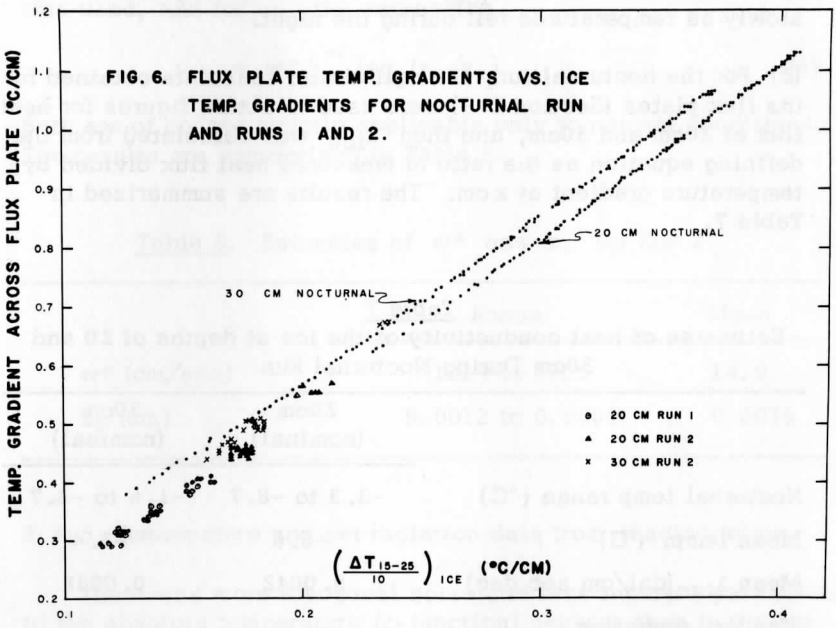

Fig. 6. Flux-plate temperature gradients versus ice temperature gradients for Runs 1 and 2 and the Nocturnal Run.

may be due to the interaction of the temperature coefficients of glass and ice during the night-long cooling process. Temperatures at 20cm decreased 5.4°C (-3.3° to -8.7°) and those at 30cm fell 3.1°C (-1.6° to -4.7°). The temperature coefficient of λ_{ice}, as given in the Smithsonian Meteorological Tables (1951) is negative and slightly non-linear, at least between 0 and -10°C. The Smithsonian Tables quote the following values of λ_{ice}:

Temp. (°C)	λ_{ice} (cal/cm sec degC)
0	0.00535
-10	0.00554
-20	0.00581

Values of λ_{glass} for various glasses, from the International Critical Tables (1927), indicate a positive and almost linear temperature coefficient near 0°C. This information is in qualitative agreement with the observed trend: at the beginning of the night (left side of the curves in Fig. 6) the slopes (and therefore the values of λ_{ice}) were relatively low, increasing slowly as temperatures fell during the night.

(2) For the nocturnal run, the calibration constants obtained for the flux plates (Section 2.9) were used to obtain figures for heat flux at 20cm and 30cm, and then λ_{ice} was calculated from the defining equation as the ratio of measured heat flux divided by temperature gradient at z cm. The results are summarized in Table 7.

Table 7

Estimates of heat conductivity of the ice at depths of 20 and 30cm During Nocturnal Run

	20cm (nominal)	30cm (nominal)
Nocturnal temp range (°C)	-3.3 to -8.7	-1.6 to -4.7
Mean temp. (°C)	-6.6	-3.4
Mean λ_{ice} (cal/cm sec deg)	0.0042	0.0038
Standard deviation (percentage of mean)	0.8	1.1

Values of λ_{ice} determined by this method, while showing reasonable agreement between levels, are about 30 percent less than the values estimated by the first method, and about 25 percent less than the value quoted in the Smithsonian Tables. A possible reason for the discrepancy might be the non-applicability of a flux-plate calibration obtained in sand to actual measurements in ice. Because it was closer to other published values of λ_{ice}, the value determined by comparison with glass 0.0057 cal/cm sec degC) was used in later calculations.

2.3.4 Wind profile parameters in Run 2

w* and z_0 were calculated from wind speeds at 20 and 160cm for 15-minute runs during Run 2. Results from the anemometers at 40 and 80cm were not used because the calibrations of these instruments were less reliable. To estimate w*, the expression

$$u_2 - u_1 = w^* k^{-1} \log_e (z_2 + z_0)/(z_1 + z_0) \qquad (5)$$

was used, and for z_0 the expression

$$u_{z1} = w^* k^{-1} \log_e (z_2/z_0) \qquad (6)$$

Both are of course strictly applicable only to neutral conditions. The results are summarized in Table 8.

Table 8. Estimates of w* and z_0 for Run 2

	Range	Mean
w* (cm/sec)	12.9 to 17.5	14.9
z_0 (cm)	0.0012 to 0.0065	0.0036

2.3.5 Temperature and net radiation data from shading trials

There was more electrical noise and less inherent sensitivity in the absolute temperature (2-junction) sensors than in the temperature difference (4-junction) sensors throughout the ice layer.

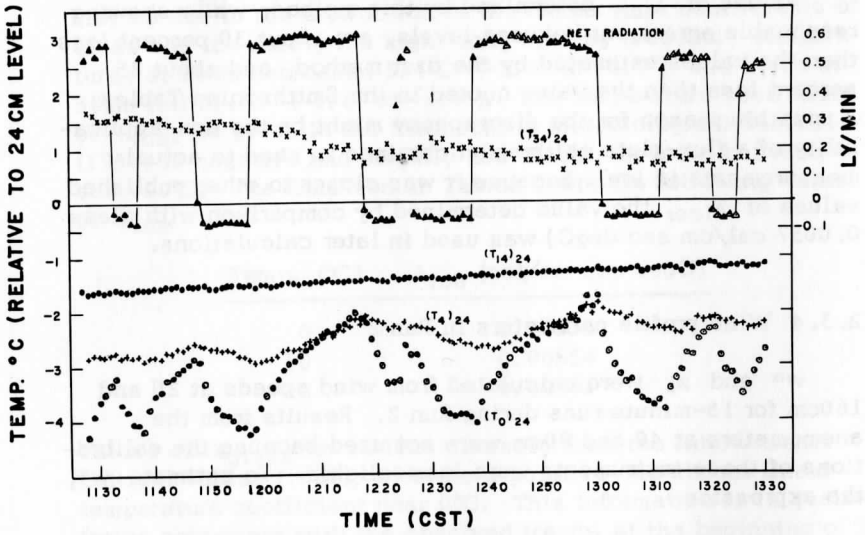

Fig. 7. Run 1, Net radiation and ice temperature data, 24 February 1963.

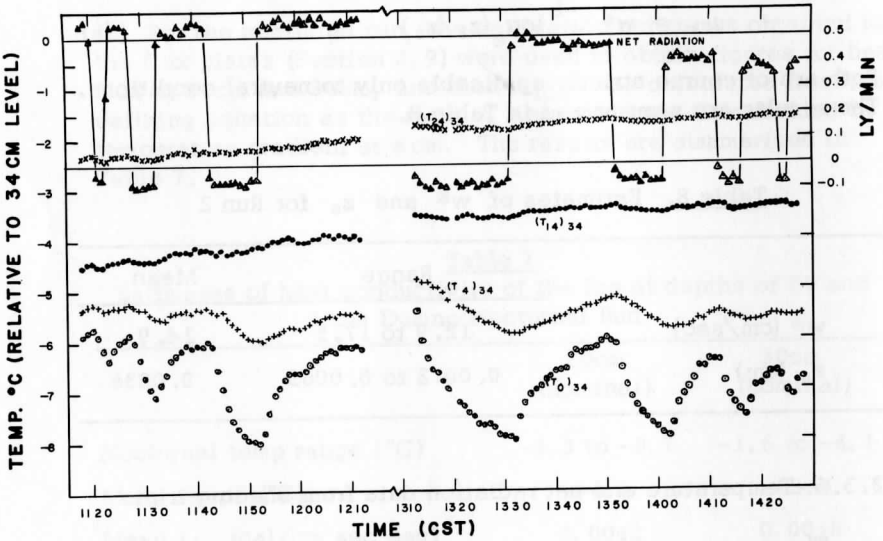

Fig. 8. Run 2, Net radiation and ice temperature data, 26 February 1963.

Accordingly, the latter were used alone in the analysis whenever possible. In Figs. 7 and 8, which are temperature and net radiation records of Runs 1 and 2, all temperatures have been referred, using temperature difference results alone, to arbitrary levels in the ice iteself rather than to the 2m level in the water. Reference to Section 2.22 will show that no provision was made for a 4-junction temperature difference sensor between 2m and 35cm when the instrument was constructed. This defect will be corrected in future modifications of the instrument.

For Run 1, the 24 cm level was chosen as the reference level because the behaviour of temperatures at 34cm suggested that there was water rather than ice at that level. In Run 2, the 34cm level seemed to be frozen, and it was used as the reference. Some graphical plotting and drawing of profiles suggested that a linear extrapolation of temperatures beyond the 4 to 0.3cm layer to the surface would produce errors never greater than 0.1°C. In Figs. 7 and 8, therefore, the captions $(T_0)_{24}$ and $(T_0)_{34}$ refer to temperatures extrapolated to the surface and referenced to 24 and 34cm respectively. This method of arbitrary referencing to lower levels in the ice was considered to be valid for examining the effects of short-period pulses (up to 40 minutes), which did not penetrate even to the 14cm level.

With the electrical noise level at the minimum of $\pm$ 1 microvolt, the temperature difference sensors could be read to about $\pm$ 0.01°C with assurance during most of Runs 1 and 2. Throughout Run 3 however, the noise level was about ten times greater than in the earlier runs. With two inches of snow above, no trace of possible heating pulses was revealed, so that any temperature amplitudes must have been less than about 0.2°C at the ice surface. Because of the lack of detectable thermal response, the results of Run 3 have not been put into diagram form.

The accidental displacement of the screen for a few minutes during the 20-minute shaded interval in Run 1 is clearly seen by its results in Fig. 7. There is no reason to suppose that radiation errors were important in the thermojunctions near the surface. For instance, the $(T_{14})_{24}$ record in Fig. 7 shows no response to shading, and according to Table 6, the radiation passing through the 15cm level is only about 15 percent less than the radiation passing through the 0.3cm level. In Fig. 8, the $(T_{14})_{34}$ record shows more variation, which however does not appear to be always related to the shaded cycles and could equally well be electrical noise.

For later calculations, the amplitudes of temperature cycles were determined by finding the difference between the temperature at the end of a shaded half-period and the temperature at the end of the corresponding unshaded half-period. Thus, two amplitudes were determined for each period during each run, except for the case of the 40-minute period in Run 2 when only one value could be obtained because of the time break in the record. Approximate corrections were applied to the several half-periods (see Table 2) which were not of standard length.

Amplitudes of net radiation were given by the magnitude of the difference between the means of equilibrium values during corresponding shaded and unshaded half-periods. In addition, using the assumptions of Section 3.3 concerning ice transmissivity, net radiation amplitudes (ΔR_n) corrected for ice transmissivity to short wave radiation were calculated. The expressions used were:

Unshaded

$$\text{Corrected } (R_n)_{\text{unshaded}} = (R_n)_{\text{observed, unshaded}} - 0.48\, R_s(1-r) \tag{7}$$

Shaded

$$\text{Corrected}(R_n)_{\text{shaded}} = (R_n)_{\text{observed, shaded}} - 0.48\, R_s(1-r)0.08 \tag{8}$$

so that the final, "corrected" ΔR_n was given by:

$$\Delta R_n = (R_n)_{\text{corrected, unshaded}} - (R_n)_{\text{corrected, shaded}} \tag{9}$$

In (8) the value 0.08 refers to the sky radiation fraction, which was assumed constant for Runs 1 and 2 in view of the possibility of some error in its determination during Run 2 (see Section 3.2).

2.3.6 Estimation of surface heat flux

From one of the basic equations for one-dimensional heat-flow in a homogeneous medium,

$$B = -\lambda\, \partial T/\partial z \tag{10}$$

we obtain, by differentiating with respect to z and then integrating through the depth affected by the heat flow, the heat flux at the surface,

$$B_0 = \lambda \int_0^z (\partial^2 T/\partial z^2)\, dz \tag{11}$$

where λ of course, is assumed to be independent of z. This expression may be put into an approximate, linearized form for the particular sensor placement in these studies as follows:

$$B_0 = \lambda[(\Delta T_{0-4})/4 - (\Delta T_{4-14})/10] \cdot (14/7)$$

$$= 0.1\lambda(5\Delta T_{0-4} - 2\Delta T_{4-14}) \qquad (12)$$

where we assume, on good evidence from Figs. 7 and 8, that the heating pulses generated at the surface did not penetrate beyond 14cm. Relation (12) is in a grossly simplified form because of the sparseness of sensing levels in the 0 to 14cm layer, and we would expect it to yield an underestimate of B_0, especially for the shorter pulses. However, using the equation, B_0 and ΔB_0, values were calculated for both runs using the previously determined value (Section 3.3) of λ_{ice}. Plotted values of B_0 formed patterns very closely resembling the form of the $(T_0)_{24}$ and $(T_0)_{34}$ results, as would be expected by the form of (12). Because of the similarity to T_0 results, estimated B_0 values have not been included in Figs. 7 and 8.

It was not considered worthwhile to use other methods to obtain other estimates of B_0. Federer found for concrete that no one method was significantly better than the other, and none gave satisfactory estimates of B_0 because his sampling system, like the one used in this study, did not provide a sufficiently intensive coverage in depth or time.

2.4. Discussion

2.4.1 $\Delta B_0/\Delta Rn$ and $\Delta T_0/\Delta Rn$ ratios in relation to theory

Federer has discussed at length some of the major predictions following from Lettau's theory. In the present work, the only variable which it was possible to examine for its effects on thermal response was the period of the forcing function. Ratios of the amplitudes of surface heat flux to net radiation, and surface temperatures to net radiation, as determined for Runs 1 and 2 by the method described in Sections 3.5 and 3.6, are set out in Table 9. The theoretical values involving ΔT_0 in Table 9 were computed for a thermal admittance of ice of 0.397 cal/cm^2 deg C(min)$^{\frac{1}{2}}$. The information contained in Table 8 has been plotted in Fig. 9

Table 9
Ratios of $\Delta B_0/\Delta Rn$ and $\Delta T_0/\Delta Rn$ for Runs 1 and 2

Period (min)		Run 1 $\frac{\Delta B_0}{\Delta Rn}$ *	Run 1 $\frac{\Delta T_0}{\Delta Rn}$ *	Run 1 $\frac{\Delta T_0}{\Delta Rn}$	Run 2 $\frac{\Delta B_0}{\Delta Rn}$ *	Run 2 $\frac{\Delta T_0}{\Delta Rn}$ *	Run 2 $\frac{\Delta T_0}{\Delta Rn}$	Theoretical values $\frac{\Delta T_0}{\Delta Rn}$
4	1st	---	---	---	0.4	2.0	1.0	1.9
	2nd	---	---	---	0.2	1.6	0.7	1.9
10	1st	0.4	3.1	1.6	0.5	3.9	2.0	3.1
	2nd	0.5	3.0	1.7	0.5	4.2	1.8	3.1
20	1st	0.5	4.0	2.1	0.7	6.8	3.3	4.3
	2nd	0.7	4.8	2.4	0.9	6.8	3.1	4.3
40	1st	0.6	5.8	3.1	---	---	---	6.1
	2nd	0.6	6.3	3.4	0.7	7.2	3.6	6.1

(*these ratios were calculated using "corrected" Rn values)

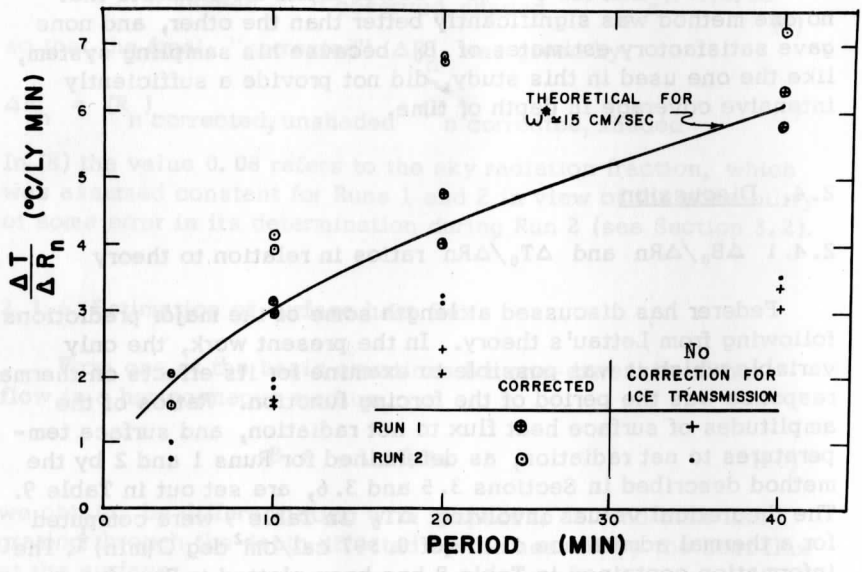

Fig. 9. Ratios of ice surface temperature amplitude to net radiation amplitude vs. period for Runs 1 and 2.

The ratios involving ΔB_0 seem to be dependent on period, and this is in fact predicted by the theory. Theoretical values of the $\Delta B_0/\Delta R_N$ ratio for the conditions of Run 2 ($w^* = .15$ cm/sec, $z_0 = 0.0036$ cm and $(\lambda c)^{\frac{1}{2}} = 0.397$ cal/cm^2 deg C(min)$^{\frac{1}{2}}$) are shown in Table 10.

Table 10

Theoretical ratios $\Delta A_0/\Delta B_0$ for the conditions of Run 2

Period (min):	2	4	10	20	40
Ratio	0.87	0.85	0.80	0.75	0.69

The fact that the trend of the measured ratios is opposite to that predicted by theory is probably ascribable to gross inadequacy of the measuring system used, particularly for sensing the shorter periods.

In Table 9 and Fig. 9, we see that, while corrected and uncorrected $\Delta T_0/\Delta Rn$ ratios for Run 2 maintain the approximate trend predicted by theory, agreement is by no means close. The data from Run 1, when the w^* value was undetermined, fit the theoretical curve better. For small periods and high thermal admittance, w^* is not an important variable. The data are too sparse to attempt any statistical analysis, and the only conclusion we can draw is that more and better data are required.

2.4.2 Use of a square-wave forcing function

Lettau's theory assumes a forcing function which is a harmonic function of time. The question arises as to how serious with respect to the theoretical predictions is a departure from the harmonic form to the square wave used in practice. An empirical examination of this question was made by performing a harmonic analysis of the square wave given by +1 (13 points) to -1 (13 points). The results are presented in Table 11. Since the variance of all the even-numbered harmonics is exactly zero, only the variances of the odd-numbered harmonics are listed in the table.

Table 11. Harmonic Analysis of a Symmetrical Square Wave

Harmonic	Variance (percent)	Phase angle (°) (position of first maximum value)
1	81.4	90
3	9.4	76
5	3.7	62
7	2.1	49
9	1.5	35
11	1.3	22
13	0.6	7

We see that 81 percent of the total variance of a symmetrical square wave is explained by the first harmonic, which has a phase angle of 90°. On the other hand, if the forcing function were the harmonic function assumed in theory, it would be a pure first harmonic (i.e., all of its variance would be explained by its first harmonic).

Such a marked predominance of the first harmonic in a square wave of the forcing function means that the radiation-dependent cycles which we examine in air and ice will also be principally explained by their first harmonics. For the data-treatment in this thesis, it has been assumed that the observed temperature cycles, for instance, were pure first harmonics. For the level of accuracy achieved in measurement, this seems a reasonable assumption. But in future work (see Section 5), where improvements in measure-

ment accuracy can be looked for, it will be desirable to harmonically analyse the results to isolate the first harmonic. In order to allow equilibrium to be attained and thereby gain more reliable analyses, it would seem necessary to modify the sequence of half-periods as used in the present work and to have, say, three successive periods of the same length instead of one alone.

The theory predicts the phase angles of the secondary cycles as well as the relation of their amplitudes to the amplitude of the forcing function. To determine the phase angle of the first harmonic of the surface temperature cycle for instance, it would be essential to perform a harmonic analysis because there is no means of approximating it by inspection as there is for the amplitude. It was decided to defer the examination of phase angle effects until the improved program of shading and unshading described above could be carried out.

2.5. Recommendations for Future Work

2.5.1 Prior examination of amplitude values predicted by theory

A thorough examination of predicted amplitude ratios involving ΔA_0, ΔB_0, and ΔT_0, versus ΔRn values in relation to wide ranges of period, w^* and z_0 for an ice-air system is necessary before further field work is undertaken. As has been noted in Section 4.1, for the periods so far used (4 to 40 minutes) the difficulties of accurately measuring the amplitudes ΔB_0 and ΔA_0 are considerable.

2.5.2 Design of improved experiments

The period range covered, for instance, might well have to be enlarged in order to enter a region in which amplitude ratios of heat fluxes are more favourable to satisfactory measurement. At the same time, there is an upper limit imposed on period because of interference from the concurrent diurnal cycle of net radiation. For whatever period range is found to be possible, it might be that accurate measurements of ΔA_0 and ΔB_0 are not possible. However, satisfactory estimates of ΔT_0 could still be made, using a similar sensor system to the one described in this thesis, preferably in conjunction with an infrared bolometer to provide a check.

2.5.3 Improvement of measurements in ice

The possible usefulness of an electrical resistance method (Houle, 1961) was mentioned earlier (Section 2.4). This method, as described in the paper quoted, would measure ice thickness to the nearest cm. Apart from their utility in determining Rn values corrected for transmission, in situ measurements of radiation penetration in ice have a good deal of intrinsic interest. An instrument which has a uniform spectral response is required for the in situ calibration of solar cells. The solarimeter described by Ward (1957) is compact, inexpensive and can be expected to have a uniform spectral response. This instrument could be used as a comparison standard in an examination of the usefulness of solar cells under ice, with mechanical protection and electrical insulation perhaps provided for the solar cells by polyethylene, which in thin films at least, is almost transparent to short wave radiation (e.g., see Funk, 1959).

It is apparent that the heat flux plates used in the present trials are of no use for daytime measurements in ice because of their radiation error. However, it would be worthwhile to retain them on the equipment in order to obtain an estimate of λ_{ice} under nighttime conditions for possible later use in estimating B_0 during shading trials. In this connection, it is highly desirable to establish an accurate value for λ_{glass} of the plates themselves.

Even if it does not prove worthwhile to measure B_0 because of its near-equality with Rn, information about temperatures at depth in the ice in relation to shading cycles would be valuable for the study of phase and amplitude relationships. As was mentioned in Section 4.2, perhaps three successive periods of the same length could be run, to provide satisfactorily equilibrated data for harmonic analysis. A greater intensity of temperature sensing levels throughout the profile in ice and water is desirable, especially in the first 10cm. Simultaneously, an increase in the sensitivity of the temperature difference measurements would be possible by increasing the numbers of junctions in each thermopile. The degree of areal integration at each level could then also be increased.

2.5.4 Experimental modifications of the ice surface

2.5.4.1 Surface roughness changes

To produce variations in z_0, a supply of 1cm wooden cubes, sufficient to cover ten percent of the surface area of a semicircle of radius 5m (the probable layout in practice, with the arc of the semicircle facing the northwest) is already available for future use. The use of a Pitot tube is planned, to measure wind speeds in the lowest 10cm, in conjunction with Thornthwaite cup anemometers above.

2.5.4.2 Albedo changes

If practicable under winter conditions, an interesting experimental modification would be to paint the ice surface with a black water-based paint. This modification, as for the surface roughness changes mentioned above, would best be done at a time when temperatures were 10 to 15°C below freezing to prevent any serious melting effects. One foresees the following physical changes with a black ice surface: (1) low albedo and more energy absorbed for heating the ice; and (2) absorption of energy in depth much reduced or eliminated, thus rendering the ice more like a conventional solid medium for heat flow.

2.6 Acknowledgments

The author wishes to thank Dr. H. H. Lettau, C. R. Stearns, H. L. Hamilton, J. P. Kearns, J. T. Scott and A. B. Super of the Department of Meteorology and Dr. C. B. Tanner and C. A. Federer of the Department of Soils for advice and assistance during the course of the work.

2.7. References

Federer, C.A., "Thermal response of a dry surface to shading cycles of short period," Master's Thesis (Soils), University of Wisconsin, 1962.

Funk, J.P., "Improved polyethylene-shielded net radiometer," J. Sci. Instru., 36 (6), 267-270, 1959.

Houle, J. L., "Two instruments for the measurement of ice thickness," Canadian Defence Research Board, Defence Research Northern Laboratory, Tech. Note No. 5/61, 1961.

"International Critical Tables," McGraw Hill, N.Y., 1927.

Lettau, H. H., "Theory of surface-temperature and heat-transfer oscillations near a level ground surface," T. A. G. U., 32, 189, 1951.

Lettau, H. H., "Synthetic climatology," Berichte des Deutschen Wetterdienstes, No. 38, 127-136, 1952.

Lettau, H. H., "Research problems in micrometeorology," Task 65-58-0026, prepared under contract DA-36-039-SC-80063 (USAEPG), University of Wisconsin, 1959.

Lienesch, J. H., "Experimental investigations of the thermal response of the air-soil system to controlled radiation pulses," Annual report — "Studies of the three-dimensional structure of the planetary boundary layer," Contract DA-36-039-SC-80282 (USAEPG), University of Wisconsin, p. 5-26, 1961.

List, R. J. (Editor), Smithsonian Meteorological Tables, 6th Edition, Smithsonian Institution, Washington, D.C., 1951.

Priestley, C. H. B., "Heat conduction and temperature profiles in air and soil," J. Australian Instit. Agric. Sci., 25, (2), 94-107, 1959.

Priestley, C. H. B., "Turbulent Transfer in the lower atmosphere," Univ. of Chicago, 1959.

Scott, J. T., and Ragotzkie, R. A., "Heat budget of an ice-covered inland lake," Task No. NR 387-022, ONR Contract No. 1202(07), University of Wisconsin, 1961.

Smithsonian Meteorological Tables, Ed. R. J. List, 6th Edition, Smithsonian Institution, Washington, D.C., 1951.

Stearns, C. R., "Micrometeorological installation on Lake Mendota," Final report: "Studies of the three-dimensional structure of the planetary boundary layer, Contract No. DA-36-039-SC-80282 (USAEPG), University of Wisconsin, 1962, pp. 7-46.

Ward, W. H., "Two portable thermistor radiometers," J. Sci. Instru., 34, 317-321, 1957.

Scanner's note:

This page is blank.

Report on Wind Profile Modification Experiments Using Fields of Christmas Trees on the Ice of Lake Mendota

Charles Stearns

Department of Meteorology
University of Wisconsin

Abstract: The experiments on wind profile structure within and above an artificial Christmas tree forest "planted" on the Lake Mendota ice were made in March 1964. Profile changes were measured within and outside the forest. The results show that at a given downwind distance within the trees the wind profile shape will be duplicated with winds of different velocities and direction for two specific areas of 4.0 and 2.1 m^2 per Christmas tree. The results also show that air flow and weather conditions under which the experiment is done must be carefully chosen so that profiles within the trees may be unambiguously related to the undisturbed conditions.

3.1 Introduction

The first experiments on wind profile modification using a rather sparse field of Christmas trees were performed March 21, 1963, on the Lake Mendota ice — as reported by Stearns and Lettau (1963) —and left a great deal to be desired. The gap at the downwind edge of the otherwise circular array of trees resulted in uncertainties as to what was actually happening downwind from the stand of trees. The anemometer mast which was moved through the trees had an insufficient number of anemometers yielding only relatively poor information about the wind profile shape at the several points within the trees. In addition, no information on air temperature profile modification by

the trees was available in the winter of 1962/63. Therefore, similar experiments were made in the winter of 1963/64, with several improvements added.

3.2 Layout of Christmas Trees

Approximately 500 left-over Christmas trees were collected in January of 1964 and trimmed to a height of 160 cm. Some trees such as the white and red pines would have a spike projecting 50 cm or more above the first set of branches at the top of the tree. This spike was shortened in order to reshape the pine trees and make them similar to the balsams and spruces. Also, trees with an unusually large branch were trimmed to conform to the rest of the trees. In a few cases one tree, if large enough, would be cut into two specimens of uniform shape. Approximately 20 cm of the trunk was allowed to project beyond the lowest branch so that the tree could be "planted" into pre-drilled holes with the lowest branch resting on the ice. The same effective silhouette area of 0.3 m^2 per tree was maintained as in the 1963 experiment.

The trees were planted in a circular pattern to decrease the dependence on wind direction. The pattern consisted of 11 concentric circles of trees spaced 1.45 m apart with the trees also spaced approximately 1.45 m apart along the arc of each circle. Naturally an integral number of trees had to be used for each circle. The total number of trees used was 420 and the total area to the outside of the outer row of tree branches was about 880 m^2. This results in a specific area (SA) of 2.1 m^2 per tree which is about one-half of the specific area used for the 1963 Christmas tree experiment. Fig. 1 is a photograph of the Christmas trees planted on the Lake Mendota ice. The average height of the trees was estimated to be 135 cm when compared to the anemometer levels of the wind profile masts.

3.3 Results of Data Collected

3.3.1 Data Collection System

Twenty-two Thornthwaite 3-cup anemometers were available for this experiment. A remote mast located approximately 50 m southwest of the trees was used to monitor the unmodified flow. Anemometers were placed at 40, 80, 160, 320 and 640 cm levels above the ice. The mast shown in Fig. 2 which was moved to

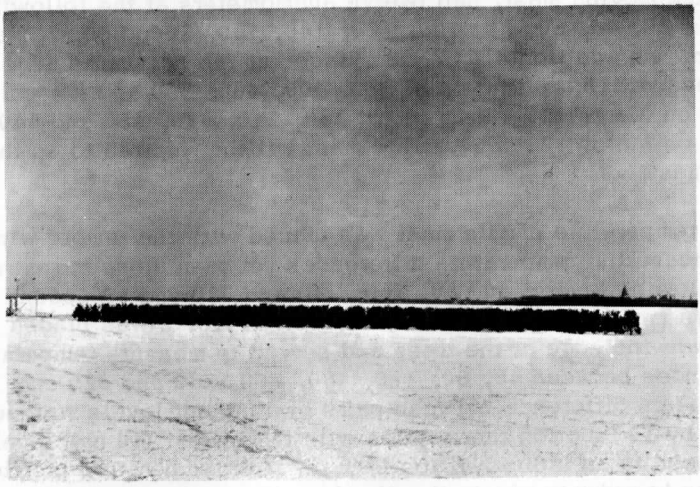

Fig. 1. Christmas Tree "Planted" on the Lake Mendota ice.

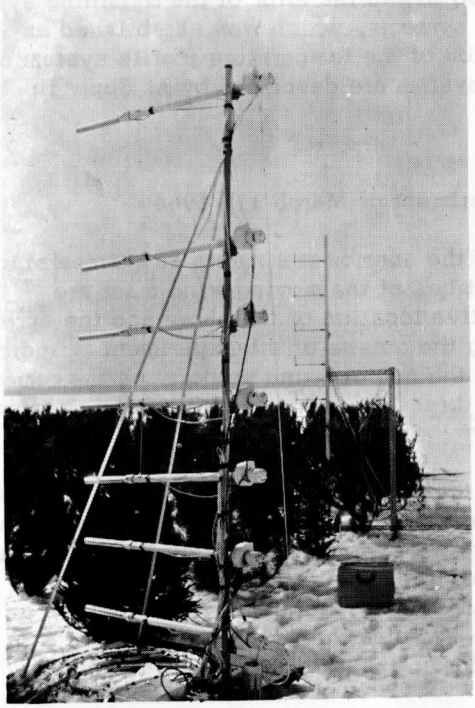

Fig. 2. Wind and Temperature Profile Masts at Downwind Edge of Christmas Trees.

the several locations inside and outside the trees and here referred to as the moving mast, had twelve anemometers at the following levels: 20, 40, 60, 80, 100, 120, 140, 160, 200, 240, 280 and 320 cm. An additional mast was placed at the downwind edge of the trees with anemometers at 320, 400, 480, 560 and 640 cm levels on March 11, 1964, and at 160, 240, 320, 480 and 640 cm levels on March 12, 1964. This mast will be referred to as the fixed mast.

A temperature profile mast was placed with the remote wind mast measuring temperature differences between adjacent pairs of the following levels: 40, 80, 160, 240 and 320 cm. A second temperature profile mast which may be seen in Fig. 2 was placed at the downwind edge of the trees and served to measure temperature differences between 40, 80, 120, 160, 200, 240 and 320 cm. The temperature difference between pairs of adjacent levels was detected by 10 junction thermopiles with the lowest (40 cm) level referenced to an individual ice bath for both temperature profile systems in order to obtain the absolute temperature. The temperature difference between the 320 cm level and the ice bath was also measured to check the sum of the adjacent temperature differences. The two temperatures agreed within the error of the recording system in both temperature profile systems, which was established as $\pm$ 0.005°C. The construction of the temperature profile system and the anemometer recording system are described by A. Super in Section 1 of this report.

3.3.2 Christmas tree experiment of March 11, 1964

The physical layout of the anemometer masts and temperature masts and the several positions of the moving wind mast are shown in Fig. 4. The relative location of the shore and the spread of the wind direction during the course of the experiment is indicated in Fig. 3. Fig. 5 presents the 640 cm wind velocity on the remote mast and the average wind direction during each 10 minute period of the experiment.

During the experiment the wind direction varied from 188° to 222° and the distance to the upwind shore was about 600 m. The tree tops on the rising shore were about 40 m above the ice giving a ratio of 1 to 15 for the obstacles' height to the fetch distance. This was insufficient for fully developed air flow over the ice as is well illustrated in Fig. 6 because the wind profile shows a curvature which is typical for an inversion. There was heating

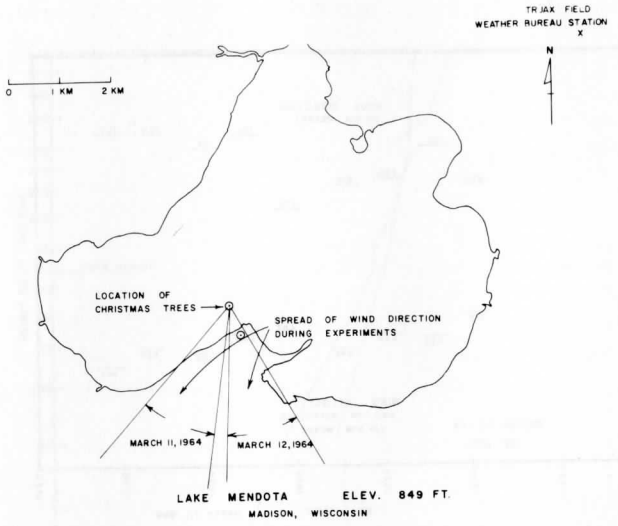

Fig. 3. Map of Lake Mendota with wind direction range observed during Christmas tree experiments of March 11 and 12, 1964.

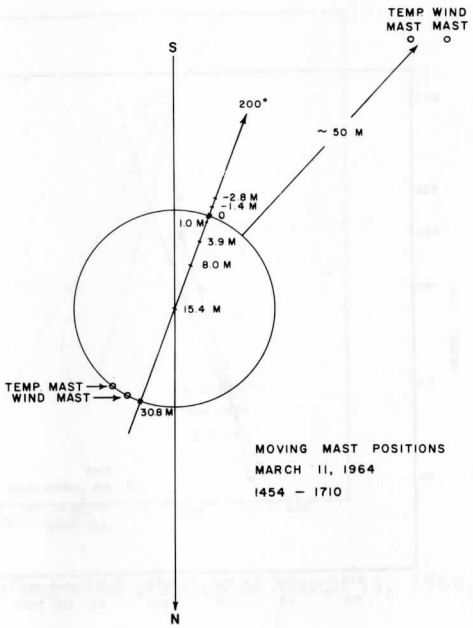

Fig. 4. Wind mast positions within and outside Christmas trees on March 11, 1964.

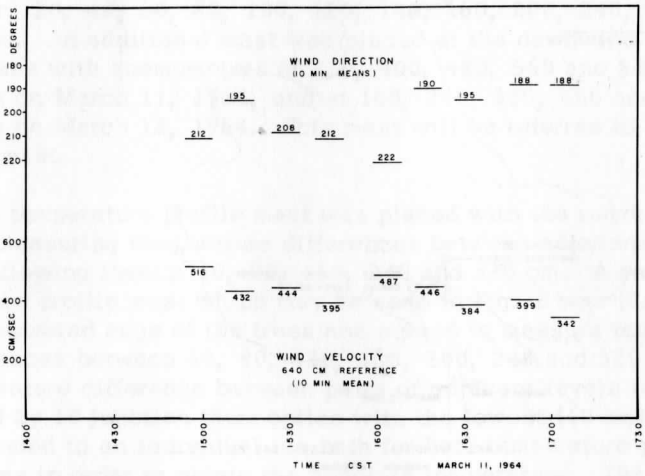

Fig. 5. Wind velocity at 640 cm level on remote mast and wind direction during Christmas tree experiment of March 11, 1964.

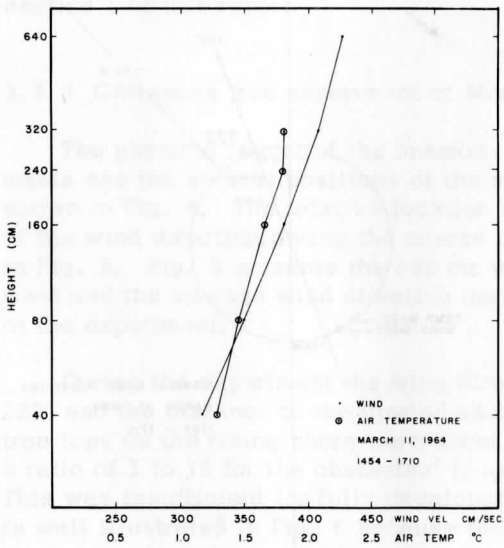

Fig. 6. Unmodified mean wind and temperature profile for March 11, 1964.

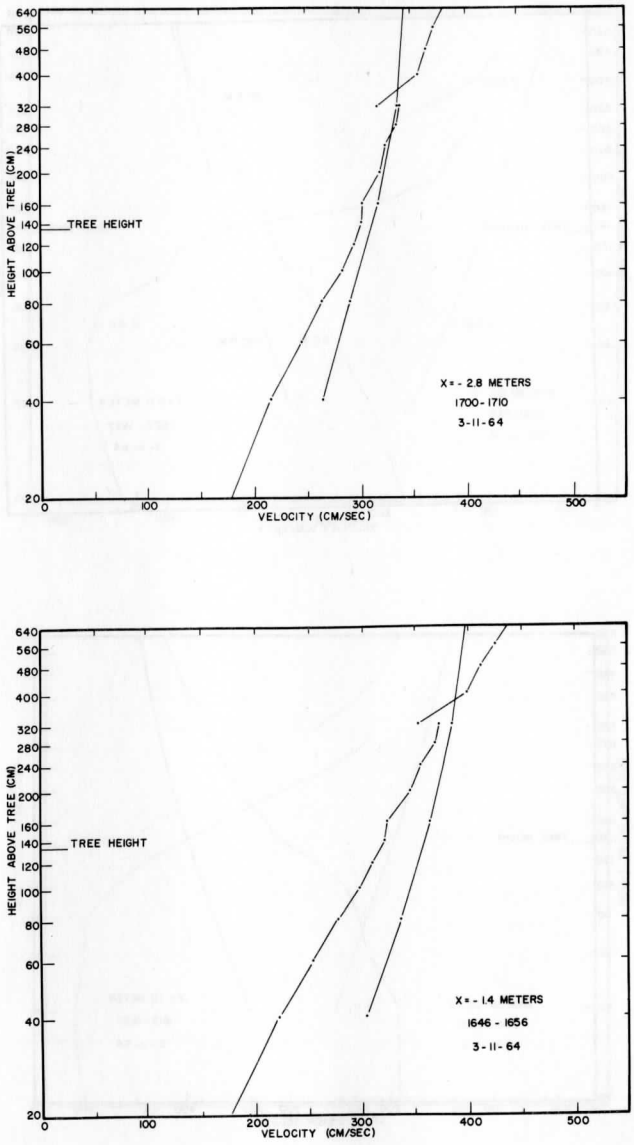

Fig. 7a. Modified and unmodified wind profiles of March 11, 1964, at x = -2.8 m and -1.4 m.

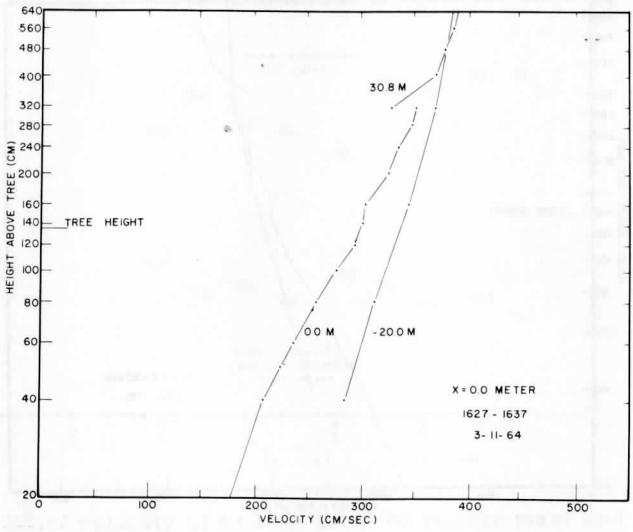

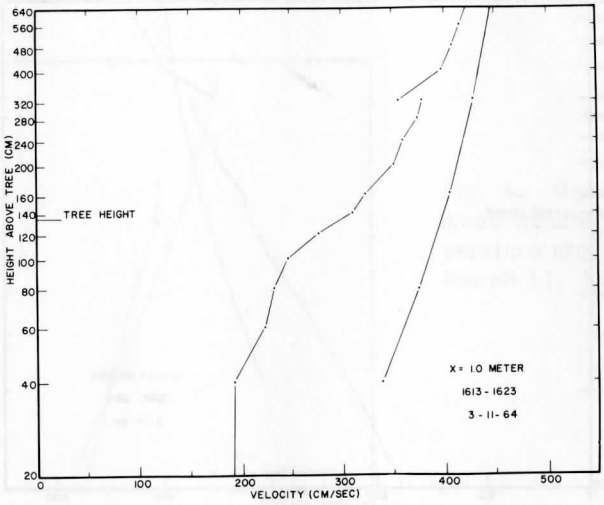

Fig. 7b. Modified and unmodified wind profiles of March 11, 1964, at x = 0 m and 1.0 m.

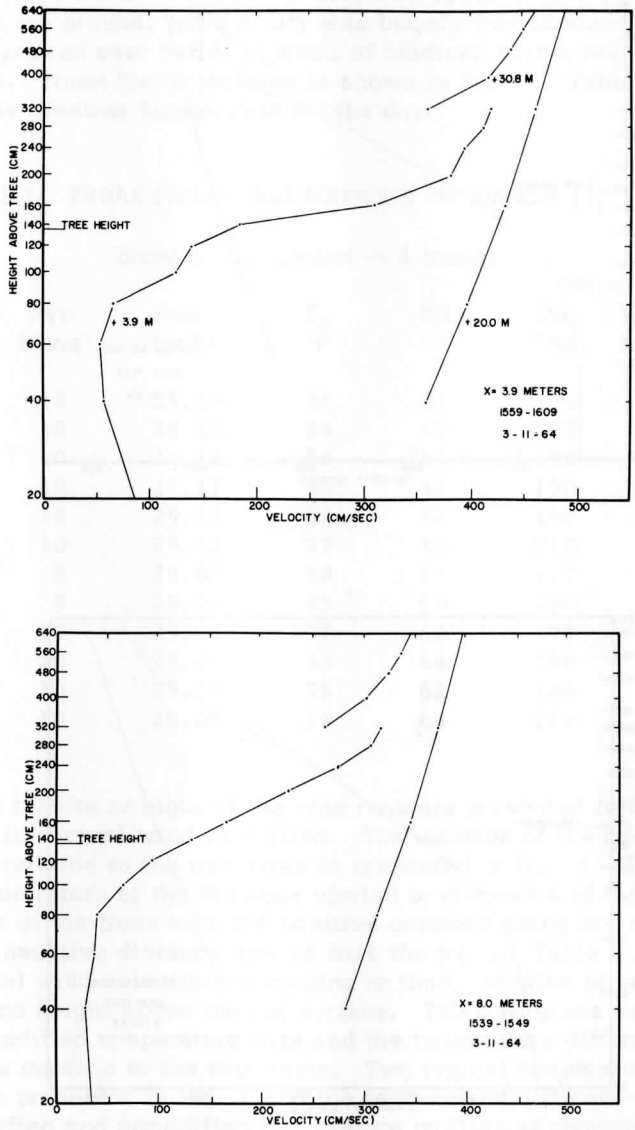

Fig. 7c. Modified and unmodified wind profiles of March 11, 1964, at x = 3.9 m and 8.0 m.

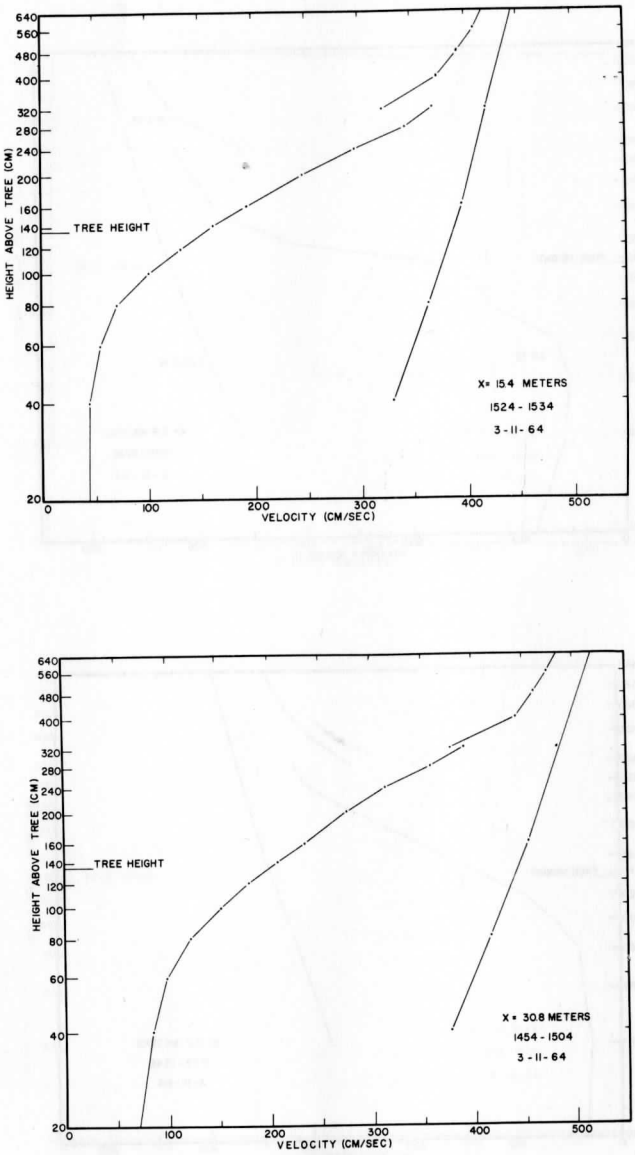

Fig. 7d. Modified and unmodified wind profiles of March 11, 1964, at x = 15.4 m and 30.8 m.

over the surrounding land and the ice surface was meling. The U. S. Weather Bureau station at Truax Field recorded 3 inches of snow on the ground, but the city was largely free of snow and the air had passed over build-up areas of Madison before reaching the lake. Truax Field location is shown in Fig. 3. Table I presents the Weather Bureau data for the day.

TABLE I. TRUAX FIELD OBSERVATIONS OF MARCH 11, 1964

Snow on the ground — 3 inches

Hour CST	Sky 10ths	Pres. inches	T_a °F	RH	Wind Dir. Deg.	Wind Vel. Knots
0900	10	29.19	31	61	190	7
1000	10	29.18	34	59	190	10
1100	10	29.18	35	57	190	9
1200	10	29.17	36	57	190	10
1300	10	29.14	37	57	190	13
1400	10	29.12	37	59	210	11
1500	8	29.09	38	57	190	11
1600	9	29.08	38	60	190	11
1700	10	29.07	37	62	190	8
1800	10	29.08	35	64	180	7
1900	10	29.08	35	62	180	5
2000	10	29.08	35	64	180	6

The results of eight of the nine runs are presented in Fig. 7 and are the actual wind velocities. The location of the moving mast in relation to the tree array is presented in Fig. 4. The x dimension refers to the distance upwind or downwind of the leading edge of the trees with the positive distance being downwind and the negative distance upwind from the trees. Table II lists the actual wind velocities according to time, location of moving mast, and height above the ice surface. Table III gives modified and unmodified temperature data and the temperature differences at levels common to the two masts. Two typical temperature profiles are presented in Fig. 8 and the temperature difference between the modified and unmodified temperature profiles at common levels in Fig. 9. It is obvious that solar radiation intercepted by the trees is used for heating the air during the day and, of course, changes the sign of the Richardson number $Ri = \frac{g}{T} \frac{\Delta\theta/\Delta z}{(\Delta u/\Delta z)^2}$. The values

TABLE II. Wind Velocities in cm/sec according to Time, Location and Height above ice surface for March 11, 1964

Height (cm)		Time CST	1454-1504	1508-1515	1524-1534	1539-1549	1559-1609	1613-1623	1627-1637	1646-1656	1700-1710
		Location	30.8m	30.8m	15.4m	8.0m	3.9m	1.0m	0.0m	-1.4m	-2.8m
320	Moving Mast		392	361	368	316	418	378	351	374	336
280			359	330	342	307	412	373	346	370	334
240			314	287	295	275	394	359	333	356	323
200			276	248	246	227	381	350	324	347	318
160			236	205	193	167	310	322	302	325	301
140			208	180	161	132	183	309	300	322	300
120			180	154	130	93	139	275	292	311	293
100			152	131	101	65	124	245	275	298	281
80			122	107	70	39	65	231	257	278	262
60			98	92	54	37	54	222	235	254	243
40			83	81	44	28	57	192	208	222	215
20			71	66	43	35	86	191	177	178	178
640	Fixed Mast		483	450	416	345	459	422	390	437	378
560	at x = 30.8 m		474	443	408	337	449	416	385	428	379
480			460	432	392	324	436	408	377	414	362
400			442	418	374	304	416	398	369	401	354
320			379	365	321	262	360	355	327	355	316
640	Remote Mast		516	432	444	395	487	446	384	399	342
320			482	416	420	371	460	427	369	386	333
160			453	389	395	345	432	403	343	365	316
80			416	359	363	313	397	374	312	337	290
40			377	329	330	282	358	337	285	304	263
Wind Direction			212°	195°	208°	212°	222°	190°	195°	188°	188°

TABLE III. Temperature in °C at the remote mast and at the downwind edge of the trees for March 11, 1964

Height (cm)	Time CST 1454-1504	1508-1518	1524-1534	1539-1549	1559-1609	1613-1623	1627-1637	1646-1656	1700-1710
					Modified Temperature				
320	2.445	2.367	2.503	2.448	2.709	2.494	2.634	2.371	2.234
240	2.640	2.469	2.625	2.593	2.777	2.499	2.616	2.283	2.105
200	2.778	2.567	2.712	2.702	2.850	2.527	2.637	2.252	2.053
160	2.992	2.729	2.871	2.868	2.982	2.609	2.695	2.234	2.003
120	3.213	2.944	3.060	3.075	3.106	2.667	2.769	2.224	1.959
80	3.452	3.173	3.268	3.299	2.966	2.799	2.849	2.228	1.913
40	3.580	3.182	3.325	3.340	2.947	2.740	2.770	2.088	1.743
					Reference Temperature				
320	2.067	1.851	1.855	1.778	1.646	1.739	1.671	1.821	1.983
240	2.067	1.876	1.853	1.758	1.614	1.730	1.649	1.783	1.930
160	1.952	1.738	1.707	1.605	1.503	1.601	1.535	1.698	1.848
80	1.773	1.567	1.522	1.374	1.246	1.369	1.311	1.462	1.582
40	1.578	1.365	1.320	1.147	0.998	1.098	1.035	1.180	1.260
					Modified Temperature minus Reference Temperature				
320	0.388	0.516	0.648	0.670	1.063	0.775	0.963	0.550	0.251
240	0.573	0.593	0.772	0.835	1.163	0.769	0.967	0.500	0.175
160	1.040	0.991	1.266	1.263	1.479	1.008	1.160	0.536	0.155
80	1.679	1.606	1.746	1.925	1.720	1.436	1.538	0.766	0.331
40	2.002	1.817	2.005	2.193	1.949	1.642	1.735	0.908	0.483

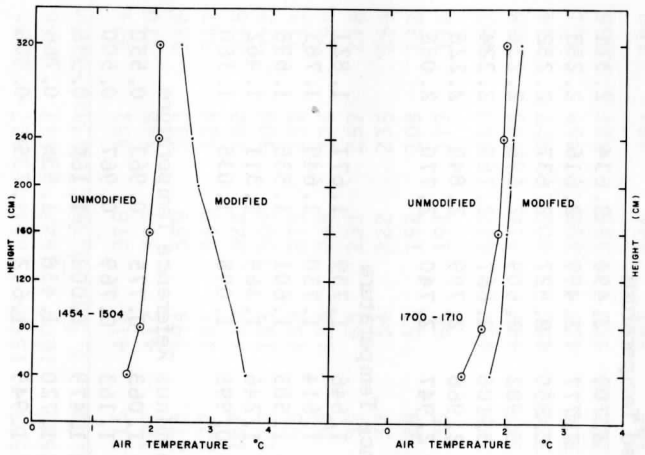

Fig. 8. Two modified and unmodified air temperature profiles for March 11, 1964

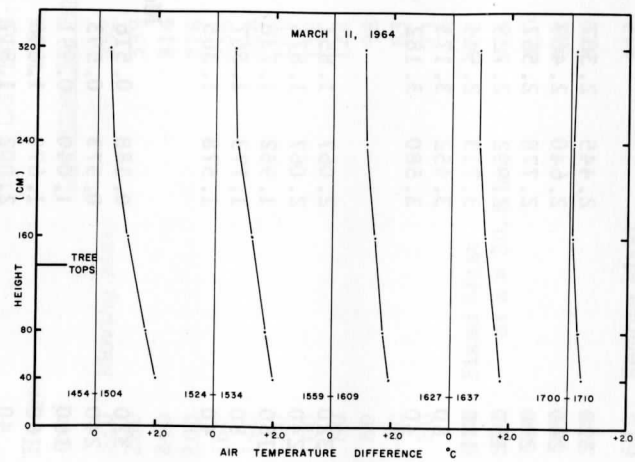

Fig. 9. Temperature difference between modified and unmodified air for March 11, 1964.

TABLE IV. Values of windshear, temperature difference, and Richardson number for unmodified and modified conditions on March 11, 1964.

		1454 - 1504			1508 - 1518		
	Level (cm)	Δu cm/sec	ΔT °C	Ri	Δu cm/sec	ΔT °C	Ri
Reference Mast unmodified	320 - 160	29	.115	0.078	16	.113	0.25
	160 - 80	37	.179	0.037	27	.171	0.067
		39	.195	0.018	30	.202	0.032
Fixed mast modified	320 - 240	78	-0.323	-0.015	74	-0.102	-0.005
	240 - 160	78	-0.352	-0.016	82	-0.206	-0.009
	160 - 120	56	-0.221	-0.910	51	-0.012	-0.012

obtained are summarized in Table IV but are not really valid for either the remote wind and temperature or the modified wind and temperature profile, since equilibrium conditions have not been reached in either case. Because of the spacing of the anemometers at the fixed mast on this day it was not possible to calculate the Richardson number at the downwind edge of the trees except during the first two runs when the moving mast was at the back edge of the trees.

In the analysis of the experiments of the winter 1962/63, the wind data at the several levels were referred to the remote 320 cm anemometer for calculations of the velocity ratios in order to make comparisons between the different profiles, and to calculate vertical velocities. It is obvious from Fig. 7 that this method will not work with the experiments in 1963/64. Thus, to reduce the dependency on an individual anemometer, the mean velocity was calculated for each profile. The results are presented in Table V. The mean velocity at the remote mast was calculated according to the formula $\bar{u}_R = \int_{z_1}^{z_2} u dz = z_1(0.56u_2 + 0.44u_1)$ where $z_2 = 2z_1$, and the wind velocity between z_1 and z_2 is considered a logarithmic function of height. The 40, 80, 160 and 320 cm levels were used for this calculation. The mean velocity $\bar{u}_m$ for the moving was calculated from 40 cm to 320 cm with the anemometer value weighted according

to the distance to the anemometer below it. The mean velocity $\bar{u}_f$ of the fixed mast was similarly calculated for all available levels.

The behavior of $\bar{u}_m$ of the moving mast to the remote mast or the fixed mast is very important for the calculation of vertical velocities and the distribution of horizontal velocities outside and in the trees. Fig. 10 presents ratios of $\bar{u}_m/\bar{u}_R$, $\bar{u}_m/\bar{u}_f$, $\bar{u}_m/\bar{u}_{640}$ as a function of x from the leading edge of the trees. It is obvious that none of the ratios show a consistent variation with respect to x. The ratio $\bar{u}_m/\bar{u}_f$ was used for the construction of the velocity ratios about the trees presented in Fig. 11. It is obvious from the graph that more detailed information is required about the wind velocity in the vicinity of the leading edge of the trees.

Two ten-minute runs were made at the beginning with the moving anemometer mast at the downwind edge of the trees, x = 30.8 m. The two runs are shown in Fig. 12 as the ratio of $u_z/\bar{u}_m$. The value of $\bar{u}_m$ are 246 and 221 cm/sec. and the two profiles agree with each other very well, differing by at most 5 percent of the velocity ratio. Knowing the shape of the profile of $\bar{u}/\bar{u}_m$ at any point the velocity distribution could be determined by as few as three anemometers.

3.3.3 Christmas Tree Experiment of March 12, 1964

The Truax Field Weather Bureau data for the day listed in Table VI reveals that melting had reduced the snow on the ground by one inch. Due to the wind direction, this day was not favorable for the Christmas tree experiment but the deteriorating condition of the lake ice was threatening to shorten our stay, so the experiment was done anyway in the hope of getting some useful information. Fig. 3 also presents the spread of wind direction during the course of the experiment and shows that the ratio of height to fetch is reduced to about 1 to 12 in relationship to the lake shore. Fig. 14 gives the wind direction and at velocity 640 cm as a function of time during the course of the experiment. The fixed and remote wind masts were located at the same position as on March 11, but the moving mast was shifted along a slightly different line from the previous day. The positions are illustrated in Fig. 13. The mean wind and temperature profile at the remote location in Fig. 14 are very similar to the previous day except the air temperature is about 2° higher.

The moving mast was placed 5.8 m upwind of the trees and then a ten-minute record of wind velocity at all points was obtained. Then

TABLE V. Ratio of the Velocity at a given level to the mean velocity of the particular mast for March 11, 1964

(Height (cm)	Time CST Location	1454-1504 30.8 m	1508-1518 30.8 m	1524-1534 15.4 m	1539-1549 8.0 m	1559-1609 3.9 m	1613-1623 1.0 m	1627-1637 0	1646-1656 -1.4 m	1700-1710 -2.8 m
		$u/\bar{u}_m$	$u/\bar{u}_m$	$u/\bar{u}_m$	$u/\bar{u}_m$	$u/\bar{u}_m$	$u/\bar{u}_m$	$u/\bar{u}_m$	$u/\bar{u}_m$	$u/\bar{u}_m$
320		1.580	1.632	1.745	1.725	1.520	1.200	1.100	1.093	1.062
280		1.458	1.492	1.626	1.675	1.498	1.185	1.084	1.080	1.056
240		1.275	1.300	1.400	1.502	1.433	1.140	1.045	1.040	1.021
200		1.120	1.121	1.168	1.240	1.385	1.110	1.015	1.015	1.005
160		0.960	0.927	0.915	0.912	1.128	1.021	0.946	0.950	0.953
140		0.845	0.815	0.763	0.720	0.665	0.981	0.940	0.942	0.950
120		0.732	0.696	0.616	0.508	0.505	0.873	0.915	0.910	0.926
100		0.619	0.593	0.478	0.355	0.450	0.768	0.861	0.871	0.884
80	Moving Mast	0.496	0.485	0.332	0.213	0.236	0.734	0.805	0.814	0.830
60		0.398	0.416	0.256	0.202	0.196	0.705	0.736	0.743	0.769
40		0.337	0.366	0.208	0.153	0.207	0.610	0.652	0.650	0.680
20		0.288	0.298	0.204	0.192	0.312	0.600	0.555	0.520	0.563
$\bar{u}_m$ cm/sec.		246	221	211	183	275	315	319	342	316
		$\bar{u}/\bar{u}_f$	$u/\bar{u}_f$	$u/\bar{u}_f$	$u/\bar{u}_f$	$u/\bar{u}_f$	$u/\bar{u}_f$	$u/\bar{u}_f$	$u/\bar{u}_f$	$u/\bar{u}_f$
640		1.070	1.061	0.078	0.088	1.078	1.047	1.050	1.066	1.057
560		1.038	1.015	1.055	1.062	1.052	1.031	1.035	1.045	1.033
480		1.008	1.019	1.015	0.021	0.022	1.011	1.013	0.010	1.010
400	Fixed Mast	0.968	0.980	0.969	0.960	0.975	0.989	0.992	0.977	0.988
320		0.831	0.861	0.832	0.825	0.844	0.881	0.879	0.865	0.883
$\bar{u}_f$ cm/sec.		456	424	386	317	427	403	372	410	358
		$u/\bar{u}_R$	$u/\bar{u}_R$	$u/\bar{u}_R$	$u/\bar{u}_R$	$u/\bar{u}_R$	$u/\bar{u}_R$	$u/\bar{u}_R$	$u/\bar{u}_R$	$u/\bar{u}_R$
640		1.148	1.113	1.122	1.151	1.132	1.115	1.102	1.100	1.096
320		1.071	1.070	0.070	0.080	1.070	1.070	1.060	1.062	1.068
160		1.007	1.002	1.008	1.006	1.005	1.010	0.985	1.005	1.012
80		0.925	0.925	0.926	0.914	0.924	0.936	0.896	0.928	0.930
40	Remote Mast	0.837	0.847	0.842	0.823	0.833	0.845	0.819	0.836	0.843
$\bar{u}_R$ cm/sec.		450	388	392	343	430	399	348	363	312
$\bar{u}_m/\bar{u}_R$		0.547	0.570	0.538	0.535	0.640	0.790	0.918	0.943	1.010
$\bar{u}_m/\bar{u}_f$		0.540	0.522	0.547	0.578	0.645	0.783	0.858	0.835	0.883
$\bar{u}_m/\bar{u}_{640}$		0.492	0.500	0.491	0.494	0.581	0.726	0.825	0.819	0.878

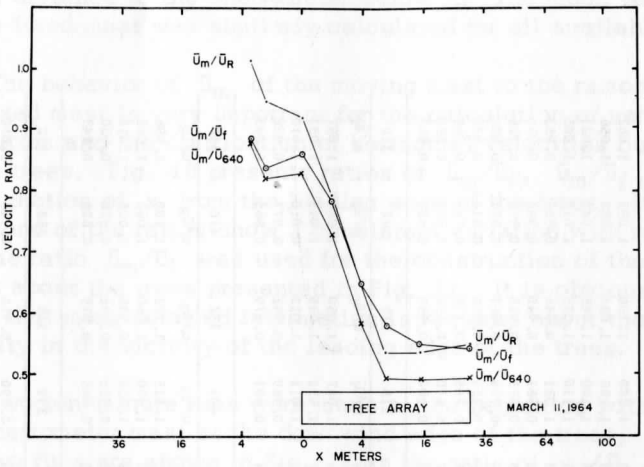

Fig. 10. Velocity ratios between the moving and the remote and fixed profile and the mean 640 cm velocity of the remote and fixed mast as a function of position March 11, 1964.

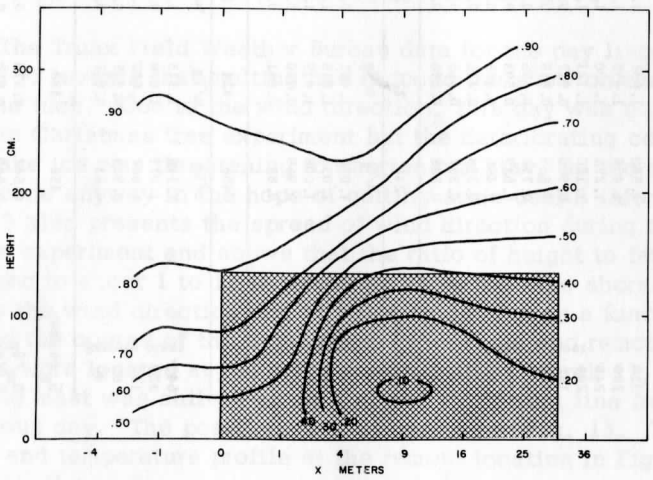

Fig. 11. Velocity ratio distribution about the trees compared to the fixed mast at the back edge of the trees March 11, 1964.

TABLE VI. Truax Field Observations of March 12, 1964

Snow on the ground — 2 inches

Hour CST	Sky 10ths	Pres. inches	T_a °F	RH	Wind Dir. Deg.	Wind Vel. Knots
0900	10	29.22	34	73	290	6
1000	10	29.24	34	73	180	5
1100	3	29.23	37	67	60	6
1200	1	29.23	41	62	180	5
1300	4	29.21	42	60	180	6
1400	5	29.21	43	60	180	6
1500	7	29.20	43	63	170	9
1600	8	29.18	43	60	180	13
1700	7	29.17	42	65	140	10
1800	7	29.16	40	62	150	9
1900	6	29.14	36	70	130	9
2000	4	29.14	37	67	150	10

the moving mast was shifted downwind through the trees, with ten-minute recordings at each of the points in Fig. 13. A total of 14 profiles were collected and the results of 12 profiles are presented in Fig. a, b, c, d, e, f, g, and h. Profiles at $x = -2.9$ m and at $x = 70.8$ m are not presented. The remote profile with anemometers at 40, 80, 160, 320 and 640 cm is undisturbed during the experiment as is the fixed mast at the back row of trees with anemometers at 160, 240, 320, 480 and 640 cm (note that these levels are different from the ones used at the fixed mast on the previous day). Table VII presents the actual velocities. The agreement at 640 cm between the fixed and remote masts on an individual run looks very poor, however, the average of all runs of this day is 453 cm/sec on the fixed mast and 451 cm/sec on the remote mast. The velocity differences between the 640 cm anemometers on the remote mast and fixed mast are too large to depend on differences in heating by the trees and are not correlated with wind direction. Fig. 17 presents two typical temperature profiles for the day and Fig. 18 the temperature differences at common levels between the modified and unmodified air. The temperature values are given in Table VIII.

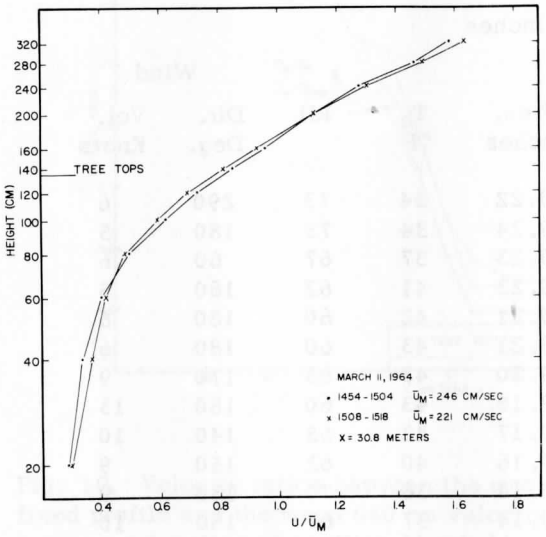

Fig. 12. Comparison between the velocity ratios of two runs at the same location March 11, 1964.

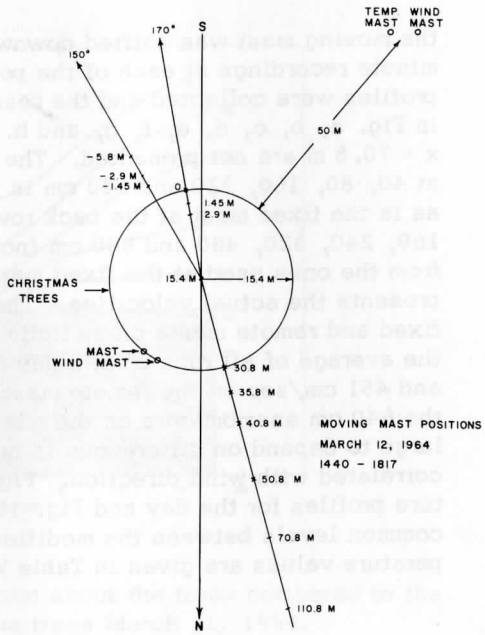

Fig. 13. Wind Profile mast locations within and outside the Christmas trees on March 10, 1964.

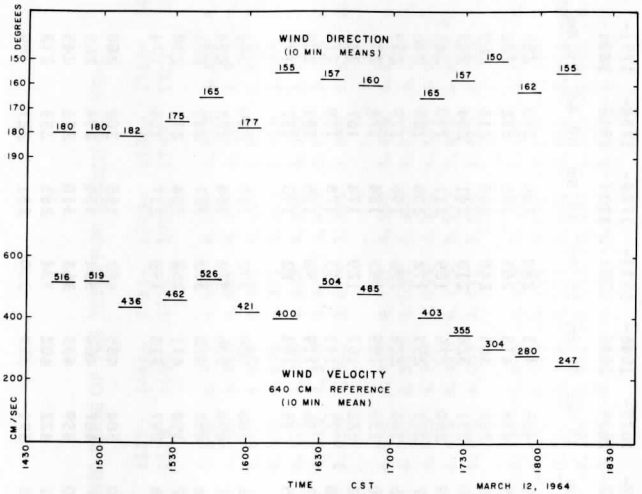

Fig. 14. 640 cm wind velocity on remote mast during experiment of March 12, 1964.

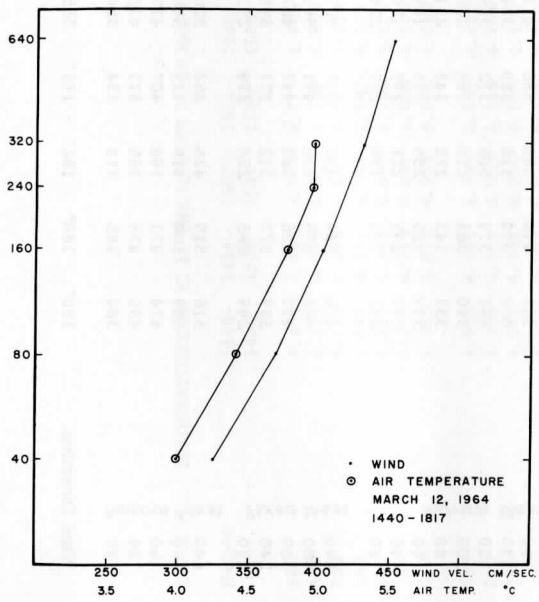

Fig. 15. Remote mean wind and temperature profile of March 12, 1964.

TABLE VII. WIND VELOCITY IN cm/sec ACCORDING TO TIME, LOCATION AND HEIGHT ABOVE ICE SURFACE FOR MARCH 12, 1964.

Height		Time (CST)	1440-1450	1454-1504	1507-1517	1526-1536	1540-1550	1556-1606	1612-1622	1629-1639	1646-1656	1711-1721	1724-1734	1738-1748	1751-1801	1807-1817
(cm)		Location	-5.8m	-2.9m	-1.45m	0	2.1m	4.2m	8.4m	15.4m	30.8m	35.8m	40.8m	50.8m	70.8m	110.8m
320			426	462	386	451	484	362	389	465	443	280	300	240	285	242
280			421	455	379	444	479	358	379	438	415	265	285	232	280	241
240			403	431	362	424	458	340	345	382	363	240	260	215	269	234
200			394	419	349	409	444	320	300	331	328	218	241	204	262	229
160	Moving Mast		392	414	340	386	411	263	219	260	276	189	217	190	245 ?	214 ?
140			369	390	318	380	384	187	157	223	253	172	208	185	246	218
120			362	379	306	372	355	115	96	186	228	156	196	179	239	212
100			350	365	290	354	280	94	70	139	199	143	184	174	233	207
80			333	343	272	343	231	73	62	122	167	129	174	167	223	198
60			319	325	255	333	189	73	58	71	141	113	173	159	214	187
40			290	295	227	295	170	71	57	56	119	98	155	151	200	173
20			243	246	184	257	225	91	65	55	104	82	143	137	175	149
640	Fixed Mast		478	524	453	507	527	416	416	508	520	332	365	280	304	256
480			462	508	436	491	509	397	401	490	506	324	354	272	294	248
320			410	456	383	447	467	352	374	454	473	303	327	249	273	227
240			339	377	313	377	395	294	327	398	411	258	284	211	238	194
160			249	285	234	279	291	224	248	297	315	195	217	155	174	143
640	Remote Mast		516	519	436	462	526	421	400	504	485	403	355	304	280	247
320			503	500	419	439	506	404	377	487	464	384	334	294	265	233
160			474	471	394	407	477	376	350	459	435	363	310	278	245	215
80			435	433	359	373	435	345	321	422	402	334	283	255	218	197
40			384	385	318	334	380	308	283	371	357	300	251	227	189	172
Wind Direction			180°	180°	182°	175°	165°	177°	155°	157°	160°	165°	157°	150°	162°	155°

TABLE VIII. TEMPERATURES IN °C AT THE REMOTE MAST AND AT THE DOWNWIND EDGE OF THE TREES FOR MARCH 12, 1964.

Height (cm)	1440-1450	1454-1504	1507-1517	1526-1536	1540-1550	1556-1606	1612-1622	1629-1639	1646-1656	1711-1721	1724-1734	1738-1748	1751-1801	1806-1816
320	4.451	4.468	4.633	4.771	4.905	4.817	4.933	7.845	4.879	4.685	4.685	4.313	4.129	4.005
240	4.481	4.414	4.619	4.707	4.805	4.744	4.844	4.708	4.760	4.527	4.580	4.116	3.970	3.809
200	4.527	4.426	4.647	4.707	4.615	4.738	4.815	4.649	4.687	4.422	4.440	3.957	3.816	3.640
160	4.648	4.484	4.741	4.742	4.593	4.778	4.811	4.586	4.605	4.323	4.263	3.769	3.599	3.422
120	4.821	4.572	4.850	4.788	4.572	4.858	4.798	4.477	4.509	4.223	4.038	3.543	3.317	3.160
80	5.028	4.719	5.001	4.828	4.535	4.965	4.780	4.314	4.399	4.083	3.813	3.275	3.004	2.894
40	5.023	4.638	4.935	4.580	4.240	4.818	4.448	3.850	3.985	3.673	3.365	2.880	2.512	2.460
320	4.453	4.541	4.548	4.689	4.805	4.799	4.556	4.992	4.885	4.703	4.560	4.420	4.231	4.084
240	4.453	4.536	4.533	4.669	4.768	4.750	4.914	4.951	4.819	4.631	4.468	4.313	4.126	3.988
160	4.273	4.392	4.350	4.505	4.659	4.555	4.755	4.823	4.709	4.494	4.352	4.221	4.035	3.933
80	3.947	4.084	4.036	4.182	4.346	4.217	4.432	4.478	4.420	4.135	3.993	3.870	3.630	3.618
40	3.633	3.765	3.720	3.850	3.988	3.875	4.063	4.095	4.065	3.718	3.570	3.423	3.135	3.158
320	-0.002	-0.073	0.085	0.082	0.100	0.018	-0.023	-0.147	-0.006	-0.018	0.115	-0.107	-0.102	-0.079
240	0.028	0.122	0.086	0.038	0.037	-0.006	-0.070	-0.243	-0.059	-0.104	0.112	-0.197	-0.156	-0.179
160	0.375	0.092	0.391	0.237	-0.066	0.223	0.066	-0.237	-0.104	-0.171	-0.089	-0.452	-0.436	-0.511
80	1.081	0.635	0.965	0.646	0.189	0.748	0.348	-0.164	-0.021	-0.052	-0.180	-0.595	-0.626	-0.924
40	1.390	0.873	1.215	0.730	0.252	0.943	0.385	-0.245	-0.080	-0.045	-0.205	-0.543	-0.623	-0.698

TABLE IX. RATIO OF THE VELOCITY AT A GIVEN LEVEL TO THE MEAN VELOCITY OF THE MAST FOR MARCH 12, 1964.

	Time (CST)	1440-1450	1454-1504	1507-1517	1526-1536	1540-1550	1556-1606	1612-1622	1629-1639	1646-1656	1711-1721	1724-1734	1738-1748	1751-1801	1807-1817
Height (cm)	Location	-5.8m $u/\bar{u}_m$	-2.9m $u/\bar{u}_m$	-1.45m $u/\bar{u}_m$	0 $u/\bar{u}_m$	2.1m $u/\bar{u}_m$	4.2m $u/\bar{u}_m$	8.4m $u/\bar{u}_m$	15.4m $u/\bar{u}_m$	30.8m $u/\bar{u}_m$	35.8m $u/\bar{u}_m$	40.8m $u/\bar{u}_m$	50.8m $u/\bar{u}_m$	70.8m $u/\bar{u}_m$	110.8m $u/\bar{u}_m$
320	Moving Mast	1.111	1.145	1.180	1.145	1.258	1.502	1.685	1.655	1.472	1.415	1.318	1.211	1.130	1.100
280		1.090	1.130	1.133	1.125	1.243	1.485	1.640	1.560	1.410	1.340	1.250	1.172	1.112	1.095
240		1.042	1.070	1.106	1.075	1.217	1.410	1.492	1.360	1.245	1.212	1.140	1.085	1.067	1.062
200		1.019	1.040	1.068	1.038	1.153	1.327	1.300	1.176	1.115	1.101	1.058	1.031	1.040	1.040
160		1.014	1.028	1.040	0.980	1.068	1.090	0.947	0.924	0.939	0.955	0.951	0.960	0.972 ?	0.974 ?
140		0.956	0.968	0.974	0.965	0.996	0.776	0.679	0.783	0.861	0.868	0.908	0.935	0.978	0.991
120		0.937	0.942	0.936	0.944	0.921	0.478	0.415	0.661	0.775	0.787	0.860	0.905	0.948	0.961
100		0.907	0.906	0.888	0.899	0.726	0.390	0.303	0.494	0.676	0.721	0.806	0.879	0.925	0.942
80		0.863	0.852	0.833	0.871	0.600	0.302	0.268	0.434	0.567	0.651	0.764	0.844	0.885	0.900
60		0.826	0.806	0.780	0.846	0.491	0.302	0.251	0.252	0.480	0.570	0.715	0.804	0.850	0.850
40		0.752	0.732	0.696	0.746	0.441	0.294	0.246	0.198	0.405	0.492	0.680	0.763	0.794	0.786
20		0.629	0.610	0.563	0.653	0.585	0.377	0.281	0.195	0.354	0.411	0.627	0.692	0.695	0.679
$\bar{u}_m$ cm/sec		387	403	327	394	385	241	231	281	294	198	228	198	252	220
		$u/\bar{u}_f$	$u/\bar{u}_f$	$u/\bar{u}_f$	$u/\bar{u}_f$	$u/\bar{u}_f$	$u/\bar{u}_f$	$u/\bar{u}_f$	$u/\bar{u}_f$	$u/\bar{u}_f$	$u/\bar{u}_f$	$u/\bar{u}_f$	$u/\bar{u}_f$	$u/\bar{u}_f$	$u/\bar{u}_f$
640	Fixed Mast	1.159	1.145	1.120	1.040	1.135	1.168	1.118	1.128	1.110	1.129	1.120	1.129	1.121	1.133
480		1.119	1.113	1.075	1.005	1.095	1.115	1.068	1.080	1.080	1.101	1.085	1.095	1.084	1.098
320		0.992	0.997	0.936	0.916	1.005	0.989	1.005	1.010	1.010	1.003	1.005	1.003	1.006	1.004
240		0.821	0.825	0.774	0.772	0.852	0.828	0.880	0.881	0.876	0.871	0.870	0.850	0.879	0.859
160		0.603	0.624	0.578	0.572	0.627	0.630	0.667	0.656	0.672	0.658	0.666	0.625	0.642	0.632
$\bar{u}_f$ cm/sec.		413	457	405	488	464	356	372	449	469	296		248	271	226
		$u/\bar{u}_R$	$u/\bar{u}_R$	$u/\bar{u}_R$	$u/\bar{u}_R$	$u/\bar{u}_R$	$u/\bar{u}_R$	$u/\bar{u}_R$	$u/\bar{u}_R$	$u/\bar{u}_R$	$u/\bar{u}_R$	$u/\bar{u}_R$	$u/\bar{u}_R$	$u/\bar{u}_R$	$u/\bar{u}_R$
640	Remote Mast	1.098	1.110	1.220	1.138	1.112	1.125	1.145	1.096	1.130	1.119	1.152	1.097	1.158	1.150
320		1.070	1.070	1.098	1.082	1.072	1.080	1.080	1.060	1.081	1.065	1.085	1.060	1.095	1.085
160		1.010	1.010	1.032	1.002	1.010	1.005	1.002	0.998	1.013	1.010	1.005	1.003	1.012	1.000
80		0.925	0.928	0.940	0.919	0.921	0.923	0.920	0.916	0.936	0.926	0.919	0.920	0.901	0.915
40		0.816	0.825	0.832	0.823	0.805	0.824	0.811	0.806	0.832	0.825	0.815	0.819	0.781	0.799
$\bar{u}_R$ cm/sec		480	467	382	406	472	374	349	460	429	360	308	277	242	215
$\bar{u}_m/u_R$		0.822	0.854	0.857	0.972	0.816	0.645	0.662	0.611	0.685	0.550	0.740	0.716	1.040	1.022
$\bar{u}_m/u_f$		0.936	0.884	0.805	0.807	0.830	0.677	0.621	0.627	0.627	0.674	0.700	0.798	0.931	0.974
$\bar{u}_m/\bar{u}_{640}$		0.778	0.773	0.735	0.813	0.730	0.576	0.567	0.563	0.584	0.539	0.635	0.682	0.864	0.873

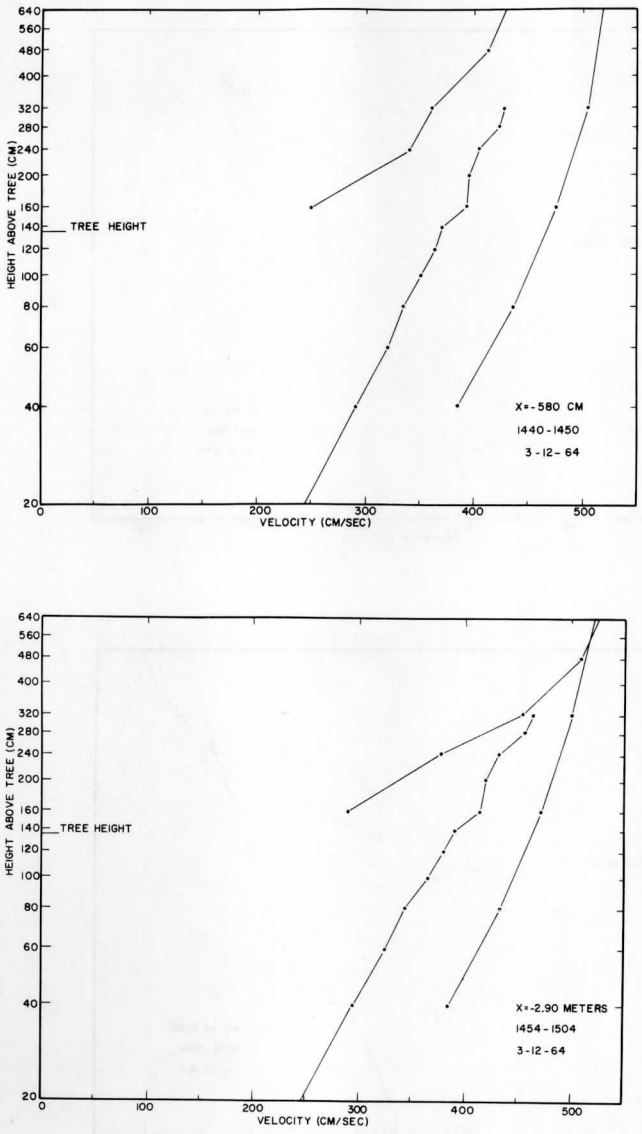

Fig. 16a. Modified and unmodified wind profiles for March 12, 1964 at x = -5.8 m and -2.9 m.

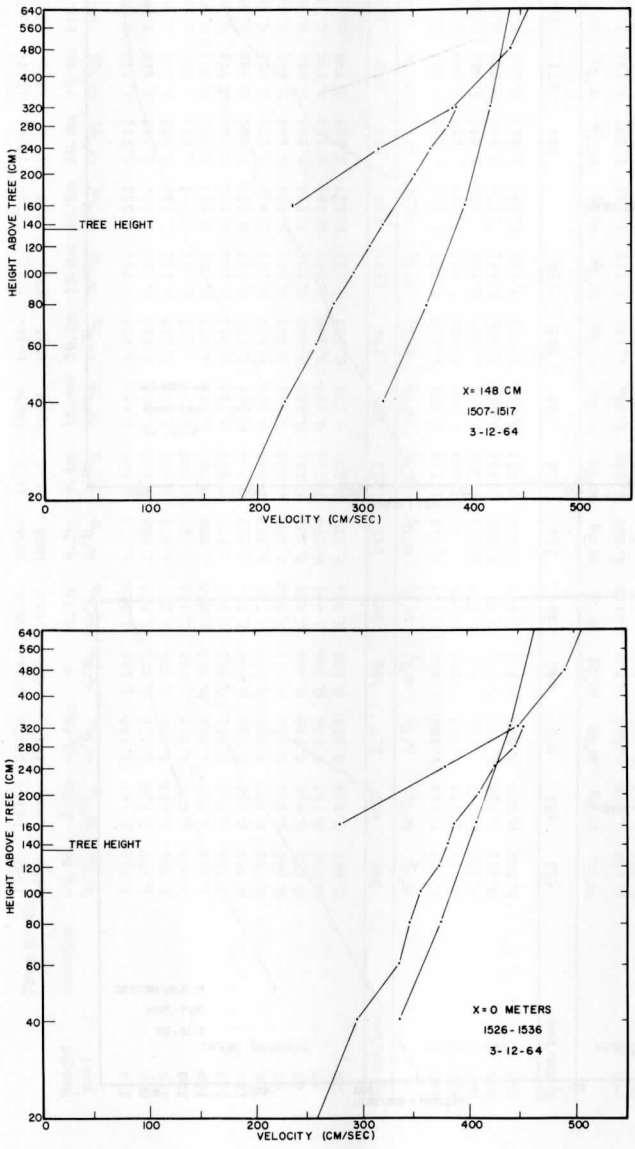

Fig. 16b. Modified and unmodified wind profiles for March 12, 1964, at x = -1.45 m and 0 m.

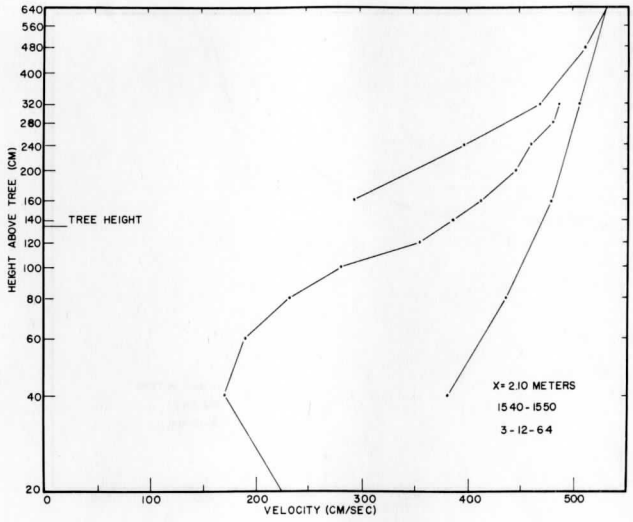

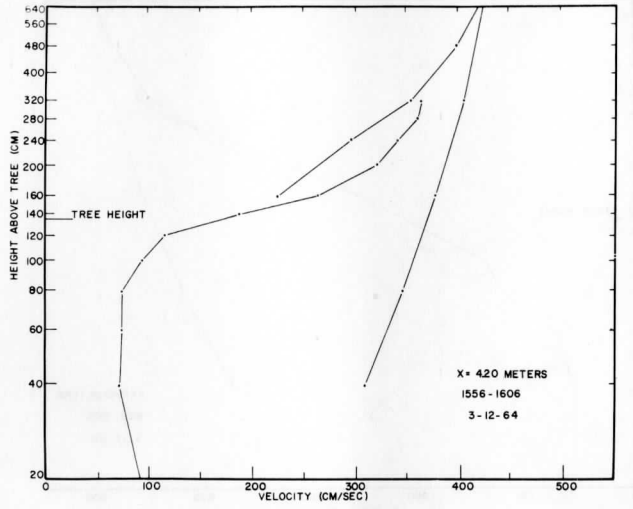

Fig. 16c. Modified and unmodified wind profiles for March 12, 1964, at x = 2.1 m and 4.2 m.

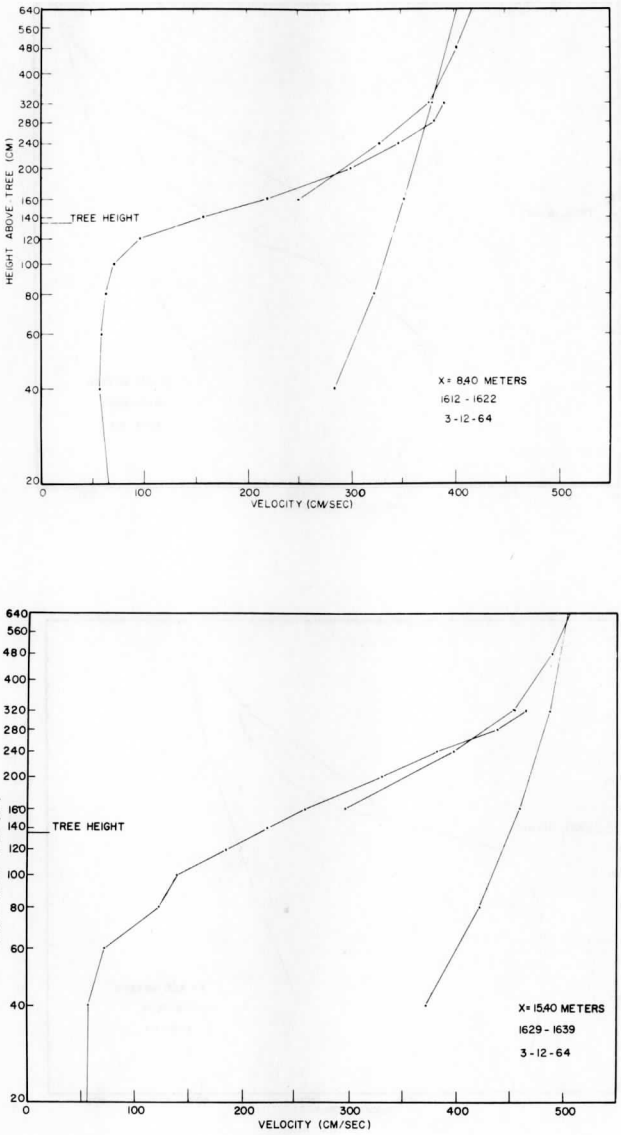

Fig. 16d. Modified and unmodified wind profiles for March 12, 1964, at x = 8.4 m and 15.4 m.

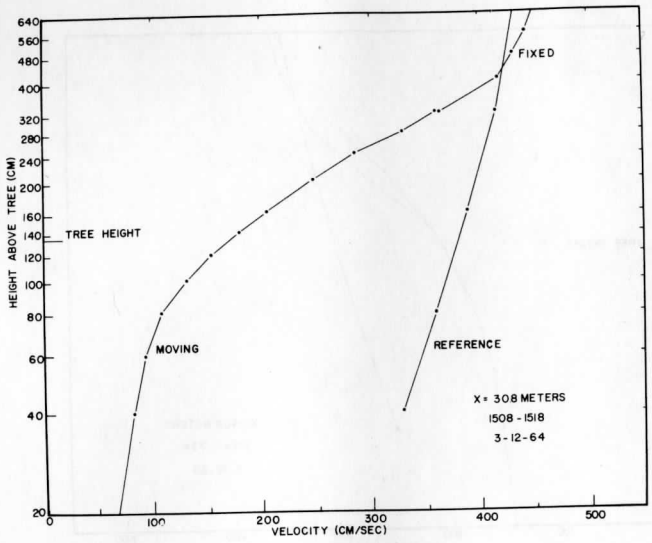

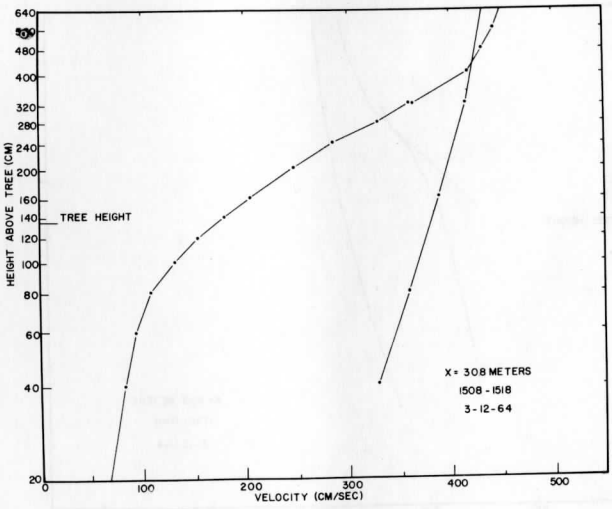

Fig. 16e. Modified and unmodified wind profiles for March 12, 1964, at x = 30.8m and 35.8m.

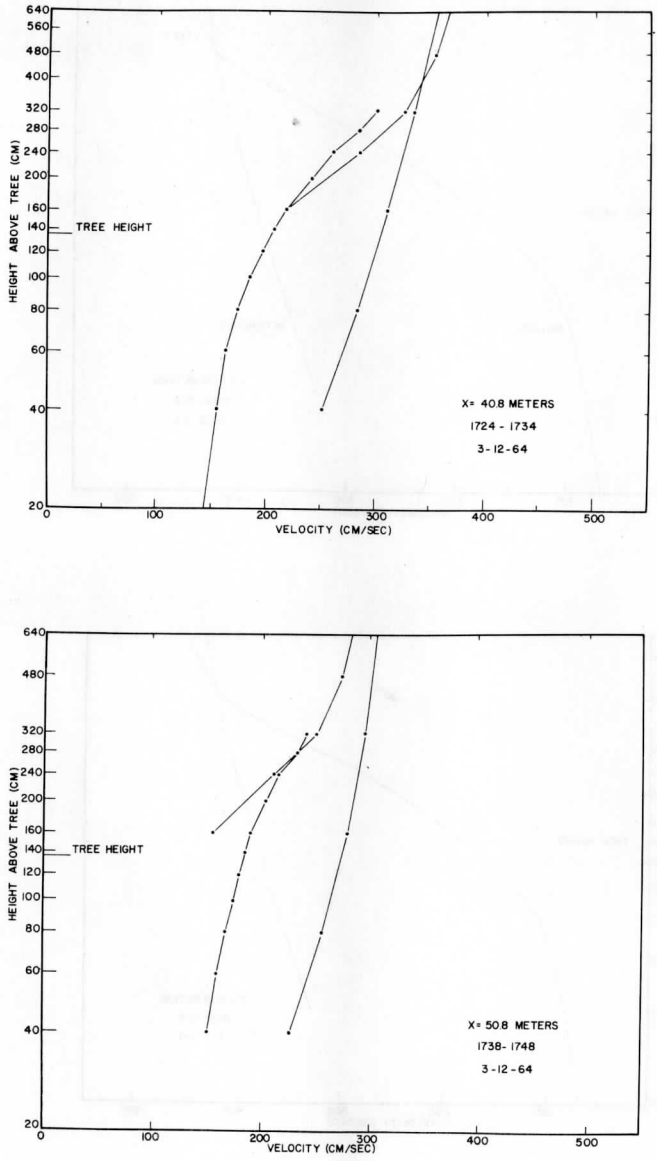

Fig. 16f. Modified and unmodified wind profiles for March 12, 1964, at x = 40.8 m and 50.8 m.

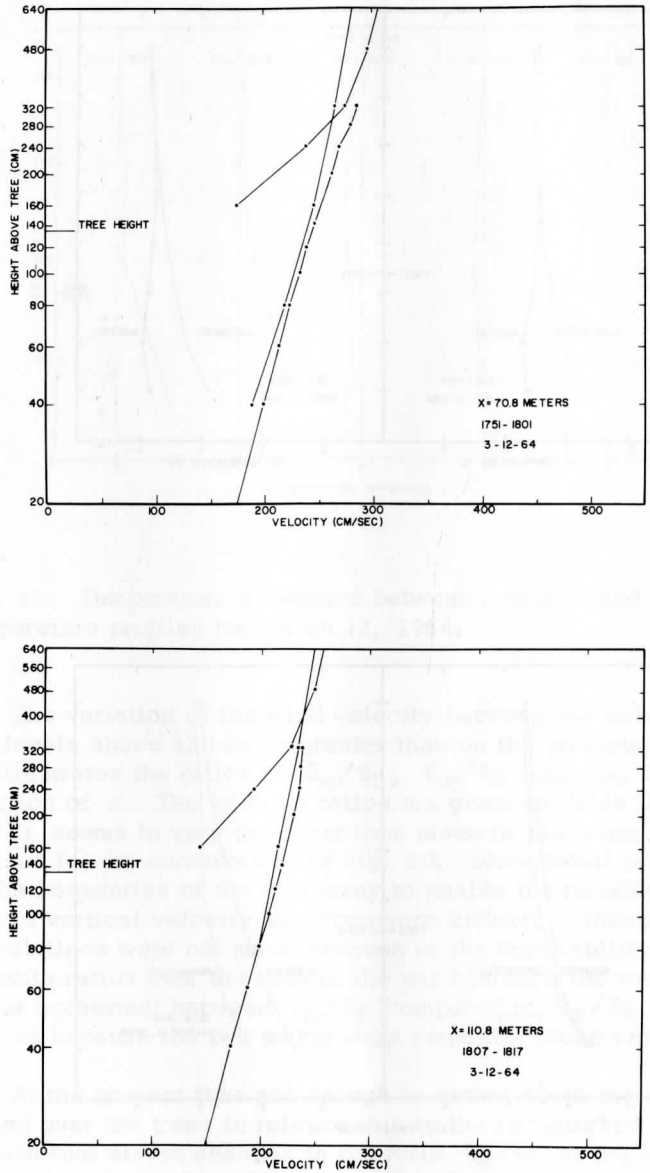

Fig. 16g. Modified and unmodified wind profiles for March 12, 1964, at x = 70.8 m and 110.8 m.

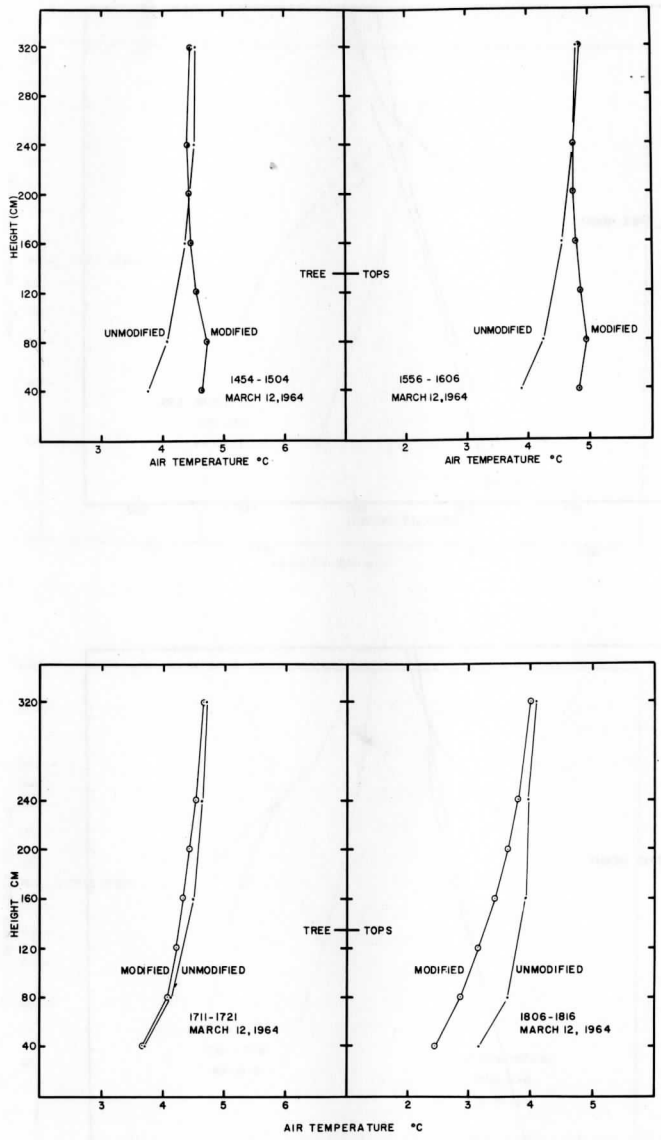

Fig. 17. Modified and unmodified air temperature profiles for March 12, 1964.

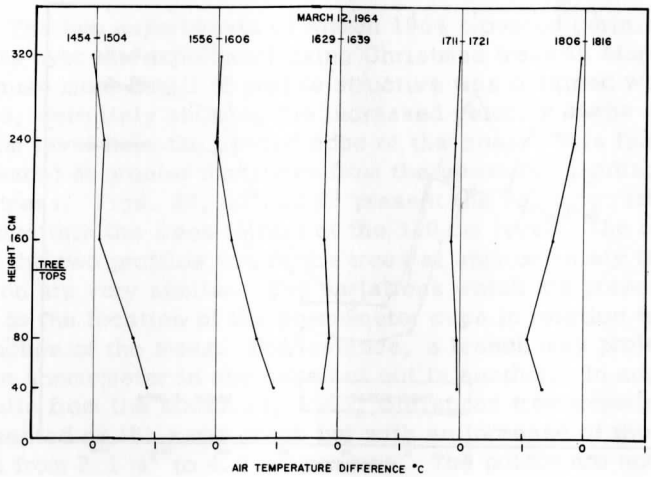

Fig. 18. Temperature difference between modified and unmodified temperature profiles for March 12, 1964.

The variation of the wind velocity between the three masts at the levels above 320 cm is greater than on the previous day. Fig. 19 illustrates the ratios of $\bar{u}_m/\bar{u}_f$, $\bar{u}_m/\bar{u}_R$ and $\bar{u}_m/\bar{u}_{640}$ as a function of x. The velocity ratios are given in Table IX. Again $\bar{u}_m/\bar{u}_f$ seems to vary the least from place to place and accordingly is used for the construction of Fig. 20. More detail is required at the boundaries of the tree array to enable the reliable calculation of vertical velocity and momentum budgets. These interesting calculations were not made because of the unreliability of the mean velocity ratios over the path of the wind through the trees. The better agreement between $\bar{u}_m/\bar{u}_f$ compared to $\bar{u}_m/\bar{u}_R$ and $\bar{u}_m/\bar{u}_{640}$ may be because the two masts were generally close together.

At the present time not enough is known about the mean flow in and over the trees in relationship to the undisturbed flow to be certain that abrupt changes in the ratio $\bar{u}_m/\bar{u}_f$ at the leading and downwind edges of the trees are not real.

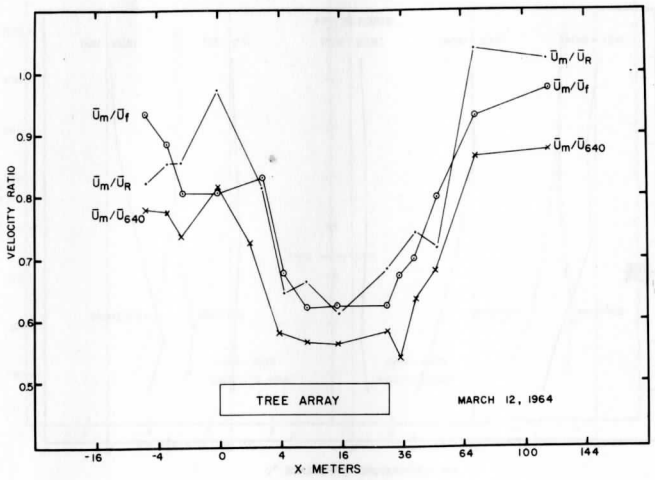

Fig. 19. Velocity ratios as a function of position, March 12, 1964.

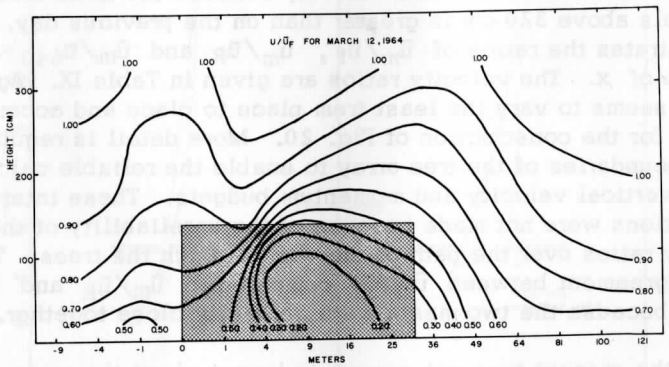

Fig. 20. Velocity ratio distribution with height and position compared to fixed mast for March 12, 1964.

3.4. Conclusions

The two experiments of March 1964 provided certain improvements over the experiment using Christmas trees in March 1963 because more detail of profile structure was obtained within the trees, definitely showing the increased velocity of the wind at the 20 cm level near the upwind edge of the trees. This feature disappeared at greater distances from the upwind or leading edge of the trees. Figs. 21, 22 and 23 present the velocity ratio of the wind within the trees to that at the 320 cm level. The results show that the two profiles within the trees at approximately the same location are very similar. The variations which are present could be due to the location of the anemometer cups in relation to individual branches of the trees. For instance, a branch may project closer to an anemometer in one case but not in another. In addition, results from the March 21, 1963, Christmas tree experiment are presented on the same graph but with an increase of the specific area from 2.1 m^2 to 4.0 m^2 per tree. The points are not as numerous with height within the trees but do show good agreement with the profiles at a smaller specific area. One may conclude that decreasing the specific area did not appreciably alter the wind profile and that a specific area of 4.0 m^2 per tree was modifying the wind structure within the trees to the maximum amount possible. This was also illustrated by results of the bushel basket experiment of February 24, 1961, where a decrease of the specific area from 0.8 m^2 to 0.4 m^2 did not significantly alter the wind profile as z_0 went from 6.0 cm to 4.0 cm compared to the charge of z_0 from 6.0 cm to 1.2 cm for a specific area change of 0.8 m^2 to 1.5 m^2 per bushel basket. On this basis there might be little gained by using a specific area less than 4 m^2 per tree. Fig. 24 shows that the undisturbed profile wind structure on March 11 and 12, 1964, were similar. These ratios are the mean of all the ten-minute runs referred to the 640 cm level.

3.5 Recommendations

The wind profiles within the trees appear to be reliable and reproducible. The relationship between the wind profile in and above the trees to the remote wind profile is very poor. This is also apparent from the results of March 23, 1963, but not as strongly as in the present results. The experiment of 1963 was carried out under much more favorable conditions.

Future experiments should be done hopefully under better fetch conditions but with an anemometer mast up to 640 cm together with

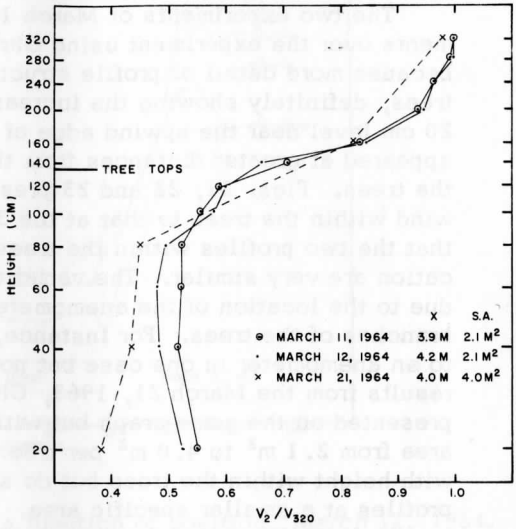

Fig. 21. Comparison between results of March 11 and 12, 1964, and March 21, 1963, at x ≈ 4 meters.

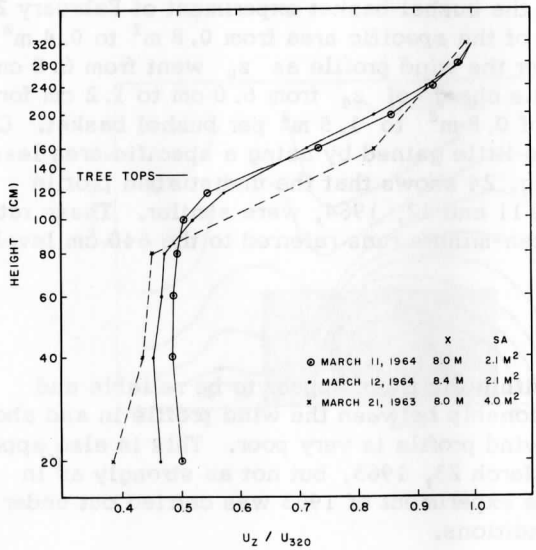

Fig. 22. Comparison between results of March 11 and 12, 1964, and March 21, 1963, at x ≈ 8 meters.

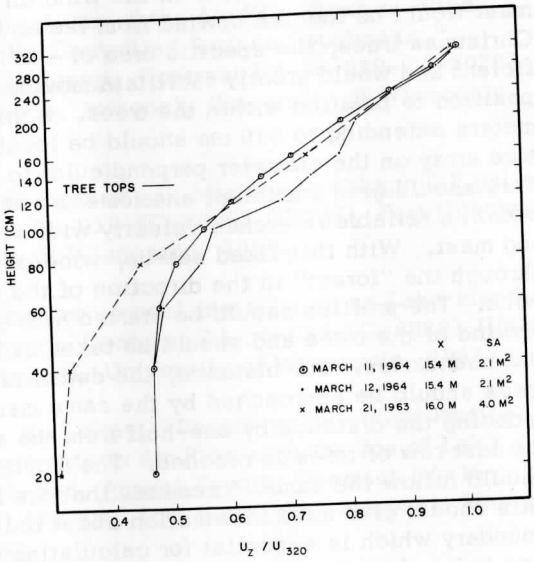

Fig. 23. Comparison between results of March 11 and 12, 1964, and March 21, 1963, at $x \approx 16$ meters.

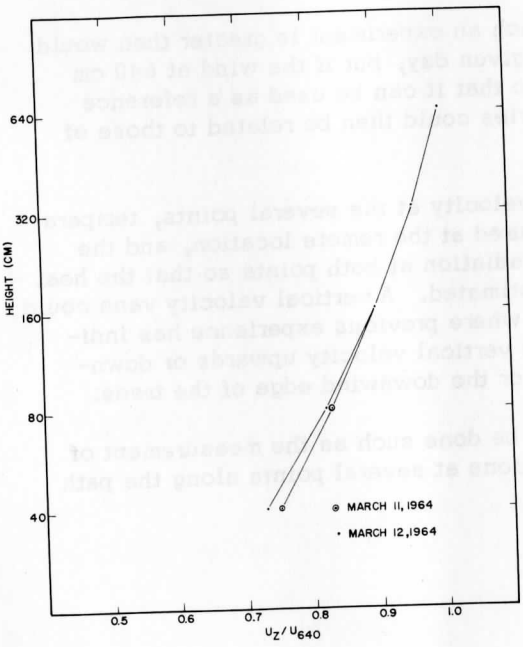

Fig. 24. Comparison between March 11 and 12, 1964, of the unmodified velocity ratios.

the temperature profile located at the center of the circular array so as to be less dependent on the wind direction. Again a remote mast would be located upwind from the array. Using similar Christmas trees, the specific area of 4 m^2 per tree would be sufficient and would greatly facilitate moving the equipment from position to position within the trees. A third mast with 5 anemometers extending to 640 cm should be located on the edge of the tree array on the diameter perpendicular to the wind direction. This should give sufficient anemometers at 320 and 640 cm to obtain a reliable reference velocity with which to compare the moving mast. With this fixed set-up, wind profiles should be obtained through the "forest" in the direction of the wind and normal to the wind. The profiles should be started from a distance at least 15 m upwind of the trees and should be taken at least twice as often at the boundaries. For instance, the downwind edge from within the trees should be approached by the same manner as the upwind edge reducing the distance by one-half from the center of the trees until the last row of trees is reached. The moving-away from the trees should follow the same increments that the boundary was approached. This should give more information about the transition at the boundary which is essential for calculating the vertical velocities induced by the trees.

The time required for such an experiment is greater than would be generally available on a given day, but if the wind at 640 cm is known sufficiently well so that it can be used as a reference then the results from one series could then be related to those of another series.

In addition to the wind velocity at the several points, temperature profiles should be measured at the remote location, and the center of the trees with net radiation at both points so that the heat budget of the trees can be estimated. A vertical velocity vane could also be used at those points where previous experience has indicated there should be a large vertical velocity upwards or downwards such as at the upwind or the downwind edge of the trees.

Other experiments could be done such as the measurement of wind and temperature fluctuations at several points along the path of the wind through the trees.

3.7 References

Kutzbach, J. E., "Investigations of the Modifications of Wind Profiles by Artificially Controlled Surface Roughness," pp. 71-114 of Annual Report, Contract DA-36-039-SC-80282 (USEPG, Fort Huachuca, Arizona), University of Wisconsin, 1961.

Lettau, H. H., "Research Problems in Micrometeorology," Final Report, Contract DA-36-039-SC-80063 (USEPG, Fort Huachuca, Arizona), University of Wisconsin, 1959.

Stearns, C. R., "Micrometeorological installation on Lake Mendota," pp. 7-46, Final Report, Contract DA-36-039-SC-80282 (USEPG, Fort Huachuca, Arizona), University of Wisconsin, 1962.

Stearns, C. R., and H. H. Lettau, "Report on Two Wind Profile Modification Experiments in Air Flow over the Ice of Lake Mendota," pp. 115-138, Annual Report, Contract DA-36-039-AMC-00878 (USAERDA, Fort Huachuca, Arizona), University of Wisconsin, 1963.

Scanner's note:

This page is blank.

4

Preliminary Note on the Effect of Terrain-Slope on Low-Level Jets and Thermal Winds in the Planetary Boundary Layer

H. Lettau

Department of Meteorology
University of Wisconsin

Abstract: The conventional explanation of nocturnal low-level jetstreams in the Central United States is that they are an effect of the daily cycle of solar heating and the resulting diurnal variation in eddy viscosity and internal friction. The supergeostrophic speed of the boundary layer maximum is assumed to be due to an inertia oscillation which begins when in the late afternoon the vertical mixing decreases, so that maximum overshoot occurs around midnight. However, this does not explain why low-level jets appear more frequently in certain geographic areas (such as Kansas and Nebraska) and are less pronounced in other similar regions. It is suggested that an additional factor favoring low-level jet stream development at night-time is a large-scale terrain-slope at which the daily cycle of solar heating sets up a systematic diurnal variation of the thermal wind. For extended slopes of suitable orientation a significant enforcement of the conventional mechanism will result. This effect is demonstrated by deriving a closed solution for, and computation of, the distortion of Ekman profiles caused by a harmonically varying thermal wind in the planetary boundary layer, as produced by solar heating of sloping ground. Certain consequences of the concept are discussed.

4.1 Introduction

A remarkable feature of atmospheric boundary layer structure is the occasional occurrence of levels with surprisingly high wind

velocity. In the vertical profile of horizontal air motion we can sometimes find an absolutely and relatively sharp velocity peak only a few 100 m above ground, i.e., well below the top of the total layer of frictional influence which, normally, is about 1,000 m thick. Such wind profile maxima appear to be best developed in certain parts of the central United States, during summertime, at the middle of the night, and about 300 to 500 m above ground. Unusually detailed and accurate wind profile measurements in the lowest 1,500 m were obtained, around the clock, during well-defined weather situation with southerly air flow, within the framework of the "Great Plains Turbulence Field Program" held in 1953 at O'Neill, Nebraska; reference is made to Lettau and Davidson (1957). Barad (1961) finds that these measurements provide still the best illustration of the development of the phenomenon, because bi-hourly sequences of wind profile data over flat Prairie country throughout several days and nights in August and September were obtained. Section 6.1 of Volume I of Lettau and Davidson (1957) contains a series of graphs which show, at the peak of the development around local midnight, a south component of air motion of 24 m/sec at about 400 m above the ground, while no more than about 12 m/sec were found about 300 m above as well as below the level of maximum speed.

In one of the earliest studies of the phenomenon, on the basis of routine pilot-balloon data, Means (1944, 1952) had introduced the descriptive term "low-level jet stream," and suggested its importance, and possible causal relationship with squall lines and severe weather types east of the Rocky Mountains. Pitchford and London (1962) have shown that there seems to be indeed a direct relationship between the occurrences of low-level jets and nocturnal thunderstorms over the Midwest United States. Gerhardt (1962) discusses a development of a nocturnal low-level jet as recorded by anemometers on the 1400-foot tower near Dallas, Texas.

In his interesting discussion, Barad (1961) summarizes other practical implications of strong low-altitude jet streams, including effects on the landing maneuvers of airplanes, parachute drops of men or material, rocket launching, etc. This special wind profile structure may also be responsible for "blow-ups" of forest fires.

Any theoretical model of the mechanism of the low-level jet has, first of all, to explain the fact that the peak velocity is definitely and considerably super-geostrophic. That is to say that the wind speed exceeds greatly the value which would be there when pressure gradient and Coriolis forces were in equilibrium, i.e., in absence of frictional forces. In the above-quoted example with

peak velocity of 24 m/sec at 400 m above the ground at O'Neill, Nebraska, the geostrophic wind was only about 12 to 14 m/sec at this level. A basic theory of the phenomenon was presented by Blackadar (1957). Assuming that the horizontal pressure gradient remained constant in time and space, the mechanism for generating the low-level jet was seen in the diurnal heating and cooling of the atmosphere at the earth's surface, and the resulting cycle of intensity of convective turbulence and/or vertical mixing. Convection is strong during daytime and serves to increase the frictional forces. If convection dies out in the late afternoon, the frictional forces decrease, and the upper layers are no longer sapped by contributions to the momentum loss by frictional surface drag. The wind aloft therefore speeds up, which means the beginning of the low-level jet formation. Following Barad's (1961) summary review of Blackadar's concepts, an analysis of the balance of forces governing the local time changes of horizontal momentum shows that such a process, once started, tends to build up and eventually to overshoot. Thus, when the frictional force due to convection and mixing drops from a large value to a small one, the wind enters a cycle that can carry it to a higher speed than it would have reached if the friction had been small all the time. As in any oscillation, the overshoot then tends to correct itself, and the wind dies down again. The time-scale of such an inertia oscillation depends on geographic latitude, and in the Central United States it may very well be that once the process has started with the initial acceleration in the late afternoon, the overshoot will culminate around midnight.

Essentially, the development of low-level jets has thus been attributed by Blackadar to the same basic mechanism which produces the normal or regular diurnal variation of wind speed in the atmospheric boundary layer. As early as 1841, Espy suggested that convection could be the cause of the opposite trends in diurnal variation of wind speed in the lower versus the upper portion of the frictional layer; later, in 1883, Koeppen added more detail, and Wagner (1936) showed that the layer of daytime maximum of wind speed which corresponds only to the lowest 10 to 20 percent of the atmospheric boundary layer, coincides with the region where eddy viscosity generally increases with height. In the remaining 80 to 90 percent, the wind is weakest at daytime and strongest at night. Incidentally, this structure of the representative vertical distribution of eddy viscosity was accepted by Rossby and Montgomery (1935) and also by Lettau (1962, b) for a theoretical model of generalized wind spirals in the barotropic boundary layer.

For an example of actual data on diurnal variation of wind speed in the lower atmosphere, references can be made to Lettau and Haugan (1960). Blackadar's (1957) contribution to the basic Espy-Koeppen theory as reformulated by Wagner (1936) was the explanation of the super-geostrophic nature of the nighttime wind maximum in the upper portion of the atmospheric boundary layer. Barad (1961) has provided an excellent illustration of this mechanism but shows that the oscillations in both wind speed and direction for real jet and theoretical model conform only in some respects. However, even though Blackadar's model is strongly simplified, it must be said that the essential features of low-level jet development are correctly predicted. Only certain additional aspects are left to be explained, essentially in the form of a refinement of the basic theory.

It is evident that the above theoretical model should apply to the atmosphere above any continental region, perhaps, with the exception of the equator where the Coriolis force vanishes. The only prerequisites are a steady and significant horizontal pressure gradient force, clear skies, and a strong summer sun which produces sufficiently strong diurnal cycles of convective turbulence. If we accept this model, then it is hard to explain why Pitchford and London (1962) have found such a sharp and well-pronounced maximum-region of occurrence of low-level jets in the Midwest United States, along a narrow South-to-North strip located about 100 km west of a line connecting Omaha, Nebraska, with Wichita, Kansas. Why is this relatively narrow region so significantly preferred by frequency of low-level jets? Blackadar's basic theory does not supply a satisfactory answer to this question.

It is known from climatology that during summertime the Great Plains region is dominated by southerly flow due to a quasi-permanent low-pressure system in the Rocky Mountain region. Since the air to the west is relatively warm, the horizontal pressure gradient (which is from west to east at the earth-air interface, i.e., at about the 950 to 900 mb level) decreases with elevation. The nighttime pilot-balloon swarm acsents during the O'Neill tests in 1953 gave clear evidence of the decrease of geostrophic speed aloft in that only a few hundred meters above the extreme nocturnal south-wind maximum the air-flow tended to be towards the south. The picturesque constellations formed by the lamp-carrying balloons after the swarm had passed through levels of about 1,500 m, i.e., after stopping the rush towards north and even beginning to drift back towards the south, was an impressive spectacle and will always be remembered by the author or other eye-witnesses of these tests. These observational facts may indicate that perhaps certain systematic diurnal

variations of the horizontal pressure gradient were involved in the low-level jet development. This possibility will be discussed in the following section.

4.2 General Remarks on Thermal Winds in the Atmospheric Boundary Layer

The purpose of this preliminary note is to demonstrate how, in principle, a periodically oscillating horizontal density gradient may affect the structure of the frictional wind spiral in the atmospheric boundary layer. Therefore, it will suffice to restrict the discussion to an otherwise conveniently simple atmospheric boundary layer model. It will be assumed that frictional forces follow from an apparent viscosity of the lower atmosphere which is independent of height and constant in time, and that inertia terms in the equation of motion are unimportant. When, under these conditions, the horizontal pressure gradient would be constant, the resulting steady-state solution of the horizontal equation of motion results in a wind profile known as the Ekman spiral. Hesselberg (1954) has discussed the possible extension of the Ekman solution to include height-dependent pressure gradient, based on his earlier work in co-authorship with Sverdrup which dates back to 1915. It is obvious that a change of the horizontal pressure gradient with height will cause a corresponding dependency of both the geostrophic and actual wind vectors on elevation. The first derivative with respect to height of the geostrophic wind defines the vector of thermal wind. The name illustrates a result easily confirmed by an elementary transformation of the geostrophic wind equation, using the hydrostatic equation and the equation of state, which demonstrates that primarily responsible for a change of geostrophic wind with height is an existing horizontal temperature gradient.

In a discussion of climatological averages of boundary layer profiles, Johnson (1962) has shown that a semi-permanent thermal wind prevails over the continental United States and that it will often mask the effects of frictional forces, resulting in interesting distortions of normal wind spirals.

To facilitate the following discussion, let us define the "shear component" versus the "advective component" of the thermal wind. The basis or reference for the distinction is the vector of geostrophic motion at the level of the earth/air interface. This nomenclature is illustrated in Fig. 1 using a finite vector difference between the geostrophic values at height zero, and z_1 which can be taken as the top of the friction layer.

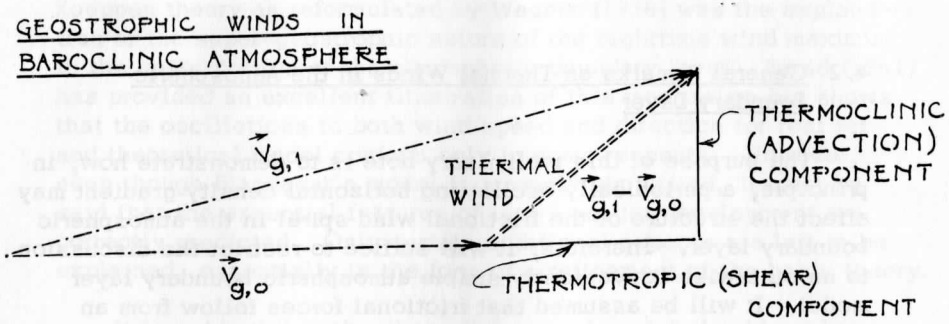

Fig. 1. Illustration of nomenclature for the definition of the two significant components of the thermal wind, using the vector of geostrophic wind at the lower boundary as reference or datum value.

When reference is made to the "Glossary of Metecrology" (published by the American Meteorological Society in Boston, 1959) a numerical weather analysis model with zero values of geostrophic advection is usually referred to as "equivalent barotropic" while the term "thermotropic model" is used to indicate either constant thermal wind or a thermal wind which changes intensity but not direction between any levels. A new terminology is suggested here with the distinction between a "thermotropic component" versus the "thermoclinic component" of the thermal wind, as an alternative to the nomenclature of geostrophic shear versus geostrophic advection component. This permits precision and conciseness of wording inasmuch as a constant thermal wind can be represented either a constant thermoclinic component, or a constant thermotropic component, or a composite of the two. These terms are illustrated in Fig. 1, and utilized in Fig. 2.

For the Ekman model of internal friction, it follows that the distortion of the spiral by a constant thermal wind can readily be computed, by the superposition of a suitably chosen linear function on the original solution. Certain mathematical complications enter only if the thermal wind varies with height, i.e., when the horizontal pressure gradient is at least a second order or parabolic function of elevation. Examples of computations for both constant thermotropic and constant thermoclinic components of the thermal wind are illustrated in Fig. 2. It can be seen that the degree of

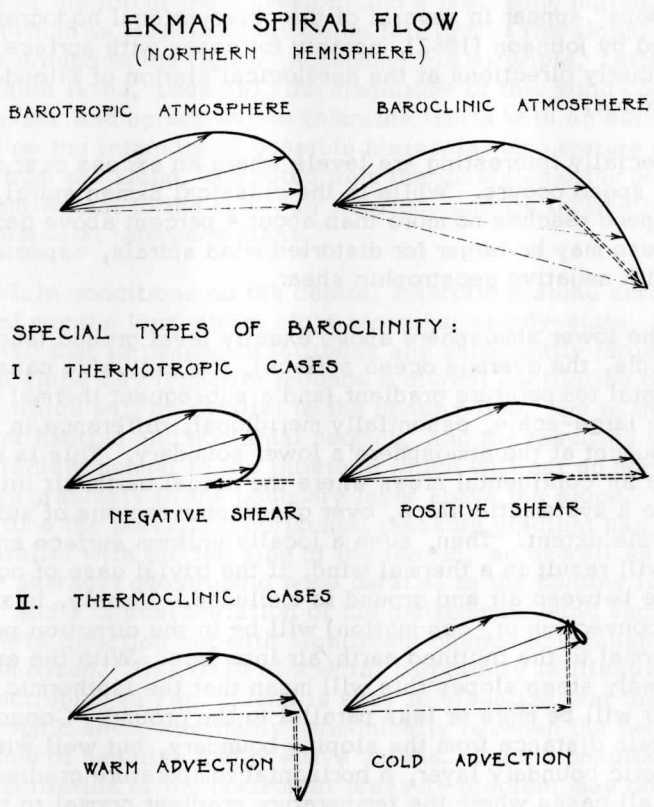

Fig. 2. Ekman spiral distortions by constant thermal wind, for the four elementary types of baroclinity using nomenclature as defined in Fig. 1. Note that all spirals are constructed for conditions of the Northern Hemisphere.

deformation of the original Ekman spiral is greatly dependent on magnitude and direction of the thermal wind, in relation to the surface-geostrophic wind vector. Negative geostrophic shear and/or warm-air advection tend to influence predominantly the directional changes of the actual wind profile, while positive geostrophic shear and cold-air advection affect more the speed distribution. The directional change of the geostrophic wind vector in cold-air advection has the opposite sign in comparison with frictional turning, and may cancel, or overrule the latter, which can result in a "loop"

as shown by the spiral at the lower right of Fig. 2. Actually, such "loops" appear in several of the observational hodographs presented by Johnson (1962), notably for cases with surface wind from northerly directions at the aerological station of Ellendale, North Dakota.

Especially interesting are levels where an excess over geostrophic speed occurs. While in the classical Ekman spiral, the actual speed reaches no more than about 4 percent above geostrophic, this excess may be larger for distorted wind spirals, especially for cases with negative geostrophic shear.

In the lower atmosphere above exactly level ground (such as, for example, the average ocean surface), the exclusive cause of a horizontal temperature gradient (and a subsequent thermal wind) will be a large-scale, essentially meridional, difference in the energy budget at the atmosphere's lower boundary. This is not true any more for continental areas where the actual earth/air interface may have a systematic slope, over geographic regions of sufficiently large-scale extent. Then, even a locally uniform surface energy budget will result in a thermal wind, if the trivial case of no heat exchange between air and ground is excluded. Namely, heat diffusion (convection or, conduction) will be in the direction perpendicular or normal to the inclined earth/air interface. With the exception of extremely steep slopes this will mean that the isothermic surfaces in the air will be more or less parallel to the ground. Consequently, at a certain distance from the sloping boundary, but well within the atmospheric boundary layer, a horizontal temperature gradient must exist in all cases where the temperature gradient normal to the boundary is different from zero. For average daytime conditions, the air will be getting cooler, and, correspondingly, for average nighttime conditions the air will be getting warmer, if one moves away from a point at the boundary in a strictly horizontal direction parallel to the fall-line of the slope.

A highly interesting example of a persistent thermal wind due to a large-scale terrain slope can be found in the atmosphere over the central antarctic plateau. According to Dalrymple, Lettau, and Wollaston (1963), the region surrounding the South Pole (up to distances of more than 200 km) represents an inclined plane with a slope of approximately 1 : 560 ascending in the direction of the 152th meridian East of Greenwich. These authors have shown that during the antarctic winter night, the vertical profiles of air motion throughout the inversion layer (which includes the lowest 800 m of atmosphere) can be described by the superposition of a frictional spiral

effect (which means a fixed rate of turning relative to the wind vector at the top of the inversion) and a prevailing horizontal thermal wind (which is perpendicular to the fall line of the slope, with the higher ground to the right). According to Dalrymple, Lettau and Wollaston (1963, page 36), the magnitude of this wind component is 6 m/sec and agrees within tolerable limits with an estimate based on the intensity of possible horizontal temperature gradients away from the slope, computed from the inversional temperature gradient normal to the snow/air interface and its inclination against the horizontal reference plane.

While conditions on the central antarctic plateau during the several months long winter night are quasi steady-state, it must be expected that in temperate latitudes any sufficiently large-scale terrain slope may primarily produce a diurnal oscillation of thermal winds which will be parallel to the contour line, due to the cycle of solar heating and nocturnal cooling, and the resulting temperature gradient normal to the interface which will set up horizontal density gradients in the boundary layer above the slope. If at the same time the prevailing horizontal pressure gradient happens to run parallel with the fall line of the terrain, an overall (or, 24-hourly average) geostrophic wind parallel to the contour line will exist, and a diurnal variation of the geostrophic wind vector without change in direction but with significant change of intensity will be superimposed. This case of special baroclinity is illustrated under "thermotropic" in Fig. 2, and is easy to visualize that the actual geostrophic shear alternates harmonically between the two depicted extremes of negative and positive values. Such a peculiar see-saw oscillation of the horizontal pressure gradient may occur over sloping terrain so that the pressure gradient remains at all hours of the day parallel to the fall line. This will produce in the lower atmosphere a diurnal variation of geostrophic wind and shear, parallel to the contour lines on the slope, so that the extreme value of surface-level geostrophic speed happens either during daytime, or at nighttime. Which one of these two alternatives occurs will depend on the orientation of the slope. For example, with generally southerly geostrophic winds above an east-facing (or westwards ascending) terrain (such as the slope between the Mississippi River and the Rocky Mountains), the diurnal cycle of solar heating will tend to weaken the geostrophic south component at the surface (900 to 850 mb level) during daytime, and strengthen it during the nocturnal cooling period. If the same generally southerly flow would be assumed to exist on an eastward ascending (or west-facing) slope (as for certain regions between the Mississippi and the Appalachians) the diurnal cycle of surface-geostrophic speed would be reversed

in comparison with the westward ascending slope. Due to thermal winds set up by surface heating, the process is in both cases restricted to the atmospheric boundary layer. It shall be investigated in the following section how a frictional wind spiral of the Ekman type is actually distorted by such diurnal cycles of thermal winds, as a necessary supplement to the steady-state conditions pictured on Fig. 2.

In this connection it may be recalled that Bleeker and Andre (1951) have discussed the diurnal variation of precipitation, especially its relative high occurrence at summer nights in the region east of the Rocky Mountains, in terms of topographical effects. They pictured the region as a broad central plain framed by slopes at the western and eastern meridional borders, i.e., due to the Rocky Mountains, and the Appalachians, respectively. They apparently think in terms of a gigantic valley-circulation of a continent-wide scale. However, Bleeker and Andre did establish not much more than the fact that a large-scale low-level wind convergence coincides with the area of precipitation activity, which is insufficient to explain a causal relation. In the following an entirely different aspect of circulations induced by heating of sloping terrain will be discussed.

4.3 Mathematical Model of Ekman Spiral Flow for Harmonically Varying Thermal Wind

Let u and v denote the two components of the vector of horizontal air motion, $f = 2\omega \sin \phi$ = Coriolis parameter (with ω = earth's angular speed of rotation, and ϕ = geographic latitude), and let U and V denote the two components of the horizontal vector of geostrophic motion. When p = atmospheric pressure, and ρ = air density, the defining equations are

$$U = -(\partial p/\partial y)/\rho f \; ; \qquad V = (\partial p/\partial x)/\rho f \; . \tag{1}$$

For convenience let us assume that at all times $\partial p/\partial y = 0$, while $\partial p/\partial x$ has a mean value, and, due to diurnal cycles in heating and cooling at a sloping plane boundary (with the fall line parallel to the x-direction) a harmonic variation of frequency ω. Here we disregard the extremely slight difference between the mean solar and the sidereal day. Then, we have a strictly thermotropic case of baroclinity in which the geostrophic wind is completely described by

$$V = \bar{V} + \Delta V \cos \omega t \; , \tag{2}$$

where t = time, and the over-bar indicates a 24-hourly average. When reference is made to the discussion in Section 4.2, it can be concluded that $\bar{V}$ and also ΔV may either be constants, or linear functions of height (z). In the following, $\bar{V}$ will be assumed independent of height, and the amplitude ΔV of the thermotropic component a linear function of height.

Let a raised dot indicate a partial derivative with respect to time, while a prime denotes a partial derivative with respect to height. Assuming that inertia accelerations are unimportant, the equations of horizontal motion are, for $\partial p/\partial x = 0$,

$$u^{\cdot} - (v - V)f = Ku'', \tag{3a}$$

$$v^{\cdot} + uf = Kv'', \tag{3b}$$

where K is an apparent viscosity which will be assumed to be independent of time and height. Equations (3a, b) express equilibrium between local accelerations, pressure gradient acceleration, Coriolis acceleration, and frictional acceleration.

The problem will be to find forms $u(z, t)$ and $v(t, z)$ which satisfy (3a, b), which are harmonically varying time functions of frequency ω according to (2), and also satisfy the boundary condition of zero-motion at $z = 0$, with an approach to geostrophic motion (i.e., $u \to 0$, $v \to V$) at sufficiently large distance from the ground. Defining a set of height-functions ($\bar{u}$, u_1, u_2, $\bar{v}$, v_1, v_2) in an entirely formal manner, we may write

$$u(z, t) \equiv \bar{u}(z) + u_1(z) \cos \omega t + u_2(z) \sin \omega t, \tag{4a}$$

$$v(z, t) \equiv \bar{v}(z) + v_1(z) \cos \omega t + v_2(z) \sin \omega t, \tag{4b}$$

so that u_1, u_2, v_1, v_2 are amplitudes, and $\bar{u}$, $\bar{v}$ mean values. It follows upon differentiation that

$$u^{\cdot} = -\omega u_1 \sin \omega t + \omega u_2 \cos \omega t, \tag{5a}$$

$$u' = \bar{u}' + u_1' \cos \omega t + u_2' \sin \omega t, \tag{5b}$$

$$u'' = \bar{u}'' + u_1'' \cos \omega t + u_2'' \sin \omega t, \tag{5c}$$

and a similar system for $v^{\cdot}$, v', v'', according to (4b).

Taking the 24-hourly mean of (3a, b) produces the classical Ekman equations,

$$-(\bar{v} - \bar{V})f = K\bar{u}'' \; ; \qquad \bar{u}f = K\bar{v}'', \tag{6}$$

which are solved by the well-known Ekman spiral expression,

$$\bar{u} = \bar{V}e^{-\eta}\sin\eta \; ; \qquad \bar{v} = \bar{V}(1 - e^{-\eta}\cos\eta), \tag{7}$$

where η is an abbreviation for $z\sqrt{f/2K}$. The previously stated boundary conditions are satisfied by (7). Upon introducing (2) and (4a, b) into (3a, b), and consideration of (6), a comparison of factors which accompany the two harmonic time functions ($\sin\omega t$, and $\cos\omega t$, respectively), results directly in the following four equations,

$$\omega u_2 - f(v_1 - \Delta V) = K u_1'', \tag{8a}$$

$$-\omega u_1 - f v_2 = K u_2'', \tag{8b}$$

$$\omega v_2 + f u_1 = K v_1'', \text{ and} \tag{8c}$$

$$-\omega v_1 + f u_2 = K v_2''. \tag{8d}$$

Now, eliminate u_1 in equations (8b) and (8c), whereupon,

$$v_2(\omega^2 - f^2) = K\omega v_1'' + K f u_2''. \tag{9a}$$

Differentiate (8d) twice partially with respect to height z, multiply the result by K, whereupon, after rearrangement of terms,

$$K f u_2'' = K\omega v_1'' + K^2 v_2''''. \tag{9b}$$

Thus, after elimination of u_2'' in (9a) and (9b), and slight rearrangement of terms,

$$v_2(\omega^2 - f^2) - K^2 v_2'''' = 2K\omega v_1''. \tag{10a}$$

In an exactly corresponding manner, u_2 can be eliminated in equations (8a) and (8d); then, differentiate (8c) twice with respect to z, and eliminate u_1'' from the resulting equations, whereupon

$$v_1(\omega^2 - f^2) + f^2\Delta V - K^2 v_1'''' = -2K\omega v_2''. \tag{10b}$$

It can readily be verified that equations (10a, b) are satisfied by the two expressions

$$v_1 = -\Delta V^*(1 - e^{-\xi}\cos\xi), \tag{11a}$$

$$v_2 = \Delta V^* e^{-\xi}\sin\xi, \tag{11b}$$

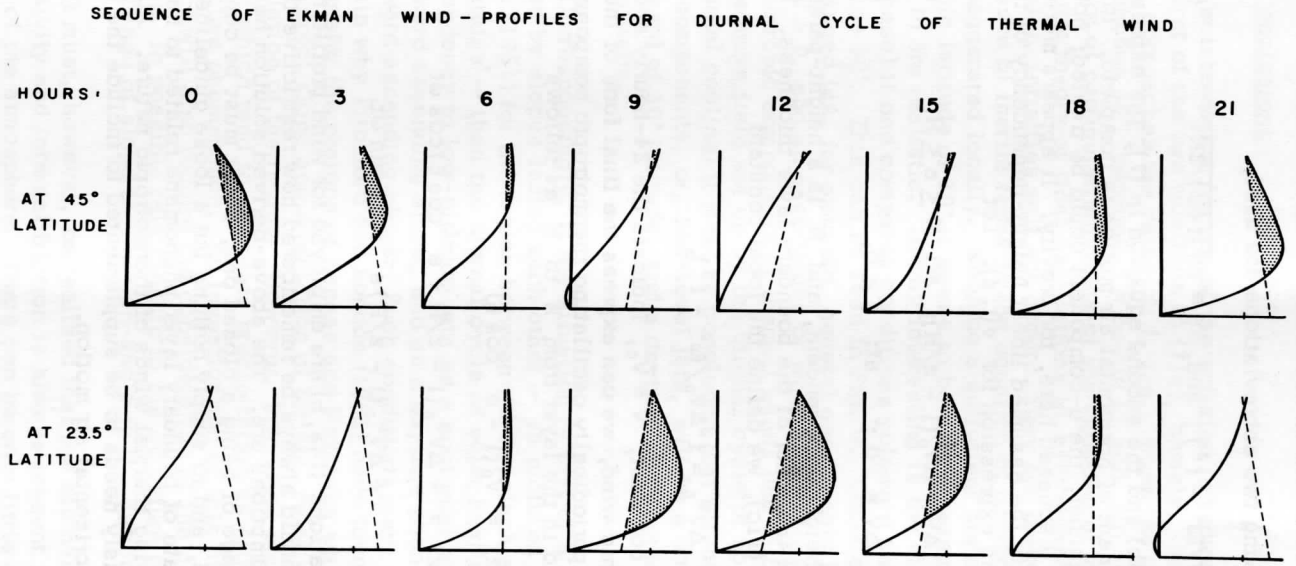

Fig. 3. Example of a 3-hourly sequence of computed diurnal variation of vertical profiles of air motion, of an extended Ekman-type, assuming harmonically varying geostropic shear (dashed lines) or, height-independent but time-varying thermal wind in the planetary boundary layer. Note the varying intensity of supergeostrophic component, and phase-differences poleward and equatorwards of 30° latitude.

where the following two abbreviations are used,

$$\Delta V^* \equiv f^2 \Delta V/(\omega^2 - f^2)\,; \text{ and, } \xi \equiv z\sqrt{(f+\omega)/2K}. \qquad (11c)$$

Together with (4b) and the second equation in (7), the expression for the v-component of horizontal air motion is complete. In a corresponding manner, the u-component could be treated; however, this will not be discussed here, for brevity. It appears more important to specify the assumed linear height-dependency of the amplitudes in the expression for $v(t, z)$. Let

$$\Delta V = \Delta V_0 (1 - z/H); \quad \text{at:} \quad 0 \leq z \leq H, \qquad (12a)$$

$$\Delta V = 0\,; \quad \text{at:} \quad z \geq H, \qquad (12b)$$

where ΔV_0 is height-independent, and H is a height-parameter which will be of the order of the boundary layer thickness. If, in agreement with (11c), we define the local constant

$$\Delta V^*_0 = f^2 \Delta V_0/(\omega^2 - f^2), \qquad (13)$$

and let another constant, $\bar{V} = \bar{V}_0$, indicate the 24-hourly average of the geostrophic wind, we can express the final form of the profile distortion by a periodically oscillating thermotropic component of the thermal wind in the layer from z to H as follows

$$\bar{v}(z) = \bar{V}_0 (1 - e^{-\eta} \cos \eta)\,, \qquad (14a)$$

$$v(z, t) - \bar{v}(z) = -\Delta V^*_0 (1 - z/H + e^{-\xi} \cos \xi) \cos \omega t + \Delta V^*_0 (1 - z/H) e^{-\xi} \sin \xi \sin \omega t. \qquad (14b)$$

Before equations (14a, b) are employed for wind profile representation, it should always be remembered how restrictive the underlying assumptions are. The above-derived solution has the obvious advantage of being a closed one, but it must be considered to be restricted, and to supply nothing but a loose guideline for the possible estimate of boundary layer phenomena related to harmonically time-varying thermal winds of thermotropic nature. Also, the solution obviously needs to be supplemented to include the u-component of horizontal air motion.

4. Conclusions

An interesting feature of the solution is indicated by (13), or the first of the two relations in (11c), namely, that it breaks down if ω approaches the value of f, i.e., when the geographic latitude approaches 30°, because $f = 2\omega \sin \phi$, and $\sin 30° = 1/2$. This feature of particular solutions of the equation of motion is well known from the theory of tidal oscillations in hydrosphere and atmosphere. Actually, infinities will not occur. They are prevented by the appearance of inertia terms in the equation of motion, if any amplitude is exaggerated locally. Keeping a sufficient distance from the geographic latitude of 30° it seems to be safe to assume that equations (14a, b) are realistic. Highly interesting is the difference in sign (or phase) if one compares conditions poleward and equatorward of latitude 30°. This can be seen in Fig. 3. Other conditions being unchanged (as, for example, general geostrophic flow from the south, or, $\bar{V} > 0$, and an east-facing or westward ascending slope with thermotropic components of thermal winds due to the horizontal temperature field set up by the diurnal cycle of solar heating and nocturnal cooling) it must be concluded that strongest supergeostrophic components, or, low-level jets, will be a nocturnal phenomenon poleward of 30° latitude, and a daytime phenomenon equatorwards of 30° latitude.

Correspondingly, if the situation is that of a broad central plain framed by slopes facing each other — as pictured by Bleeker and Andre (1951) for the region between the Appalachians and the Rocky Mountains — then the diurnal cycle of solar heating may produce the tendency to low-altitude jets as a nocturnal phenomenon on the westward ascending slope, and as a daytime phenomenon on the eastward ascending slope. Such conditions may, at least partly, explain why Pitchford and London (1962) have found that low-level jets prefer the regions of Kansas and Nebraska which seem to have the correct slope and orientation of terrain, relative to the general circulation of the region. However, low-level convergences may result which tend to stimulate precipitation as either a daytime or nighttime phenomenon. An investigation of this highly interesting aspect will also require the consideration of the u-component of air motion, in possible relationship to the curvature of the terrain, i.e., the change of slope inclination-angle in the direction of the fall line.

It must, however, be realized that the diurnal variation of eddy diffusivity and internal friction is always present in the boundary layer of the atmosphere. There can be only little chance that the above predicted daytime type of low-level jet can be observed on

eastward ascending slopes of the Central United States in a similar form as the nocturnal type, because at daytime the strong mixing opposes the formation of levels with pronounced and extreme wind maxima. Future investigations of observed wind data will be necessary to verify these aspects of the above developments.

Concerning the theoretical structure, it will be necessary to remove the restriction imposed by the Ekman assumption that $K' = K^{\cdot} = 0$. It can readily be seen from the steady-state solutions resulting in equi-angular spirals — reference is made to Lettau (1962a) — that supergeostrophic speed at certain levels of the spiral solution, i.e., the tendency to low-level jet streams, is enhanced in parts of the frictional layer where $K' < 0$.

In reality there will always be a tendency to a free or inertia oscillation of the wind in the boundary layer, due to the strong daily reduction of eddy diffusivity K from afternoon values to night values, according to Blackadar's (1957) basic theory. This will be superimposed on forced diurnal variations with solar-day period imposed by horizontal density gradients above sloping terrain, provided that the slope is sufficiently large-scale. Additional features are caused by effects of the sign of K', as suggested by Wagner (1936), and the diurnal variation of K' which may be different in different strata of the atmospheric boundary layer. All in all, the complete picture of diurnal wind variations in the lower atmosphere can be highly complicated.

As far as the above-discussed effect of geographic latitude — see Fig. 3 — is concerned, it is perhaps promising to attempt to test its validity by an analysis of aerological stations along one and the same mountain slope which stretches in a meridional direction from tropical to temperate latitudes. For this investigation, the west-facing slopes of the Andes Mountains in South America appear to offer the best opportunities, and a study of available wind data has been started.

5. References

Barad, M.L.: "Low Altitude Jet Streams." Scientif. American, 205, pages 120-131, 1961.

Blackadar, A.K.: "Boundary Layer Wind Maxima and their Significance for the Growth of Nocturnal Inversions." Bulletin Amer. Meteorol. Soc., 38, pages 283 - 290, 1957.

Bleeker, W., and M. J. Andre: "On the Diurnal Variation of Precipitation Particularly over Central United States, and its Relation to Large-Scale Orographic Circulation Systems." Quart. Journal Roy. Meteor. Soc., 77, pages 260-271, 1951.

Dalrymple, P., H. Lettau, and S. Wollaston: "South Pole Micrometeorological Program, Part II, DATA Analysis." Techn. Report ES-7, Earth Sciences Division, QMR and E Command, Natick, Mass., 1963.

Gerhardt, J. R.: "An Example of a Nocturnal Low-Level Jet Stream." Journal Atmosph. Sciences, 19, pages 116-118, 1962.

Hesselberg, T.: "The Ekman Spirals." Archiv. Meteorol., Geoph., and Bioklimat., A7, 329, 1954.

Johnson, W. B., Jr.: "Climatology of Atmospheric Boundary-Layer Parameters and Energy Dissipation, Derived from Gregg's Aerological Survey of the U. S." Section 7 of Final Report, Contract DA-36-039-SC-80282, Univ. of Wisconsin, 1962.

Lettau, H., and B. Davidson, eds.: Exploring the Atmosphere's First Mile, Pergamon Press, New York and London, 1957.

Lettau, H. and D. A. Haugan: "Wind," Section 1 of Chapter 5, in Handbook of Geophysics, MacMillan Comp., New York, 1960.

Lettau, H.: "Equiangular Wind and Current Spirals." Section 8 of Final Report, Contract DA-36-039-SC-80282, Univ. of Wisconsin, 1962(a).

Lettau, H.: "Theoretical Wind Spirals in the Boundary Layer of a Barotropic Atmosphere." 35, Beitr. Phys. d. Atmosph., pages 195-212, 1962(b).

Means, L. L.: "On Thunderstorm Forecasting in the Central United States." Monthly Weather Review, 80, pages 165-189, 1952.

Pitchford, K. L., and J. London: "The Low-Level Jet as Related to Nocturnal Thunderstorms over Midwest United States." Journal Applied Meteorol., 1, pages 43-47, 1962.

Rossby, G-G., and R. Montgomery: "The Layer of Frictional Influence in Wind and Ocean Currents." Mass. Inst. Techn., Meteor Papers No. 3, 1935.

Wagner, A.: "Zur Theorie des Taeglichen Ganges der Wind Verhaeltnisse." Gerlands Beitr. z. Geophys., 47, 172, 1936.

Scanner's note:

This page is blank.

INDEX OF DISTRIBUTION

Commanding General
U. S. Army Materiel Comd
ATTN: AMCRD-RV-A
Washington, D.C. 20315 1

Chief, Rsch & Development
Department of the Army
ATTN: CRD/M
Washington, D.C. 20310 1

Commanding General
U. S. A. Combat Devel. Comd.
ATTN: CDCMR-E
Fort Belvoir, Va. 22061 1

Commanding General
U. S. Continental Army Comd.
ATTN: Recon Br ODCS For Intel
Fort Monroe, Virginia 23351 1

Commanding General
U. S. Army Electronics Comd
ATTN: AMSEL-EW
Fort Monmouth, N.J. 07703 1

Commanding General
U. S. Army Missile Command
ATTN: AMSMI-RRA
Redstone Arsenal, Ala 35809 1

Commanding General
U. S. Army T&E Comd
ATTN: NBC Directorate
Aberdeen Prg Gnd, Md 21005 1

Commanding Officer
U.S.A. Cold Regions R&E Labs
ATTN: Environmental Rsch Br
Hanover, N.H. 03755 1

Commanding General
Natick Laboratories
ATTN: Earth Sciences Div
Natick, Mass. 01762 1

Commanding Officer
U. S. Army Ballistic Rsch Labs
ATTN: AMXBR-B
Aberdeen Proving Gnd, Md 21005 1

Commanding Officer
U.S. Army Ballistic Rsch Labs
ATTN: AMXBR-IA
Aberdeen Provg Gnd, Md 21005 1

Director
U.S. A. Eng Waterways Exp Sta
ATTN: WESSR
Vicksburg, Miss. 39181 1

Director
U. S. Army Elct Labs
ATTN: AMSEL-RD-SM
Fort Monmouth, N.J. 07703 1

Commanding Officer
U.S. Army Elct R&D Actv
ATTN: Met Dept
Ft. Huachuca, Ariz 85613 1

Commanding Officer
U.S. Army Elct R&D Activity
ATTN: Environmental Sciences
Dept
White Sands Msl Range, N.M. 1
88002

Commanding General
U.S. Army Edgewood Arsenal
ATTN: SMUEA-CS-0, Ops Rsch Grp
Edgewood Arsenal, Md. 21010 1

Commanding Officer
U. S. Army Frankford Arsenal
ATTN: SMUFA-1140
Philadelphia, Pa. 19137 1

Commanding Officer
U. S. Army Picatinny Arsenal
ATTN: SMUPA-TV-3
Dover, New Jersev 07801 1

Commanding Officer
U. S. Army Dugway Proving Gnd
ATTN: Meteorology Div
Dugway, Utah 84022 1

President
U. S. Army Artillery Bd
Fort Sill, Okla. 73504 1

Commanding Officer
USA Arty Cbt Developments Agcy
Fort Sill, Okla. 73504 1

Commandant
U. S. Army Arty & Msl School
ATTN: Target Acquisition Dept
Ft. Sill, Okla. 73504 1

Commanding Officer
US Army CDC Comm-Elct Agcy
Fort Huachuca, Ariz. 85613 1

Commanding General
USAEPG
ATTN: C, FTFD
Fort Huachuca, Ariz. 85613 1

Commanding General
Deseret Test Center
Fort Douglas, Utah 84113 1

Commanding General
U. S. Army T&E Command
ATTN: AMSTE-EL
Aberdeen Proving Gnd, Md 21005 1

Commanding General
U. S. Army T&E Command
ATTN: AMSTE-BAF
Aberdeen Proving Gnd, Md 21005 1

Commandant
U. S. Army CBR School
ATTN: Micromet Sec, Lt Col Saunders
Ft. McClellan, Ala. 36205 1

Chief, Comm-Electronics
Department of the Army
ATTN: Elct Sys Directorate
Washington, D.C. 20315 1

Asst CofS for Intel
Department of the Army
ATTN: ACSI-DSRSI
Washington, D.C. 20310 1

Commander
Air Weather Service (MATS)
ATTN: AWSSS/TIPD
Scott AF Base, Ill. 62226 1

Commander
AF Cambridge Rsch Labs
ATTN: CRXL
L. G. Hanscom Field
Bedford, Mass. 01730 1

Commander
USAF Cambridge Rsch Labs
ATTN: CRZW
1065 Main Street
Waltham, Mass 02154 1

Chief of Naval Research
ATTN: CODE 427
Department of Navy
Washington, D.C. 20350 1

Commanding Officer
U. S. Naval Weather Service
U. S. Naval Air Station
Washington, D.C. 20390 1

Officer in Charge
U. S. Naval Weather Rsch Fac
U. S. Naval Air Sta, Bldg R-28
Norfolk, Va. 23501 1

Director
Atmospheric Sciences Programs
National Sciences Foundation
Washington, D.C. 20550 1

Director
Bureau of Rsch & Development
Federal Aviation Agency
Washington, D.C. 20553 1

Chief, Fallout Studies Br
Div of Biology & Medicine
Atomic Energy Commission
Washington, D.C. 20545 1

Office, Asst SECDEF (R&E)
The Pentagon
ATTN: Tech Library
Washington, D.C. 20301 1

Director, Met Systems
Office of Applications (FM)
Natl Aeronautics & Space Adm
Washington, D.C. 20546 1

Chief, U. S. Weather Bureau
24th and M Streets
ATTN: Librarian
Washington, D.C. 20235 1

Robt A. Taft Sanitary Engng Cen
Public Health Service
4676 Columbia Parkway
Cincinnati, Ohio 45202 1

National Cen for Atmospheric Rsch
ATTN: Library
Boulder, Colorado 80301 1

Defense Documentation Center
Cameron Station
Alexandria, Va. 22314 20

Commanding Officer
U. S. Army Biological Labs
ATTN: K. L. Calder
Ft. Detrick, Fredrick, Md.
21701 1

Scientific & Tech Info Agcy
ATTN: NASA Rep (S-AK/DL)
P. O. Box 5700
Bethesda, Md. 20014 1

Commanding General
CDC Experimentation Cen
Fort Ord, Calif. 93941 1

Director, Meteorology Dept
University of Arizona
Tucson, Ariz. 85717 1

Director
U. S. Water Conservation Lab
Agricultural Rsch Svc, USDA
Route 2, Box 816-A
Tempe, Arizona 85281 1

Director
Pac SW Forest & Range Ex Sta
USDA Forest Service, Box 245
Berkeley, Calif. 94704 1

Director, Meteorology Dept
Univ. of California at L. A.
Los Angeles, Calif. 90052 1

Director, U. S. Salinity Lab
P. O. Box 672
ATTN: Dr. Richards
Riverside, Calif. 92502 1

Department of Irrigation
ATTN: Mr. Pruitt
University of California
Davis, Calif. 95616 1

Dept of Agricultural Engng
University of California
ATTN: Dr. F. A. Brooks
Davis, Calif. 95616 1

Meteorology Department
San Jose State College
San Jose, Calif. 95113 1

Chief, Radio Propagation Lab
U. S. Natl Bureau of Standards
Boulder, Colo. 80301 1

Dept of Civil Engineering
Colorado State University
ATTN: Dr. J. E. Cermak
Fort Collins, Colo. 80521 1

Forest Service Exper Sta
Colorado State University
ATTN: M. Marinelli, Jr.
Rm 221, Forestry Bldg
Fort Collins, Colo. 80521 1

Director, Meteorology Dept
Florida State University
Tallahassee, Florida 32301 1

Director, USDA Field Sta
(Southern Piedmont Soil
Conservation Sta)
P. O. Box 33
Watkinsville, Georgia 30677 1

Meteorology Department
University of Hawaii
Honolulu, Hawaii 96822 1

Director, Meteorology Dept
University of Chicago
Chicago, Illinois 60607 1

Department of Agronomy
Iowa State University
ATTN: Dr. R. H. Shaw
Ames, Iowa 50010 1

Director
Soil & Water Consvtn Div
Agricultural Rsch Svc (USDA)
Beltsville, Md. 20705 1

Director
Department of Civil Engng
Johns Hopkins University
Baltimore, Md. 21233 1

Executive Secretary
American Met. Society
45 Beacon Street
Boston, Mass. 02109 1

Round Hill Field Station
Mass. Institute of Technology
South Dartmouth, Mass. 02748 1

Director, Meteorology Dept.
University of Michigan
Ann Arbor, Mich. 48105 1

Director, Meteorology Dept.
Mass. Inst. of Technology
Cambridge, Mass. 02138 1

University of Minnesota
ATTN: Dean Spilhaus
Minneapolis, Minn. 55041 1

Director, Meteorology Dept
St. Louis University
St. Louis, Mo. 63120 1

Department of Soils
University of Missouri
Columbia, Missouri 62501 1

Department of Geophysics
Washington University
St. Louis, Mo. 63120 1

Director, Meteorology Dept
New York University
University Heights
New York, N.Y. 10001 1

Soil & Water Consvtn Rsch Div
Agricultural Rsch Svc (USDA)
Cornell Univ, Bailey Hall
Ithaca, N.Y. 14851 1

Scientific Rsch Institute
Oregon State College
ATTN: Atmospheric Sciences Br
Corvallis, Oregon 97330 1

Director, Meteorology Dept
Pennsylvania State Univ
University Sta., Pa. 16802 1

Dept of Oceanography & Met
Texas A&M College
College Station, Texas 77840 1

Electrical Engng Rsch Lab
University of Texas
Route 4, Box 189
Austin, Texas 78761 1

Dept of Meteorology
University of Utah
Salt Lake City, Utah 84116 1

Director, Natl Rsch Council
Natl Academy of Sciences
2101 Constitution Avenue
Washington, D.C. 20315 1

Director, Meteorology Dept
University of Washington
Seattle, Wash. 99703 1

Director, Meteorology Dept
University of Wisconsin
Madison, Wisconsin 53705 1

Department of Soils
University of Wisconsin
ATTN: Dr. C. B. Tanner
Madison, Wisc. 53705 1

Officer-in-Charge
Meteorological Curriculum
U.S. Naval Post Graduate Sch
Monterey, Calif. 92801 1

Director, Geophysical Rsch
USAF Cambridge Rsch Cen
ATTN: CRZHB (Hanscom Field)
Bedford, Mass 01730 1

Deputy for Defense R&E
Office of SECDEF
ATTN: Geophysical Sciences
Washington, D.C. 20315 1

USAF Climatic Center
Air Weather Svc (MATS)
ATTN: CCCAD
Annex 2, 225 D., St. S.E.
Washington, D.C. 20315 1

Forestry Library
260 Walter Mulford Hall
University of California
Berkeley, Calif. 94704 1

Commander
AF Cambridge Rsch Labs
ATTN: Chief, Boundary Layer Br
Bedford, Mass. 01730 1

Argonne National Lab
ATTN: Mr. Harry Moses
Meteorology Building
9700 South Cass Avenue
Argonne, Ill. 60440 1

Commanding Officer
U.S. Army Chemical School
ATTN: Micromet Br. Tech Div
Ft. McClellan, Ala. 36205 1

Prof. J. E. Pearson
University of Illinois
General Engineering Dept
Atmospheric Science Lab
Urbana, Illinois 1

Brookhaven National Lab
ATTN: Meteorology Group
Upton, Long Island, N.Y. 1

Iowa State University of
Science & Technology
ATTN: Agronomy Dept
Ames, Iowa 50010 1

Director
National Security Agency
ATTN: C3/TDL
Ft. George G. Meade, Md. 1
20755

Commanding General
U. S. Army Munitions Command
ATTN: AMSMU-RE-R
Dover, New Jersey 07801 1

Terrestrial Environment Group
R-AERO-YT
ATTN: Mr. Glenn Daniels
George C. Marshall Space
Flight Center
Huntsville, Alabama 1

U.S. Naval Ordnance Test
Station
CODE 40306
ATTN: Dr. Richard Jackson
China Lake, Calif. 93557 1

Office of Chief Engineer
Bureau of Reclamation
ATTN: CODE 755
Bldg 53, Denver Federal Cen
Denver, Colorado 80225 1

Meteorologist-in-Charge
Weather Bureau Forecast Cen
Room 911, Federal Office Bldg
Kansas City, Mo. 64106 1